UNIVERSITY OF CAPE TOWN
IYUNIVESITHI YASEKAPA • UNIVERSITEIT VAN KAAPSTAD

CENTRE FOR CATALYSIS RESEARCH

Low pressure ammonia oxidation over supported cobalt catalyst for nitric acid production

Wing-Kin Fung

Supervised by:
Professor Eric van Steen

Centre for Catalysis Research
Department of Chemical Engineering
University of Cape Town

2012

University of Cape Town

The copyright of this thesis vests in the author. No quotation from it or information derived from it is to be published without full acknowledgement of the source. The thesis is to be used for private study or non-commercial research purposes only.

Published by the University of Cape Town (UCT) in terms of the non-exclusive license granted to UCT by the author.

PLAGIARISM DECLARATION

1. I know the meaning of plagiarism and declare that all of the work in the dissertation, save for that which is properly acknowledged, is my own
2. I have used the Harvard system for citation and referencing. Each significant contribution to, and quotation in, this report from the work, or works, of other people has been attributed, and has been cited and referenced.

Signed by candidate

Wing-Kin Fung

ACKNOWLEDGEMENTS

First and foremost, I would like to thank Prof. Eric van Steen for his guidance and enthusiasm towards all the problems I have encountered throughout the duration of my thesis. This work would not be possible without him and I could not have wished for a better supervisor.

I apologise in advance to the people that I forget to mention and I thank you all for the help and support throughout this project.

I am very thankful for the support that I received from the following people:

- All my colleagues from the Catalysis Research Unit
- Helen Divey and Suzana Vasic for their help from the Chemical engineering analytical lab
- Mohamed Jaffer and Miranda Waldron from the Electron Microscopy Unit
- Trailblazer Technologies for making this project possible and specifically John Bewsey for his insight and expert opinions

I would also like to thank the financial support from the Chemical Engineering department, University of Cape Town post-graduate funding department and NRF (National Research Foundation).

Finally I would like to thank my parents for their everlasting love and support through all the years in raising me and allowing me to grow as a person. For this I am forever grateful.

SYNOPSIS

Ammonia oxidation is used in the production of nitric acid. The process is either run at high pressure or low pressure, with the latter requiring larger equipment. Platinum gauze is typically used as a catalyst operating at high temperatures (in the range of 810-940 °C). The platinum based catalyst is highly active and highly selective in producing the desired NO_x products, with some formation of the undesired by-products, i.e. N_2, N_2O and N_2O_4. However, a significant amount of platinum is lost during the process due to platinum volatilisation resulting in plant operating times varying between 2-12 months. Furthermore, the loss of platinum is the 2nd largest expense of the operation. Platinum loss can only be minimised but not eliminated, thus a variety of metal oxide catalysts for oxidation of ammonia to nitrogen oxides have been studied. Cobalt oxide seems to be the most promising alternative for platinum exhibiting a high activity and selectivity towards NO.

The aim of this study is to explore the use of a supported cobalt Co_3O_4 on silica catalyst for ammonia oxidation and compare some of the results with a commercial catalyst consisting of a pure, unsupported Co_3O_4.

Both the synthesised and commercial catalyst showed a maximum conversion of ammonia at approximately 600 °C. A supported catalyst with a low cobalt loading and smaller crystallites yielded similar conversions of ammonia compared to the pure cobalt catalyst with much larger crystallites. However, the calculated intrinsic activity constant per m^2 of Co_3O_4 revealed that the commercial catalyst was more active compared to the in-house prepared Co_3O_4/SiO_2 catalyst. Indicating that severe deactivation might have taken place on the synthesised Co_3O_4/SiO_2 catalyst under ammonia oxidation conditions using an ammonia content of 7.1 vol.-% at 450-800 °C. A high ammonia conversion can be achieved by adjusting the space time.

The NO content as a fraction of NO plus N_2O, increases with increasing temperature before the catalyst is completely deactivated at temperatures above 800 °C. The in-house prepared Co_3O_4/SiO_2 catalyst displayed a higher relative NO selectivity compared to the commercial Co_3O_4 catalyst under industrially relevant conditions at complete conversion of ammonia.

Applying the rate equation proposed by Saykov et al. (2000) and operating under a regime where Knudsen diffusion is the dominant diffusion mechanism, the in-house synthesised supported catalyst and the commercial catalyst showed severe mass transport limitations, indicating inefficient use of the catalyst. The heat transfer limitations were assumed to be negligible with minimal temperature gradients with the catalyst and boundary layer. The supported Co_3O_4/SiO_2 catalyst showed severe mass transfer limitations with the effectiveness factor less than 0.5 for particles greater than 300 microns. The mass transfer parameters (Thiele modulus, effectiveness factor, $r_{intrinsic}$ and $r_{observed}$) exhibit small changes over the catalyst bed at low conversions of NH_3 and displayed major significant changes at more industrially relevant conditions where higher conversion of NH_3 is achieved.,

The conversion of ammonia decreases rapidly at higher temperatures. It is deduced that sintering of the catalyst is not a major concern. Ammonia oxidation proceeds via the Mars and Van Krevelen mechanism. Therefore the deactivation of the catalyst might be caused by the reduction of active Co_3O_4 phase to the catalytically inactive CoO phase. Since the mechanism involves the lattice oxygen, the deactivation mechanism is thought to be reversible by utilising excess air. However for the supported catalyst, the CoO acts as an intermediate in the formation of cobalt silicate (Co_2SiO_4), resulting in an irreversible deactivation. In conclusion, a support material which can react with CoO under hydrothermal conditions, i.e. silica and alumina should be avoided in the preparation of cobalt catalysts for ammonia oxidation.

Table of contents

LIST OF TABLES

LIST OF FIGURES

NOMENCLATURE

a.u.	Arbitrary units	-
C	Concentration of reactant	mol/m^3
D	Rate of diffusion	m^2/s or cm^2/s
d_p	Diameter of particle	m or nm
d_{pore}	Pore diameter	m or nm
$\Delta G°$	Standard Gibbs free energy	J/mol or kJ/mol
ΔH^{rxn}	Heat of reaction	J/mol or kJ/mol
κ	Thermal conductivity constant	W/m.K
k_L	Mass transfer coefficient	m/s
λ	Lagrange multiplier	-
NTP	Normal temperature and pressure	-
η	Effectiveness factor	-
Φ	Thiele modulus	-
P	Pressure	atm
ρ	Density	g/m^3
r	Rate of reaction per unit mass of catalyst	mol/s.g
R	Gas constant	J/K.mol
STP	Standard temperature and pressure	-
u	Linear velocity	m/s
μ	Viscosity	g/s.m
T	Temperature	°C or K
X	Conversion of reactant	%
y	Molar fraction of compound	-

1 INTRODUCTION

Nitric acid production is a large scale process used to manufacture one of the most produced chemicals in the world. In 2002, it was estimated that close to 46 million tons of nitric acid were produced, mainly used for the production of fertiliser and explosives. Ammonia oxidation is the central catalytic process in the production of nitric acid process (Clarke and Mazzafro, 2005).

Ammonia oxidation is the reaction whereby ammonia (NH_3) is reacted with oxygen (O_2), in the presence of a catalyst, to produce nitric oxide (NO), nitrogen dioxide (NO_2) and water (H_2O). However, NO and NO_2 are not the only products, by-products such as N_2O, N_2 and N_2O_4 are formed during the oxidation of ammonia as well. The by-product N_2O is environmentally unfriendly, toxic and a strong greenhouse gas (EPA, 2009). Therefore the catalyst that is utilised must be highly selective in producing NO/NO_2 and minimise the production of the other product compounds, in particular N_2O_4. The typical catalyst that is utilised is a platinum-based catalyst, with which conversions above 90% are easily achieved at the typical operating conditions of between 810-940 °C and pressures between 1-10 atm. The higher pressure is for the production of concentrated nitric acid (Clarke and Mazzafro, 2005).

However, the major disadvantage with using the platinum-based catalyst is the significant loss of platinum due to volatilisation of this highly expensive metal. Improvements to the process have only been able to reduce the loss of platinum but could not eliminate it. Therefore, studies have been undertaken to substitute the platinum gauzes for a less expensive catalyst and to develop an alternative catalyst (Sadykov et al., 2000). Cobalt oxide (Co_3O_4), with an average crystallite size of 80 nm, showed the highest activity when comparing with the other metal oxides, thus making it a promising alternative to replace platinum as a catalyst (Sadykov et al., 2000; Schmidt-Szałowski et al., 1998). Smaller crystallites would enhance the surface area of the catalyst and increase the activity per unit mass. Smaller crystallites are typically supported to avoid high pressure drop across the reactor. Therefore the aim of this research is to synthesise a supported Co_3O_4 catalyst, evaluate its catalytic performance in terms of activity and selectivity and investigate the mass and heat transfer limitations involved with the supported catalyst.

2 LITERATURE REVIEW

2.1 Nitric acid production

Nitric acid is one of the chemicals produced worldwide in the largest amount. Nitric acid contains properties of a strong acid, powerful oxidising agent and the ability to nitrate organics. Nitric acid is used mostly in the production of ammonium nitrate for the fertiliser and explosives industry and by the end of the 19th century, its industrial importance was established through the production of explosives and dyes. Nitric acid is essential in the production of many chemicals such as pharmaceuticals, dyes, synthetic fibre, insecticides and fungicides (Clarke and Mazzafro, 2005).

In 2002, an estimated 46 million tons of nitric acid were produced and utilised around the world. Essentially, all commercial quantities of nitric acid are manufactured through the oxidation of ammonia with air to form nitrogen oxides which is subsequently absorbed by water to form nitric acid. The ammonia oxidation reaction yields a number of products namely, NO, NO_2, N_2O, N_2 and N_2O_4 (Clarke and Mazzafro, 2005; Sadykov et al., 2000). The desired product yield depends on the catalyst selectivity and the operating conditions of the process. NO and NO_2 are reactants required for HNO_3 production and thus the desired product for the initial reactions. Nitrogen compounds and especially NO_x emissions must be limited as it is regarded as one of the major environmental pollutants.

The by-product N_2O is considered a greenhouse gas with tremendous global warming potential (EPA, 2009). Nitrogen compounds NO_2 and N_2O_4 may undergo further reactions with the atmosphere which would create harmful particulate matter, ground-level ozone (smog) and acid rain. Therefore laws and regulations are in place to limit and restrict the emissions of such harmful chemicals (EPA, 2009). The operating conditions and catalysts have to be selected to maximise the production and selectivity of NO and NO_2 as the by-products, in particular N_2O, is undesired and environmentally unfriendly.

A basic reaction scheme to produce nitric acid is given as follows and illustrated in Figure 2.1:

Catalytic ammonia oxidation:

$$NH_3 + 1.25O_2 \rightarrow NO + 1.5H_2O \qquad \Delta H^{rxn}_{25\,°C} = -226\ kJ/mol$$

Oxidation of nitric oxide:

$$2NO + O_2 \leftrightarrow 2NO_2 \qquad \Delta H^{rxn}_{25\,°C} = -57.1\ kJ/mol$$

Absorption of nitrogen oxides

$$3NO_2(g) + H_2O(l) \leftrightarrow 2HNO_3(aq) + NO(g) \qquad \Delta H^{rxn}_{25\,°C} = -246\ kJ/mol$$

Commercially nitric acid is manufactured by the oxidation of ammonia with air yielding nitrogen oxides that are absorbed in water to form nitric acid. Ammonia and air are mixed such that there is an excess of oxygen and are passed over a catalyst to produce NO, H_2O and heat. The resulting gases are cooled and as the gases cool, NO is further oxidised yielding NO_2. NO is released during the formation of nitric acid and thus, prior to the absorption tower, complete conversion of NO to NO_2 is carried out in the oxidation chamber. The resulting NO_2 gas is absorbed in water to product nitric acid. The spent gas which contains residual levels of nitrogen oxides have to be removed before discharge to the atmosphere for environmental reasons (Clarke and Mazzafro, 2005).

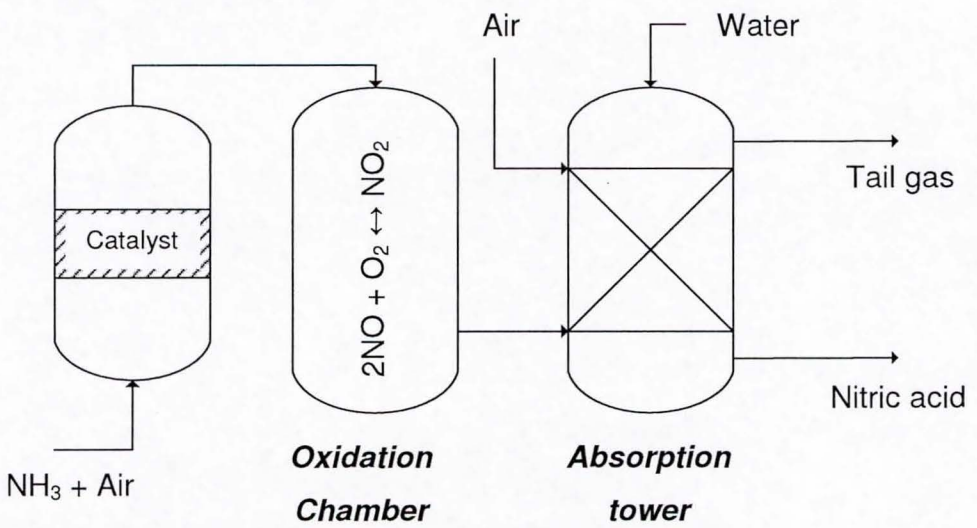

Figure 2.1: Basic process for the production of nitric acid

2.2 Ammonia oxidation

The ammonia oxidation process was first invented by Kuhlmann. By passing a mixture of ammonia and air over a platinum sponge heated to about 300 ℃ in a glass tube, nitric acid was formed. He filed a patent application for this invention in 1838 (Hunt, 1958).

However it was not until the early 20th century when the first industrial process of nitric acid production through ammonia oxidation was commercialised by Ostwald (Hunt, 1958). Ostwald further investigated the effects of variation in ammonia to air ratio, contact time and temperature of the catalyst. The catalyst used at that time consisted of a roll of corrugated platinum strip heated by a hydrogen flame. The first platinum gauze catalyst was employed by Kaiser in 1909 (Hunt, 1958). Currently, the main catalysts involved with ammonia oxidation are platinum-rhodium alloy and a platinum-palladium-rhodium alloy operating between 810-940 ℃ (Sadykov et al., 2000). The process is either run at a high pressure or at a low to moderate pressure, with the latter requiring larger equipment (Clarke and Mazzafro, 2005).

2.2.1 Thermodynamic analysis

To gain a better understanding of the process, a preliminary thermodynamic analysis on the oxidation of ammonia with oxygen was performed. To predict the thermodynamic limitations for the formation of the various product compounds, the following reactions were considered:

$NH_3 + 1.25O_2 \rightarrow NO + 1.5H_2O$ $\quad \Delta H^{rxn}_{25℃} = -226$ kJ/mol

$NO + 0.5O_2 \rightarrow NO_2$ $\quad \Delta H^{rxn}_{25℃} = -57.1$ kJ/mol

$2NO \rightarrow N_2O + 0.5O_2$ $\quad \Delta H^{rxn}_{25℃} = -98.5$ kJ/mol

$N_2O \rightarrow N_2 + 0.5O_2$ $\quad \Delta H^{rxn}_{25℃} = -33.2$ kJ/mol

$2NO_2 \rightarrow N_2O_4$ $\quad \Delta H^{rxn}_{25℃} = -57.2$ kJ/mol

The reaction between NO_2 and H_2O to form HNO_3 was not considered. Ammonia oxidation is a gas phase reaction and the calculated equilibrium constant for the gas phase of NO_2 and H_2O yielding gaseous HNO_3 was very low, thus not likely to occur. However this reaction must be considered when operating with a liquid phase as the liquid phase changes the equilibrium constant significantly.

The oxidation of NH_3 yielding NO is highly favoured and from a thermodynamic view point, complete conversion of NH_3 is expected. The conversion of NO to either NO_2 or N_2O is limited in the considered temperature range. The formation of N_2 and O_2 are thermodynamically favoured and the catalyst must inhibit the transformation of the product compounds to the undesired by-products.

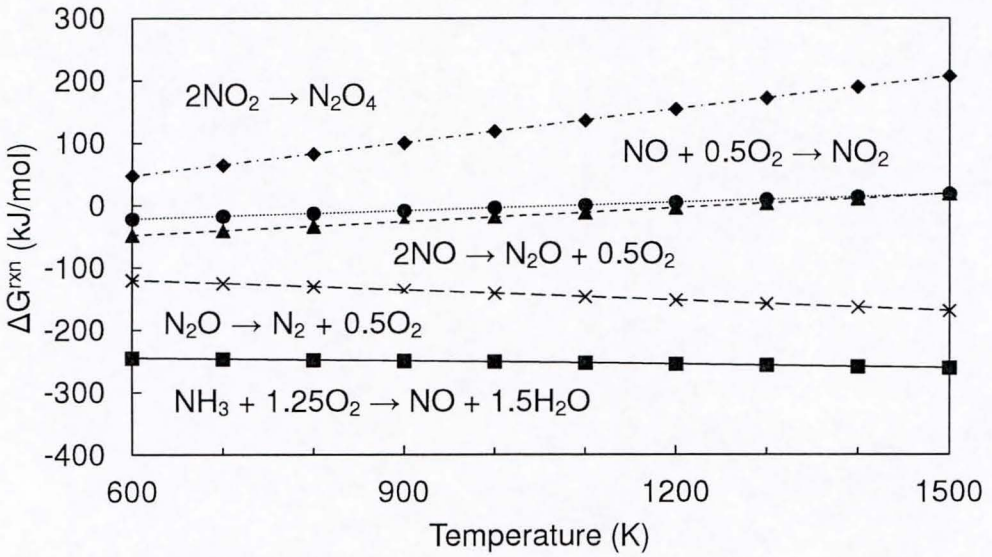

Figure 2.2: Gibbs free energy of reaction for the reactions considered in the ammonia oxidation involing NO and NO_x compounds as a function of reaction temperature

The chemical equilibrium composition was determined using Lagrange multipliers method (Smith et al., 1999).

The system composition at equilibrium can be found by solving N equilibrium equations, mass balance equations and a restriction equation represented as follows:

$$\Delta G^{\circ}_{f,i} + RTln(y_i \Phi_i \frac{P}{P_0}) + \sum_k \lambda_k a_{i,k} = 0$$

$$\sum_i n_i a_{i,k} = A_k$$

$$\sum_i y_i = 1$$

(Where $\Delta G°_{f,i}$ is the standard Gibbs free energy (J/mol) for the formation of species i at temperature T (K), R is the universal gas constant (J/mol.K), y is the molar fraction of compound i in the mixture, Φ_i is the fugacity coefficient, P and P_0 is the pressure in atm. with P_0 = 1 atm, λ_k is the Lagrange multipliers of element k, a is the no. of atoms and A is the total number of atoms of element k)

This method results in systems of non-linear algebraic equations, solved numerically using the Scilab program and the Scilab "fsolve" function. Using this method requires a good initial estimate and thus this becomes a trial and error solving method (see Appendix A.1).

The thermodynamically predicted product distribution would be represented in terms of the major and minor contributors. The distribution was reported in mole percentages of the product stream.

Figure 2.3 depicts the thermodynamically predicted product distribution of the major products during complete ammonia oxidation with a feed of 7.1 mol.-% NH_3, 19.4 mol.-% O_2 and the balance He at a pressure of 1 atmosphere. Helium was used as the inert carrier gas with a constant number of moles representing approximately 73 mol.-% of the total number of moles in the product stream. At complete conversion of NH_3 and with excess oxygen, water was determined to contribute 10 mol.-% of the total number of moles. The remaining fraction was attributed to the nitrogen containing compounds, i.e. N_2, NO, NO_2, N_2O and N_2O_4. The formation of N_2 is thermodynamically favoured and is the dominant product compound. Figure 2.4 depicts the thermodynamic product distribution of the minor nitrogen containing products and shows the increase in temperature would favour the formation of the desired NO_x products. However the formation of the desired product is still minimal with the formation of N_2 highly favoured.

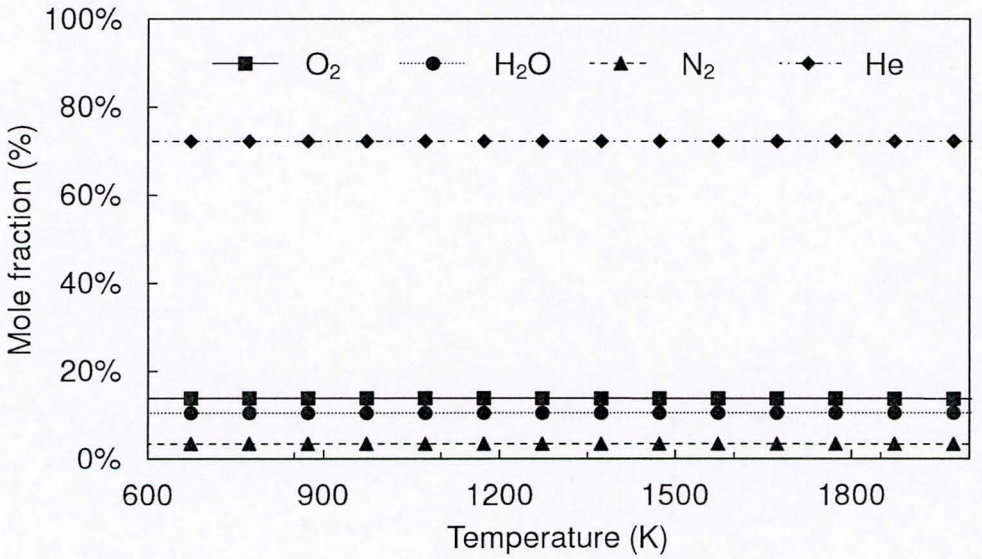

Figure 2.3: Thermodynamically controlled product distribution of the major products (O_2, H_2O, N_2 and He) as a function of reaction temperature, at which 100% NH_3 conversion is achieved with a feed (in mol.-%) of 7.1% NH_3, 19.4% O_2 and balance He at 1 atm

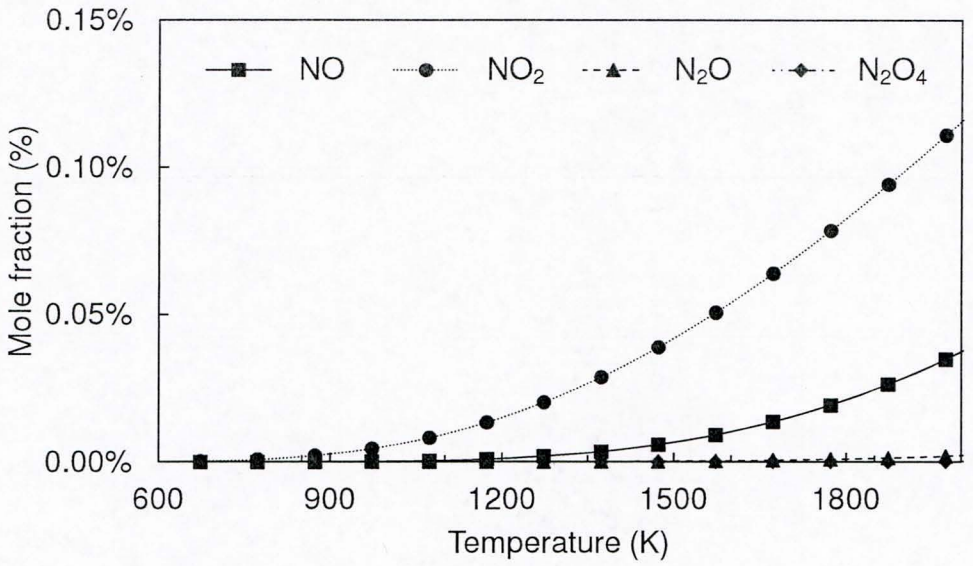

Figure 2.4: Thermodynamically controlled product distribution of the minor products (NO, NO_2, N_2O and N_2O_4) as a function of reaction temperature, at which 100% NH_3 conversion is achieved with a feed (in mol.-%) of 7.1% NH_3, 19.4% O_2 and balance He at 1 atm

The thermodynamic product distribution changes when N_2 replaces He as the balance gas (see Figure 2.5 and Figure 2.6). This would result in more feasible representation of the industrial conditions where air is used as the source of oxygen. The mole fraction of O_2 and H_2O was similar to the case where He was the balance gas. The product distribution of the nitrogen containing products changes significantly as the presence of N_2 would shift the equilibrium to reduce the formation of N_2 and favour the equilibrium formation of the other nitrogen containing products. The formation of all the nitrogen containing products increases with the increased temperature. The formation of NO_x increases by a factor of more than 10 at higher temperatures compared to the scenario where He was used as the balance gas. Therefore operating at a higher temperature would favour the formation of the desired products. However the downside is that at higher temperatures, the undesired and environmentally unfriendly by-products, N_2O and N_2O_4 are formed and should be avoided.

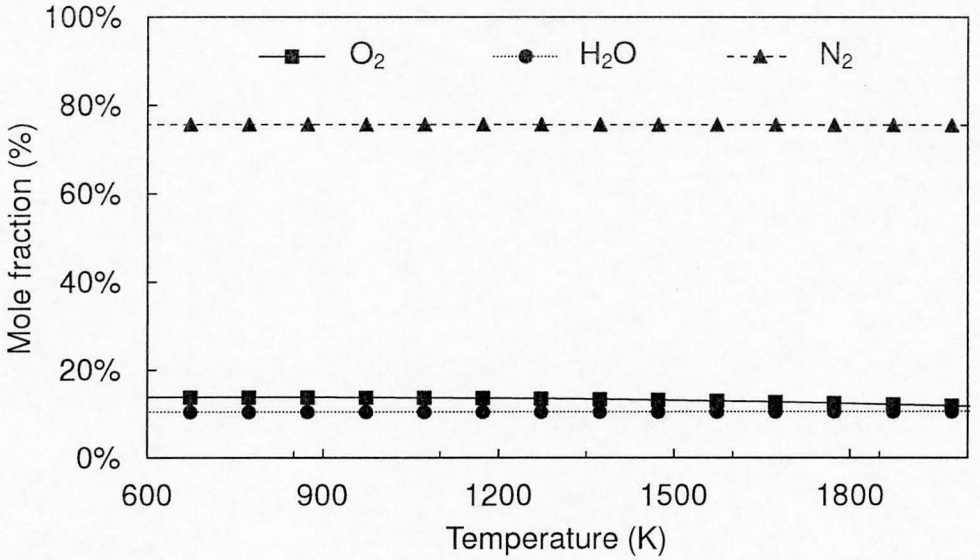

Figure 2.5: Thermodynamically controlled product distribution of the major products (O_2, H_2O and N_2) as a function of reaction temperature, at which 100% NH_3 conversion is achieved with a feed (in mol.-%) of 7.1% NH_3, 19.4% O_2 and balance N_2 at 1 atm

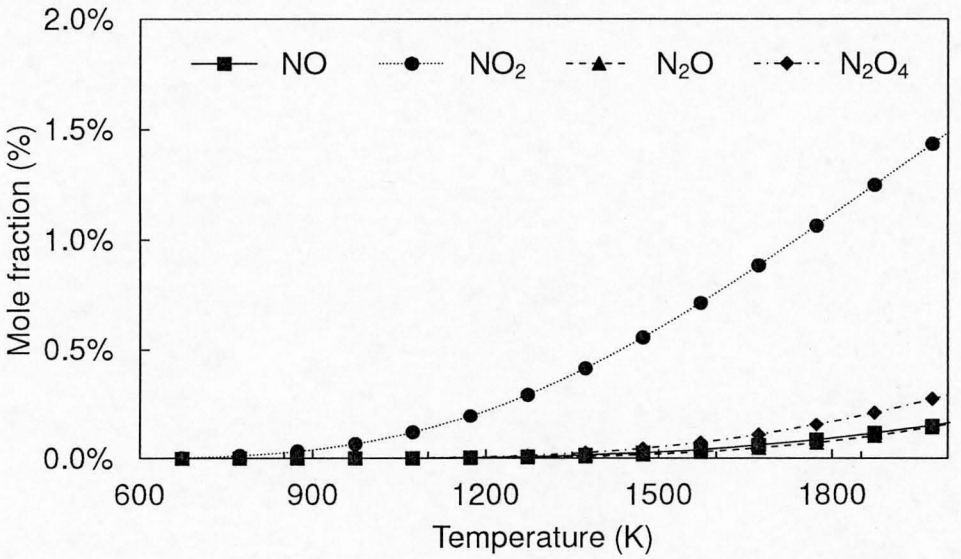

Figure 2.6: Thermodynamically controlled product distribution of the minor products (NO, NO_2, N_2O and N_2O_4) as a function of reaction temperature, at which 100% NH_3 conversion is achieved with a feed (in mol.-%) of 7.1% NH_3, 19.4% O_2 and balance N_2 at 1 atm

As mentioned before, the formation of N_2 under ammonia oxidation conditions is thermodynamically favoured. Therefore a catalyst for ammonia oxidation would be selected that inhibits the formation of N_2. The optimal catalyst is defined as the catalyst which converts all the NH_3 but completely inhibits the formation of N_2 from either ammonia or nitrogen oxides compounds. The thermodynamically predicted product distribution where no N_2 was present yielded similar results for the oxygen and water fractions but significantly different results, with a greater yield for the nitrogen oxide compounds (see Figure 2.7).

The thermodynamic yield of NO_2 decreases with increases in temperature where as the NO fraction increased with increasing temperature. The NO fraction increases at a faster rate and thus the overall formation of NO_x increases with increasing temperature. The thermodynamic yield of the undesired by-product N_2O fraction was significantly higher but decreases with increasing temperature. Similarly the N_2O_4 fraction also decreased with increasing temperature.

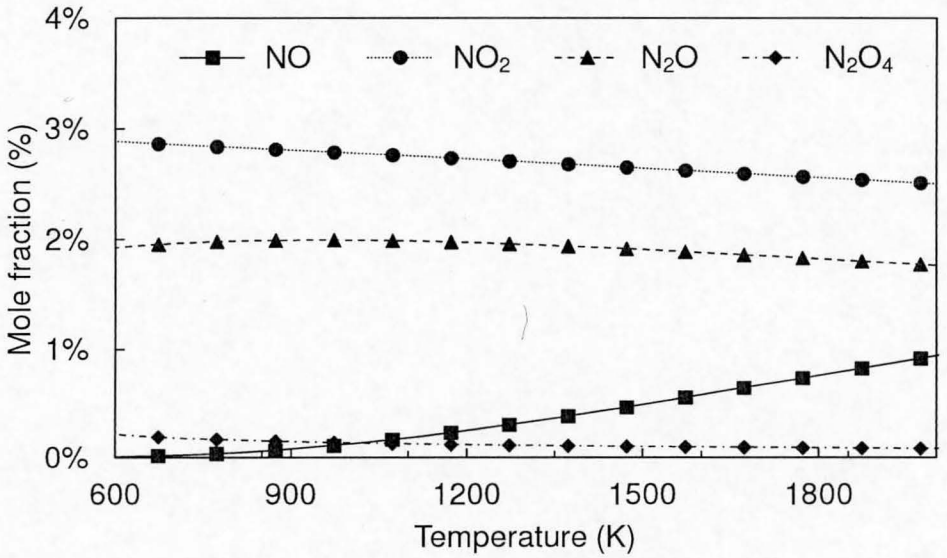

Figure 2.7: Thermodynamically controlled product distribution of the minor products (NO, NO_2, N_2O and N_2O_4) as a function of reaction temperature over an optimal catalyst, at which 100% NH_3 conversion is achieved with a feed (in mol.-%) of 7.1% NH_3, 19.4% O_2 and balance He at 1 atm

Considering all these factors and according to the thermodynamic analysis it is desired to operate at high temperatures to favour the formation of NO_x and the catalyst should inhibit the formation of, in particular N_2 but also N_2O and N_2O_4.

2.2.2 Platinum based catalyst for ammonia oxidation

In the early processes, the life times of the catalysts were very short and required a relatively large amount of platinum per unit of acid produced (Hunt, 1958; Bell, 1960). The platinum based catalyst is able to achieve high conversions (93-98%) of ammonia with the optimum reaction temperature increasing with increasing operating pressure (Clarke and Mazzafro, 2005). Under industrial operating temperatures (800-900 °C), the oxidation of ammonia on the platinum gauzes produces mainly N_2 and NO formed on the catalyst surface via the following reactions:

$$NH_3 + 1.25O_2 \rightarrow NO + 1.5H_2O \qquad \Delta H^{rxn}_{25°C} = -226 \text{ kJ/mol}$$

$$NH_3 + 0.75O_2 \rightarrow 0.5N_2 + 1.5H_2O \qquad \Delta H^{rxn}_{25°C} = -317 \text{ kJ/mol}$$

However, major problems associated with using a platinum-based catalyst are the high production costs and significant loss of platinum during the process. The platinum is slowly lost from the gauze, mainly in the form of the more volatile oxide (PtO_2). Another serious problem related to platinum losses is caused by reaction medium impact. This means that a maximum yield of NO is only achieved within 3-5 days, thus resulting in significant loss in acid production during start-up. The loss of precious metals is of financial significance and various methods, such as downstream glass fiber filters, are used to recover the lost catalyst. In spite of the recovery process, it has been reported that the loss of platinum is the second largest expense of the operation, exceeded only by the cost of ammonia feed-stock (Sadykov et al., 2000). Therefore ways to minimise this loss must be found.

2.2.3 *Improvements to the platinum based catalytic process*

Over the years, the platinum based process has undergone constant improvements. To name a few, Ning et al. (1999) found that by increasing the amount of palladium to the alloy catalysts, the losses of platinum decreases due to palladium enrichment. The action of the palladium, which accumulates on the surface and enriches the surface layer of the alloys, affects both the platinum oxidation and platinum oxide reduction (Ning and Yang, 1999).

$$2Pd + PtO_2 \rightarrow 2PdO + Pt \qquad \Delta H^{rxn}{}_{25°C} = -252 \text{ kJ/mol}$$

A brief thermodynamic analysis on the Gibbs free energy of the reaction to recover the active platinum metal using palladium, assuming that the heat of reaction was constant, indicated that the palladium reaction with platinum oxide is only favourable (spontaneous) at temperatures below 950 °C. The change in Gibbs free energy for the reaction becomes positive at temperatures above 950 °C. The conventional operating temperature for ammonia oxidation is between 800-900 °C and thus the reaction using palladium to reduce platinum volatilisation falls just within the operating temperatures (Nell and O'Neill, 1996; Pradyot, 2003).

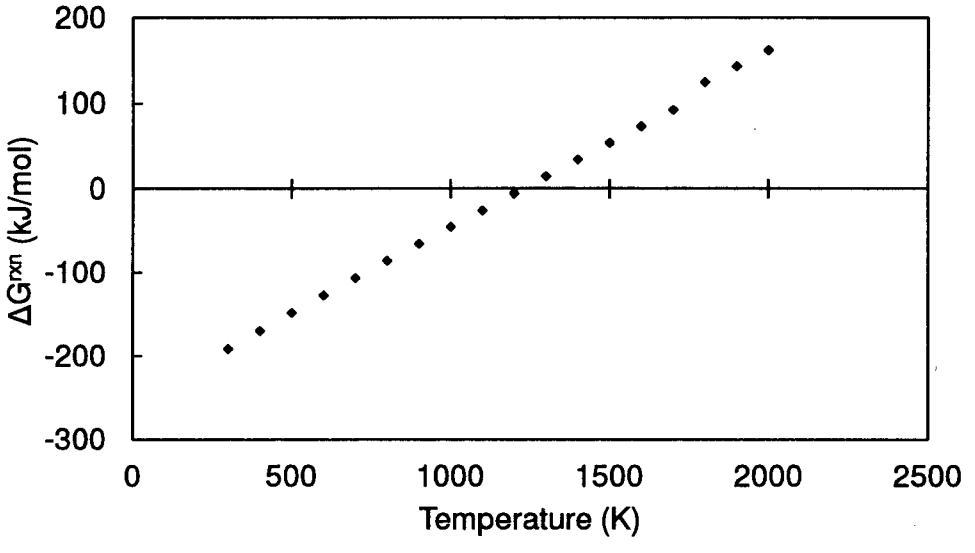

Figure 2.8: Gibbs free energy of reaction for the reaction between palladium and platinum oxide to recover the active platinum metal

Chernyshev and Zjuzin (2001) specifically looked at how the start-up process for ammonia oxidation can be improved. They found that by implementing an electrical ignition device (EID) into the process, most if not all of the disadvantages during start-up can be eliminated. The EID device uses linear heating elements arranged in a unique manner on the surface of the platinum alloy catalyst which needs to be ignited. This device has been implemented on plants in Russia, Lithuania, Hungary and Greece and yielded good results, with a time of initiating the reaction not exceeding 60 seconds. However the major disadvantages of this device is that it is dependent on technical characteristics (geometric and mechanical configurations) and it requires significant amounts of power depending on the size of the reactor. This means that the gauze composition and geometric characteristics are taken into consideration which could lead to a high cost as this device would be unique for each plant (Chernyshev and Zjuzin, 2001).

The platinum based ammonia oxidation process is a very well established process with research constantly improving the process. However, platinum losses still occur, which can only be reduced and not eliminated. All these facts encourage research towards (partial) substitution of platinum gauzes by a less expensive catalyst or to develop a new cheaper alternative catalyst. Research has shown that a metal oxide catalysts and especially the cobalt oxide catalyst may be a substitute for the commonly used catalytic platinum gauze alloy (Sadykov et al., 2000; Schmidt-Szałowski et al., 1998).

2.3 Metal oxide catalyst

Among simple transition metal oxides, the most active for ammonia oxidation are Co_3O_4, MnO_2, Cr_2O_3 and CuO with the activity decreasing in the mentioned sequence (Sadykov et al., 2000; Il'chenko and Golodets, 1975). The transition metal oxides of iron, nickel and vanadium have also been found to be moderately active. At low temperatures (below 380 °C) NO may react further or decomposes to form N_2, O_2 and N_2O as the main products over the metal oxide catalyst. At high temperatures, the selectivity towards NO dominates among the reaction products and it is said that the ammonia oxidation rate is limited by the ammonia diffusion to the catalyst surface (Sadykov et al., 2000). Therefore the selectivity towards NO attains its maximum when the oxygen completely covers the catalyst surface. The activity and selectivity towards N_2O decreases as the surface oxygen bonding strength increases (Sadykov et al., 2000).

It was found that Co_3O_4 (Co_3O_4 > MnO_2 > Fe_2O_3 > CuO > ZnO > MoO_3 > WO_3 > TiO_2) was the metal oxide catalyst that is most selective towards NO (Il'chenko and Golodets, 1975). Therefore Co_3O_4 could be a possible alternative catalyst to replace Pt as the conventional ammonia oxidation catalyst.

It has been reported that better catalytic properties are observed when the metal oxide (Co_3O_4) is further "activated" with cerium and lanthanum oxides. The addition of these metal oxides increased the activity of the catalyst as well as the selectivity towards NO. The activity and selectivity towards NO decreases as the typical Co_3O_4 catalyst is reduced to CoO under the conditions of the ammonia oxidation process (Petryk and Kołakowska, 2000). By introducing the promoters, the reduction of Co_3O_4 to CoO is inhibited.

Kim et al. (2010), who used lanthanum-based perovskite catalysts ($La_{1-x}Sr_xCoO_3$) to reduce the selectivity towards NO_x in motor engines further confirms that the introduction of promoters inhibits the formation of CoO. They concluded that the perovskite catalyst showed excellent activity for the NO oxidation reaction which was equal to or higher than the activity by the Pt-based commercial catalysts (Kim et al., 2010).

2.3.1 Co_3O_4 oxidation behaviour

Co_3O_4 catalyst is currently being used as an oxidation catalyst. Propane oxidation is an example where the cobalt oxide catalyst exhibits very high activities. Supported and unsupported nanocrystalline Co_3O_4 have been shown to be an extremely efficient catalyst for the total oxidation of propane with complete conversion achieved at reaction temperatures as low as 250 °C. Co_3O_4 catalyst was found to be critically dependent on the crystallite size of the cobalt oxide with the smaller size (higher surface area) being the most reactive. Co_3O_4 with a surface area of 99 m^2/g was shown to be the most active and highly stable (Solsona et al., 2008).

Liu et al. (2009) used various methods to prepare the Co_3O_4 crystallites and total oxidation of propane was achieved using the different preparation techniques. Crystallite sizes varied between 12~23 nm with the larger size requiring a higher temperature to achieve total oxidation of propane. It was observed that the smaller crystallites (~12nm), i.e. with the highest surface area, exhibited the highest reaction rate (Liu et al., 2009), confirming the results reported by Solsona et al. (2008).

In addition, the Co_3O_4 catalyst showed good activity and thermal stability during the high temperature methane oxidation reaction with a slight decrease in activity at temperatures above 700 °C due to the thermal decomposition of Co_3O_4 into CoO (Liotta et al., 2006).

Therefore according to literature, Co_3O_4 catalyst exhibits highly active behaviour during oxidation reactions and it is desired to have small Co_3O_4 crystallites with a high surface area, if the formation of CoO can be suppressed.

2.4 Co_3O_4 for ammonia oxidation

Schmidt-Szałowski et al. (1998) used a cobalt oxide catalyst, the active component being Co_3O_4, for ammonia oxidation which resulted in high and stable activity and selectivity towards NO. The catalyst was tested in a fluidised bed laboratory reactor. They found that much less N_2O was produced in the reaction on the Co_3O_4 catalyst than on the platinum based catalyst.

Schmidt-Szałowski et al. (1998) operated their reactions above 700 °C at atmospheric pressure and obtained conversions in the region of 90% for NH_3 to NO and < 2% conversion for NH_3 to N_2O. The residence (contact) time reported on these reactions was 1.8×10^{-2} seconds for which complete ammonia conversion was achieved. The contact time of 2×10^{-2} seconds is larger than that which has been reported for the platinum based catalyst which is approximately 1×10^{-4} seconds (Clarke and Mazzafro, 2005), this indicates that platinum has a much higher activity. However, none of the authors stated how the basis of the contact time was defined and thus a direct comparison cannot be made.

It was furthermore reported that the NO selectivity passes through a maximum of 96% using cobalt based catalyst. This high selectivity was obtained when operating at 650 °C and at atmospheric pressure at lowered ammonia content to avoid the transformation of Co_3O_4 to the less selective CoO. A residence time of 1×10^{-2} seconds was used to ensure complete conversion of ammonia (Sadykov et al., 2000).

A high selectivity towards NO was obtained in each case; however the selectivities were measured at 100% of conversion of ammonia and the catalysts were compared using the selectivities obtained. This comparison is doubtful because numerous side reactions between the products could have occurred after all the NH_3 has been converted and affect the selectivity of the measured components. Therefore the actual performance of the catalyst is not known. Selectivity should be compared at the same conversion but below 100%. At lower conversions (~50%), the kinetic performance of the catalyst can be evaluated and the higher conversions would represent the industrial relevant conditions.

The kinetic performance of the catalyst can be evaluated using an established rate law. However, despite numerous studies related to this important process, there is no generally accepted kinetic law to describe the ammonia oxidation reaction using either platinum gauze or metal oxide catalysts. Using cobalt Co_3O_4 catalyst, the ammonia oxidation rate was reported to occur via the following equation with an activation energy of approximately 37.68 kJ/mol (Sadykov et al., 2000; Schmidt-Szałowski et al., 1998) :

$$r = -r_{NH_3} = k[NH_3]^{0.36}[O_2]^{0.14}$$

(Where k is the reaction rate constant, $[NH_3]$ and $[O_2]$ are the concentrations of ammonia and oxygen near the catalyst surface respectively)

The Co_3O_4 catalyst used by Schmidt-Szałowski et al. (1998) consisted of large Co_3O_4 crystallites of ca. 80 nm. Thus the tested materials have a relatively low catalytically active surface area. Reducing the crystallite size would enhance the catalyst activity significantly.

2.4.1 Reaction mechanism of ammonia oxidation

NO, N_2O and N_2 are predominantly the only products formed over the cobalt based catalyst, it has been reported that the reaction proceeds by a Mars and Van Krevelen mechanism (Biausque and Schuurman, 2010). NO absorbs into a vacancy occupied by an oxygen species and can form a nitrite species, ONO^-. The oxygen atom can then be exchanged with the catalyst surface. NO and N_2O are formed through parallel routes from ammonia via the surface nitroxyl HNO species.

The formation of N_2 occurs via the decomposition of NO and N_2O or alternatively through the reaction of the absorbed ammonia with the oxygen surface species (Biausque and Schuurman, 2010).

2.4.2 Catalyst crystallite size effect

A decrease in size would result in a significant increase in surface area and thus leading to an increase in the activity per unit mass (see Figure 2.9), if the turn-over frequency is independent of the crystallite size.

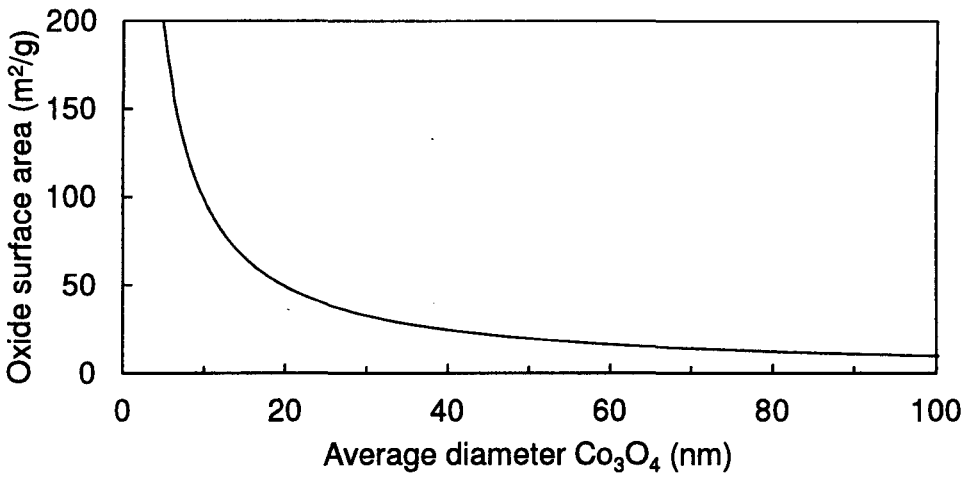

Figure 2.9: Surface area of Co_3O_4 per mass of catalyst as a function of average crystallite size

Small crystallites, around the nm range, cannot easily be applied in reactions with a high linear velocity because it would result in a high pressure drop across the reactor. Therefore nano-sized materials are typically supported. The cobalt-based catalyst (~80 nm) for ammonia oxidation reported by Schmidt-Szałowski et al. (1998) is unsupported (pure Co_3O_4) and was developed for a fluidised bed type of operation. A supported catalyst with a Co_3O_4 loading of 25% and a size of approximately 20 nm should have the same activity as an unsupported Co_3O_4 catalyst with a size of 80 nm based on the surface area of Co_3O_4, assuming the turn-over frequency is independent of crystallite size.

A smaller average crystallite size does not necessarily lead to a higher activity as seen in Fischer-Tropsch process where the activity, per unit mass of cobalt, of a cobalt catalyst passed through a maximum at an approximate size of 6 nm (Bezemer et al., 2006). However the Co° component is the active phase for the Fischer-Tropsch reaction and thus a direct comparison could not be made.

2.4.3 Silica support

The cobalt crystallites will be supported on silica (SiO_2), which is a well known porous oxide support. The function of the support is to form the size of the catalyst and add stability to the small nano-crystallites to avoid a high pressure drop across the reactor. In addition, the support should enable the formation of a well dispersed, catalytically active phase of the catalyst (Bezemer et al., 2006).

2.5 Catalyst deactivation

All catalysts show some loss in activity with time on stream. The loss of catalytic activity or deactivation can be caused under the influence of chemical, physical or thermal interactions.

Sintering of the catalytically active phase can be expected at temperatures in excess of (0.3-0.5) times its melting point (Trimm, 1980). Co_3O_4 may sinter and agglomerate, decreasing the activity with time online, without losing its structure at temperatures as low as 500 °C, thus leading to a decrease in activity (Trimm, 1995).

The main cause of catalyst deactivation for the cobalt catalyst during ammonia oxidation is the reduction of the active phase Co_3O_4 to the relatively inactive CoO. The reduction of Co_3O_4 would result in the formation of CoO in the external layer and this can be considered as catalyst deactivation since CoO does not show catalytic activity for oxidation of NH_3 to form the desired NO product (Schmidt-Szałowski et al., 1998).

The catalytic activity of Co_3O_4 catalyst is affected by both the temperature and concentration of ammonia in the reactor. Since ammonia is a reducing agent, it will lead to the reduction of Co_3O_4 to CoO.

The phase transition of Co_3O_4 to CoO in air is expected at temperatures above 900 °C where Co_3O_4 expels oxygen out of the molecule (Pradyot, 2003). Schmidt-Szałowski et al. (1998) indicated that the phase transition occurs at temperatures above 700 °C when working with 10 mol.-% NH_3 in air. This agrees with the study performed by Liotta et al. (2006) who found the same phenomenon when the Co_3O_4 catalyst was exposed to low concentration methane during methane oxidation.

The phase transition between Co_3O_4 and CoO is a result of adsorption and desorption of oxygen and is said to be reversible and can be expressed as:

$$Co_3O_4 \leftrightarrow 3CoO + 0.5O_2 \qquad \Delta H^{rxn}_{25°C} = 177 \text{ kJ/mol}$$

The kinetics of the phase transition are highly dependent on the thermodynamic driving force of desorption and adsorption reactions. Changing the partial pressure of oxygen changes the driving force for the reaction and thus the temperature range over which the reaction occurs (Hutchings et al., 2006).

According to van Steen et al. (2005), the tendency of the cobalt crystallites to oxidise is related to the cobalt oxide crystallite size and the prevalent reactor partial pressures (van Steen et al., 2005). Therefore by utilising excess air during ammonia oxidation, the cobalt Co_3O_4 phase should be recovered.

However for supported Co_3O_4/SiO_2 catalyst, the irreversible deactivation as a result of oxidation from cobalt metal to cobalt-silicate is possible (Chen et al., 2001).The thermodynamic Gibbs free energy for the reaction to form cobalt silicate was determined to be between -19.1 to -16.8 kJ/mol for a high reaction temperature between 600-1130 °C (O'Neill, 1987). Therefore, according to the thermodynamic analysis, the conventional operating temperature for the ammonia oxidation reaction falls within the temperature range where the formation of the cobalt silicate species is favourable.

$$2CoO + SiO_2 \rightarrow Co_2SiO_4 \qquad \Delta H^{rxn}_{25°C} = -27.8 \text{ kJ/mol}$$

The reaction has been observed for the Fischer-Tropsch reaction where the formation of cobalt-silicate is induced by the formation of water (van de Loosdrecht et al., 2007). This form of deactivation would be investigated and should be avoided. The operating conditions must be selected such that the phase transition is inhibited.

2.6 Industrial catalyst

Ammonia oxidation requires the use of a solid catalyst. Industrially solid catalysts are predominantly applied in the form of pellets with the exception of the Pt-based catalyst which is in a form of wire gauzes. The Co_3O_4 catalyst would be manufactured as pellets for the ammonia oxidation reaction. The physical characteristics of major importance are as follows (Perry and Green, 1997):

- Pellet size – affects pressure drop across the reactor and minimum pellet size for specific reactors (2-5 mm for fixed-beds)
- Specific surface of solid sphere – affects the rate of reaction (rate of reaction proportional to accessible surface)
- Pore diameter and distribution – accessibility to the internal surface and thus influencing the rate of diffusion
- Diffusivity and tortuosity – affect the resistance to diffusion and thus the type of diffusion mechanism

The size and type of pellet affects the mass and heat transfer through the pellet. Increase in particle size will result in both mass and heat transfer limitations. This will hinder the diffusion of ammonia to the active sites in the catalyst pore, resulting in a low rate of reaction in the particle simultaneously with higher temperatures in the pellet relative to the bulk phase (Levenspiel, 1999).

2.6.1 External and internal mass and heat transfer

A thin boundary layer exists around a catalyst particle acting in a fluid flowing reaction causing external transport limitations. Reactants have to be transported from the bulk of the fluid to the outer surface of the catalyst particle through this boundary layer. Similarly, the product compounds have to be transported from the outer surface of the catalyst, through the boundary layer to the bulk of the fluid. Heat will be transported through this boundary layer as well (Levenspiel, 1999). At steady-state, the rate of transport through the boundary layer equals the observed rate of consumption of the reactant and is governed by the mass transfer coefficient of the reactants (k_L). The mass transport coefficient is dependent on the temperature, $k_L \propto T^{0.5\text{-}2.25}$, but depends on the flow regime and type of diffusion (van Steen, 2010).

The heat transfer through the boundary layer is dependent on the heat transfer coefficient (h) and modelled in a similar manner to the external mass transport using the Chilton-Colburn analogy. At steady state, the rate of heat transfer through the boundary layer equals the heat generated by the chemical reaction in the catalyst particle. The temperature gradient over the boundary layer and the concentration difference are linked and thus the elimination of external mass transport limitations would result in the elimination of external heat transfer limitations (Levenspiel, 1999; van Steen, 2010).

$$T_{bulk\ fluid} - T_s = \frac{k_L\,(\Delta H^{rxn})}{h} \cdot (C_{A,bulk} - C_{A,s})$$

(Where $T_{bulk\ fluid}$ is the temperature (K) of the bulk fluid, T_s is the temperature (K) at the surface, k_L the mass transfer coefficient (m/s), ΔH^{rxn} is the heat of reaction (J/mol), h is the heat transfer coefficient ($W/m^2.K$), $C_{A,bulk}$ and $C_{A,S}$ is the concentration (mol/m^3) of reactant in the bulk fluid and at the surface respectively)

Therefore, experiments at which the linear velocity of the bulk fluid is changed but keeping the space time constant, would verify whether external mass transfer limitations are present by measuring the conversion/activity as a function of the linear velocity. If the conversion is independent of the linear velocity, the external mass and heat transfer limitations can be neglected.

Internal mass and heat transfer limitation would result in an observed rate of reaction, which differs from the intrinsic rate of reaction at the measured temperature and concentration on the outside of the catalyst pellet. The difference in the rate of reaction can be taken into account by defining an effectiveness factor (η).

$$\eta = \frac{r_{observed}}{r_{intrinsic}}$$

The oxidation of ammonia over Co_3O_4/SiO_2 catalyst is exothermic and expected to be non-isothermal; as a result the reaction rate inside the pellet may be greater than the rate of reaction at the outer surface or in the bulk phase. Therefore, effectiveness factor greater than 1 may be expected (Levenspiel, 1999).

A fundamental relationship exists between the temperature profile in the catalyst particle and the concentration profile. The relationship is independent on the rate

expression describing the kinetics of the reaction but dependent on the thermal conductivity of the material, effective diffusivity and heat of reaction (Levenspiel, 1999):

$$T - T_S = \frac{D_{eff.}(-\Delta H^{rxn})}{\kappa} . (C_{A,S} - C_A)$$

(Where T and T_s is the temperature (K) within the catalyst and at the surface, κ the thermal conductivity constant (W/m.K), ΔH^{rxn} is the heat of reaction (J/mol), D_{eff} is the effective diffusivity (m^2/s), C_A and $C_{A,S}$ is the concentration (mol/m^3) of reactant at the surface)

In most commercial catalysts, the surface area is characterised by the internal diffusion that is exposed by the pores. Diffusion to the surface and in the pores of the catalyst can be controlled by molecular diffusion, Knudsen diffusion or configurational diffusion (Levenspiel, 1999).

A catalyst should be evaluated for its intrinsic kinetic properties and thus mass and heat transfer limitation must be avoided.

Internal mass transfer limitations are governed by the Thiele modulus (Φ). At a given set of reaction conditions and assuming a pseudo first order reaction, the only parameter that can be varied is the radius of the catalyst particles.

$$\Phi = R_{particle} \cdot \sqrt{\frac{-r_{intrinsic} \cdot \rho}{D_{eff} \cdot C_{A,S}}}$$

(Where Φ is the Thiele modulus, R is the radius (m), r is the rate of reaction per unit mass of catalyst (mol/s.g), ρ is the catalyst density (g/m^3), D_{eff} is the effective diffusivity (m^2/s) and $C_{A,S}$ is the concentration (mol/m^3) of reactant at the external surface)

In the absence of mass and heat transfer, the observed rate of reaction is independent of the catalyst particle. Thus a series of experiments, in which catalyst particle size is varied and all other conditions are kept constant would illustrate the effect of particle size on the effectiveness factor and indicates which particle size should be utilised to avoid mass and heat transfer limitations (van Steen, 2010).

3 SCOPE OF THE STUDY

The objective of this research is to synthesise a silica supported cobalt Co_3O_4 catalyst and evaluate the catalyst performance in terms of activity and selectivity as a function of reaction temperature, by testing it in a fixed-bed reactor for ammonia oxidation. Ammonia oxidation will be carried out at atmospheric pressure (1-2 atm) and elevated temperatures (450-800 °C). The catalyst would also be evaluated based on its selectivity towards the desired NO and NO_2 products. A comparison between the synthesised catalyst and the commercially obtained Co_3O_4 catalyst would be carried out. The selectivity of the catalyst towards NO, N_2O, NO_2, N_2O_4 and N_2 will be evaluated at both low and high conversions.

Once the catalyst preparation and reaction is established, an investigation into the mass and heat transfer effects can be carried out. This is done by testing the catalyst with varying particle sizes and evaluating the performance of the catalyst. In addition, catalyst deactivation under industrially relevant conditions would be studied to conclude whether the supported cobalt catalyst is feasible for industrial use.

3.1 Hypothesis

Supported Co_3O_4/SiO_2 catalyst with small Co_3O_4 crystallites will be an effective catalyst for ammonia oxidation to NO_x if catalyst deactivation along with mass and heat transfer limitations can be avoided.

3.2 Key questions

- What catalyst (size, phase, loading) has been obtained using the incipient wetness impregnation preparation technique?
- Which cobalt phase (Co_3O_4 or CoO) was obtained using the incipient wetness impregnation method?
- Can ammonia oxidation be carried out successfully using a cobalt based catalyst at atmospheric pressure as shown in the literature?
- How has the catalyst changed after being exposed to reaction conditions (450-800 °C)?
- Does the catalyst reduce from Co_3O_4 to CoO under reaction conditions?
- What is the rate of reaction achieved using the supported Co_3O_4/SiO_2 catalyst?
- What is the selectivity of NO and NO_2 in the ammonia oxidation over a cobalt-based catalyst?
- How does the product selectivity differ between lower and higher conversion ranges?
- What are the effects of mass and heat transfer limitations?

4 EXPERIMENTAL METHODOLOGY

4.1 Catalyst preparation

Uniform catalyst pellets were prepared by the incipient wetness technique (Zhuang, 2009). Cylindrical-shaped silica pellets (Degussa†, Aerolyst 3038, d_{pellet}: 2.5 mm, l_{pellet}: 4.5 mm, S_{BET}: 270 m^2/g, d_{pore}: 12 nm) were used as catalyst support. Approximately 2 g of the silica was used for each preparation, (a Mettler AE 200 balance was used to carry out all weighing measurements with a standard deviation of 0.1 mg). The impregnation solution was made by dissolving approximately 0.97 g of $Co(NO_3)_2 \cdot 6H_2O$ (Aldrich, 98%) in 1.8 mL de-ionized water. The catalyst precursor was aged at room temperature for 20 minutes followed by drying in a ventilated oven at 120 °C for 2 hours. Subsequently, the dried precursor was calcined in air using a flow rate of 180 mL(STP)/min in a reactor at 350 °C for 2 hours (heating rate: ~5 °C/min).

A uniform catalyst with a high cobalt loading was prepared by repeating the incipient wetness impregnation a number of times on the calcined catalyst pellet. This precursor was then aged at room temperature for 20 minutes followed by drying in a ventilated oven at 120 °C for 2 hours. Subsequently, the dried precursor was calcined in air using a flow rate of 180 mL(STP)/min in a fluidized bed reactor at 350 °C for 2 hours (heating rate: ~5 °C/min).

Uniform catalyst of the different particles sizes was obtained by crushing the calcined uniform catalyst pellets to obtain a 100% passing through of a sieve of its required size range.

† 'Degussa' is now renamed to 'Evonik'

4.2 Catalyst characterisation

4.2.1 Atomic absorption spectroscopy (AAS)

The cobalt loading of the catalysts was determined using AAS. The catalyst (100 mg) was digested in a mixture of 8 mL 30 wt.-% hydrochloric acid and 2 mL 40 wt.-% hydrofluoric acid. This mixture was brought to the boil in a 250 mL Erlenmeyer flask. Once boiling, 10 mL 60 wt.-% nitric acid was added and the resulting solution was reduced to approximately 2 mL in volume. 5 mL of concentrated perchloric acid was added and the resulting solution was reduced again to 2 mL. The sample was quantitatively transferred to a 100 mL volumetric flask and made up to a volume of 100 mL with distilled water. The liquid sample was then filtered and the filtrate was analysed for its cobalt content. A Varian SpectrAA-30 spectrometer attached to a DS-15 station was used to determine the concentrations of cobalt on the catalysts.

4.2.2 Mercury porosimetry

The pore sizes of the silica support were determined using mercury porosimetry. Mercury is a non-wetting fluid at room temperature for most porous materials and can be forced into the pores by applying pressure. Mercury can thus be applied to determine the pore size for a given catalyst knowing the surface tension of mercury (0.485 N/m) and contact angle of 130°.

A Micromeritics AutoPore II 9220 was used to carry out mercury porosimetry using the following settings:

- Sample weight — ca. 0.7 g
- Evacuation time — 5 min
- Maximum head pressure — 4.45 psia
- Maximum intrusion volume — 0.1 mL/g

4.2.3 Brunauer-Emmett-Teller method (BET)

The specific surface area of the commercial catalysts was determined via N_2 adsorption/desorption according to the BET method using a Micromeritics TriStar 3000 analyser.

4.2.4 Transmission electron microscopy (TEM)

The morphology of the cobalt crystallites in the calcined supported catalyst samples was determined using a LEO TEM 912 with an acceleration voltage of 120 kV and a tungsten wire filament. The supported catalysts were finely crushed and subsequently suspended in 5 mL of methanol in 30 mL sample bottles using a blunt, smooth glass rod. The fine particles, dispersed in the methanol, were pipetted out and placed on activated carbon-coated, copper grids. This was then placed on filter paper and allowed to dry. Thereafter the samples were viewed under the Transmission Electron Microscope at different magnifications. Images were taken with a Proscan slow scan charge-couple device (CCD) digital camera, which can be used to establish the crystal size and distribution of cobalt in the catalyst.

The digital images of each catalyst sample were taken and analyzed by using a software package "Image J". On average, approximately 100 particles were manually and randomly measured to determine the average particle size and size distribution of the catalyst.

4.2.5 Scanning electron microscope (SEM)

The morphology of the industrial catalyst was determined using SEM. A scanning electron microscope (Nova NanoSEM 230) equipped with a Four Quadrant Back Scatter Detector and an energy dispersive Fissons Kevex X-ray spectrometer (EDXA) operating at 10 keV. Sample preparation involved sprinkling the sample on an aluminium stub coated with glue containing graphite. Here, graphite is used to conduct electrons, thereby preventing charge build up. The samples are then coated with carbon which does not interfere with the elemental analysis. Images were taken of this sample and analysed using software package "Image J".

4.2.6 X-ray diffraction (XRD)

X-ray diffraction data was used to identify the phases present in the catalyst and to calculate the mean particle diameter of cobalt crystallites in the catalysts. Phase identification would be carried out by comparing the catalyst XRD patterns with known reference XRD patterns containing elements/compounds suspected to be present in the catalysts.

In the case of the cobalt catalyst, the desired cobalt phase would be the Co_3O_4 phase, and thus it is desired to see only the Co_3O_4 phase in the XRD spectrum.

A Bruker D8 advanced XRD was used to obtain X-ray diffraction spectre for the different catalyst. The operational settings on the diffractometer were:

- Voltage 35 kV
- Current 40 mA
- 2θ range 15-78°
- 2θ step size 0.006 seconds
- Step duration 0.5 seconds
- X-ray source 1.78897 Å (Co Kα1)

Once the correct phase of Co_3O_4 is obtained, the Topas software associated with the XRD spectrum was used to calculate the mean particle diameter. The measurement with the XRD instrument was determined with Rietveld refinement of the parameters using the "Topas" software such that the agreement factors are within the acceptable limit, i.e. weighted profile factor (RWP) < 10 and the Bragg factor (R-bragg) < 5.

4.3 Ammonia oxidation test

4.3.1 Fixed-bed reactor set-up

The ammonia oxidation test was performed using a micro scale experimental rig with a fixed-bed reactor set-up (see Figure 4.2). The ammonia content was selected based on the flammability hazard and physical properties of ammonia. Mixtures of air and ammonia vapour of 15-28 vol.-% will ignite when sparked or exposed to temperatures exceeding 651 °C. As the operating temperature would exceed 651 °C, low ammonia content of approximately 7 vol.-% was selected. Helium would be used as the balance gas as oppose to N_2 because N_2 is expected to form in small concentrations. Excess oxygen is used to represent industrial relevant conditions and for complete conversion of NH_3.

Gas mixture (Air Liquide) containing ammonia (7 vol.-%), oxygen (19.4 vol.-%) with the balance helium was fed into the reactor at ambient pressure. Quantitative analysis of the reaction data was calculated based on the known amounts determined according to the by-pass runs and blank samples. The conversion of ammonia was determined based on the feed of ammonia which was spectrometrically determined to be 7.1 ± 0.06% ammonia and not the value quoted by the supplier (Air Liquide of 7.4%).

The gas cylinder is fitted with a pressure regulator to regulate and maintain the pressure of the cylinder and the pressure of the downstream process. The gas flows from the cylinder and passes through a 50 micron filter which traps any solid material that might be carried out of the gas cylinder and may interfere with the reaction or cause blockages within the pipelines.

The mass flow of the stream was controlled using a Brooks Instrument mass flow controller. The mass flow controller for the ammonia gas mixture was re-calibrated with the feed gas and a maximum flow rate of 564 mL(NTP)/min could be achieved (see Appendix A.2.1).

The ammonia oxidation reaction is a high temperature reaction, thus the water produced within the reaction would condense when it leaves the high temperature zone. The water knock-out cylinder which follows the reactor is essential to avoid water accumulation within the pipelines causing blockages. As ammonia will dissolve in liquid water the water knock-out cylinder was at room temperature and designed such that only the liquid water would condense out and not absorb any ammonia gas with minimal contact between the two components. The condensed liquid water was removed after each run to maintain a low level within the knock-out cylinder.

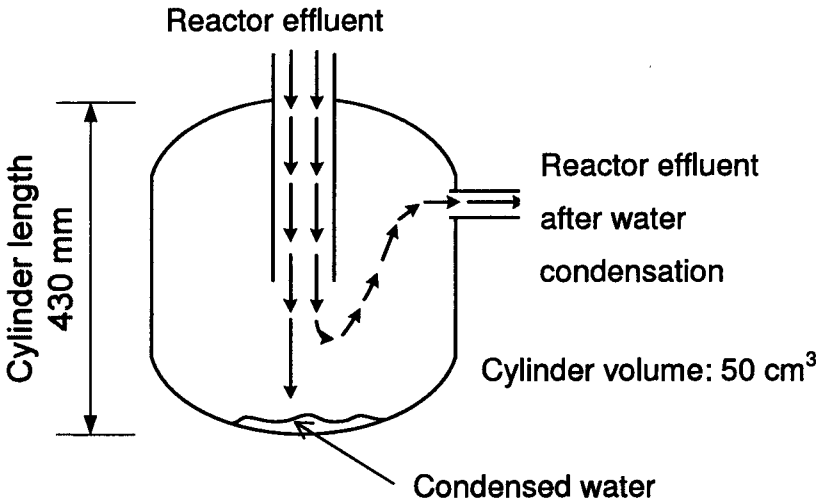

Figure 4.1: Schematic representation of the water knock-out cylinder design with indications of the flow direction

Depending on the aim of the experiment, the valves are manipulated to perform the desired experiment. The gas passes either through the gas washing flasks or through the ampoule breaker where ampoule samples can be taken. A series of gas washing flasks are used to ensure that all the ammonia is trapped within the liquid for further analysis of the catalyst.

A bubble meter which follows the gas washing flasks and ampoule breaker is in place to measure and verify the volumetric flow through the system. Eventually the gas is passed through a large flask filled with an acidic medium to ensure that all the hazardous gases (NO_x) are trapped before the gas is vented.

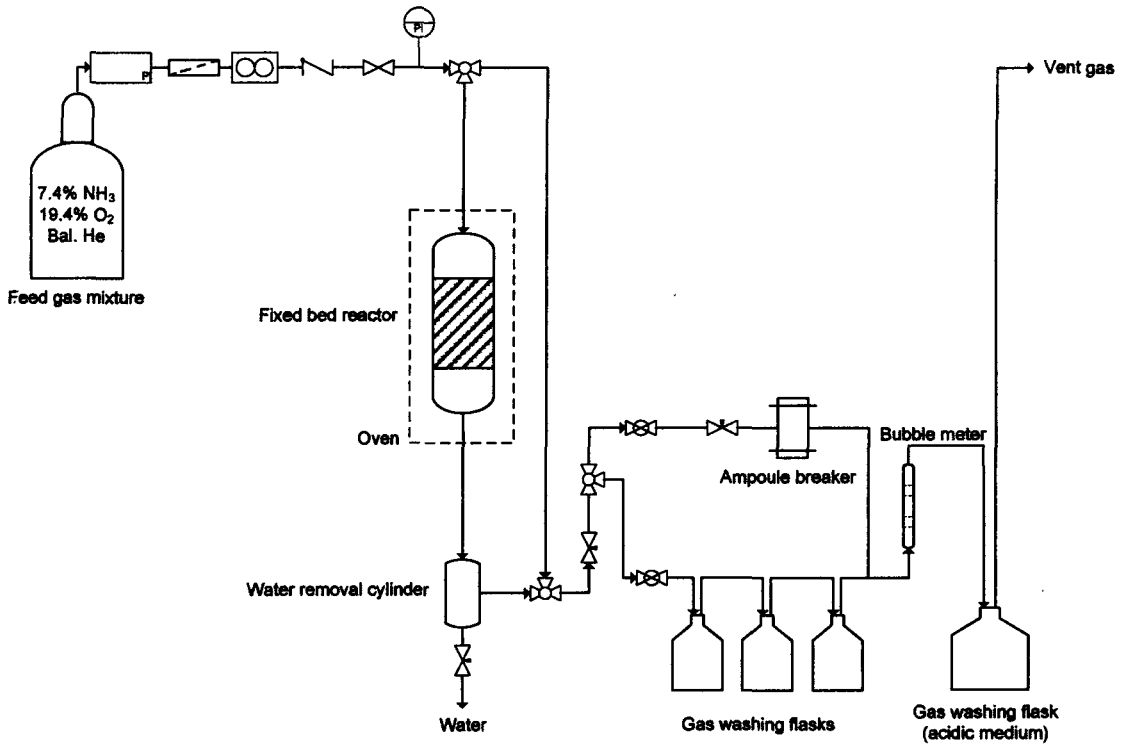

Figure 4.2: Flow diagram of fixed-bed reactor set-up for ammonia oxidation test unit

The fixed-bed reactor consisted of a quartz tube with an outer diameter (Ø) of 12 mm and an internal diameter of 9 mm, which was heated electrically by using an electrical heating element. The exterior temperature of the reactor is monitored by a Gefran 600 temperature control system. The temperature of the oven is controlled according to the set temperature while the temperature within the reactor is measured by inserting a thermocouple through a thermowell within the reactor. The temperature ramp is adjusted by the continuous auto-tuning parameter associated with the Gefran controller; this continuously reads the system oscillations and immediately seeks the control parameter values that reduce the current oscillation. The isothermal temperature zone was determined by setting the temperature exterior temperature and measuring the internal temperature across the entire length of the reactor at a temperature of 440, 645 and 875 °C respectively. A measurement was taken every 10 mm and the isothermal zone was determined where the temperature fluctuates by ± 5 °C from the set temperature. The fixed-bed set-up was determined to have an isothermal zone of 40 mm. The centre of the isothermal zone was used as the catalyst bed. The catalyst bed consisted of 20 mm and the reaction temperature was measured in the centre of the catalyst bed.

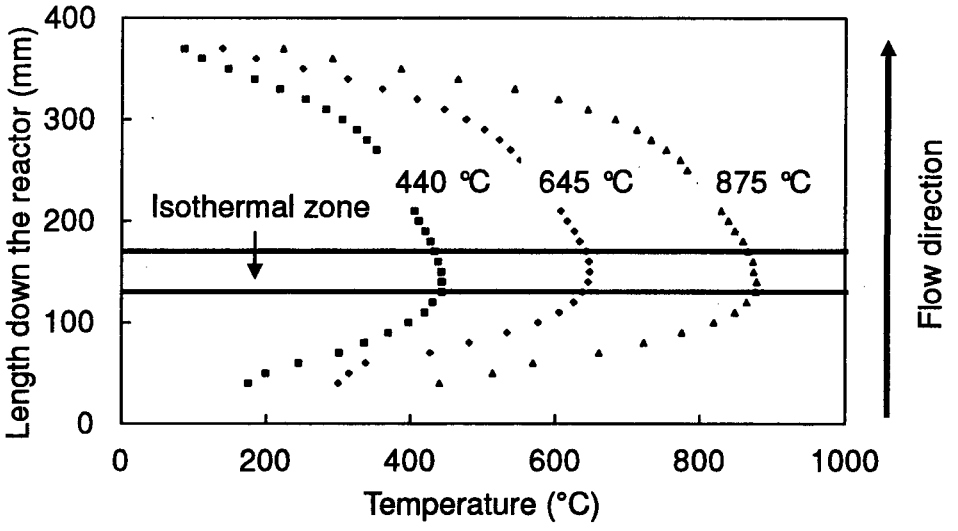

Figure 4.3: Temperature measurement across the length of the reactor at 10 mm spaces, with an interior temperature of 440, 645 and 875 °C

Catalyst was loaded into the centre of the isothermal zone. The mass of catalyst used was weighed out using a Mettler AE 200 balance which a standard deviation of 0.1 mg is associated with each measurement. Cylindrical-shaped silica pellets (Degussa†, Aerolyst 3038) were crushed to a powder (d_p < 75 microns) and approximately 300 mg of the SiO_2 was mixed with the cobalt catalyst to fill up the isothermal zone to ensure sufficient interaction between the feed gas and the catalyst. Silicon carbide (d_p: 425–600 microns) was added above the isothermal zone to serve as a pre-heating zone to minimise the temperature gradient before the reaction with the catalyst. Silicon carbide along with a plug of glass wool was also added below the catalyst bed to ensure the bed was kept in place. No pre-treatment of the catalyst is required as the active phase of a cobalt catalyst for ammonia oxidation is in the cobalt oxide phase. A schematic representation can be seen as follows.

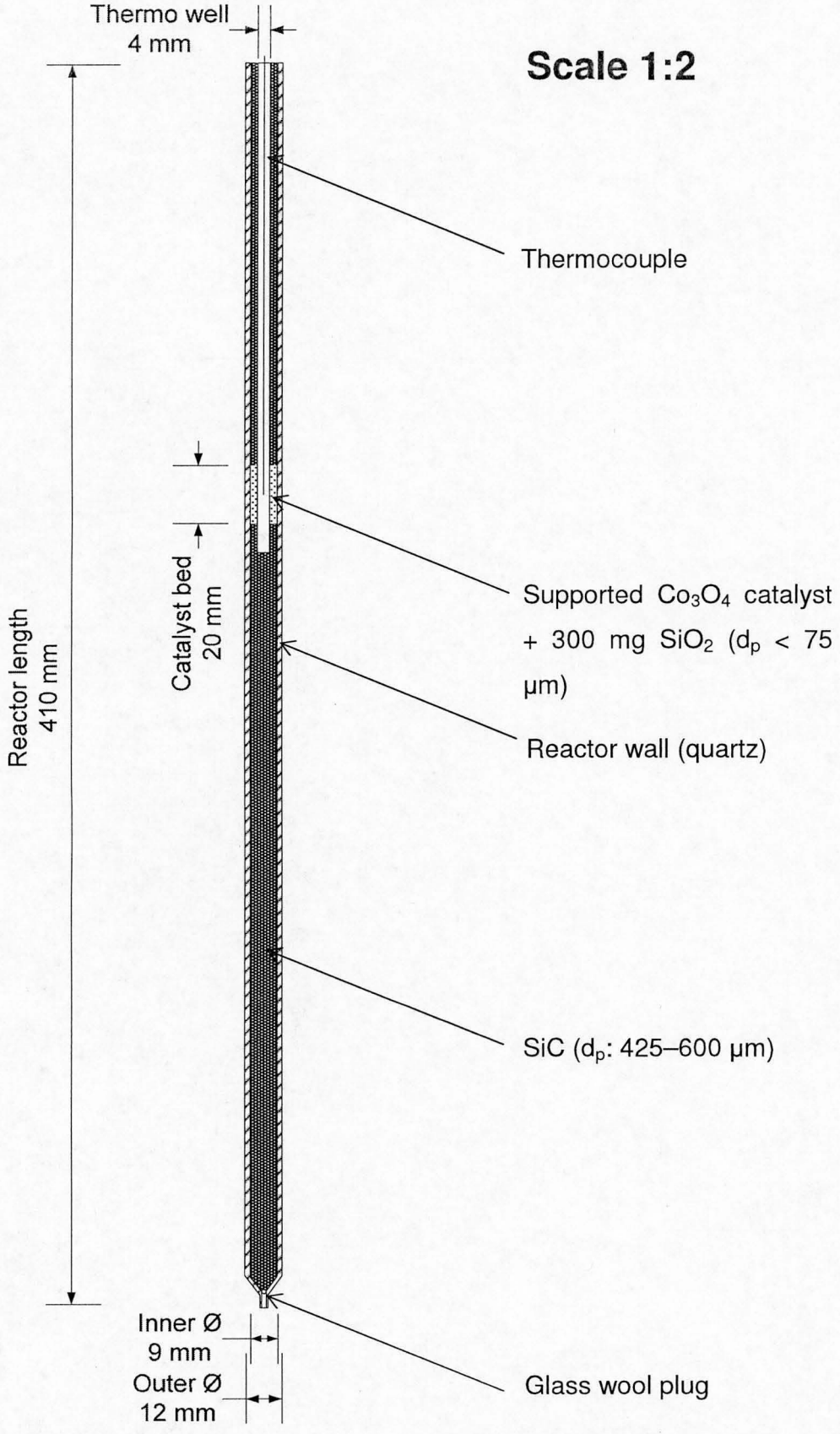

Figure 4.4: Schematic representation of the packing within the fixed-bed reactor

4.3.2 Determination of ammonia content in effluent

The composition of the ammonia content in the gas stream was determined by leading the gas mixture over the reactor or by-pass stream, through a 3-way valve to a series of 3 gas washing flasks, which ensures that the ammonia is absorbed in the liquid. The ammonia content could be determined by either a titration method or using the Nessler method for a spectrophotometric analysis. Complete absorption of ammonia was achieved within the first flask as no ammonia was detected in the second and third flasks.

The titration method can only be used to determine the ammonia content of the pure feed stream since the products of the reaction; i.e. NO and NO_2; would dissolve in an acidic medium, which would affect results during the titration of the acid with an alkali. Therefore the Nessler method is favoured, where the ammonia is trapped in deionised water and subsequently the Nessler reagent ($K_2[HgI_4]$) is added to the water and ammonia solution. The liberated ammonia rapidly reacts with the reagent to form an orange-brown product, which remains in colloidal solution, and thus the intensity of the colour directly corresponds to the concentration of ammonia in solution (Vogel, 1961).

The Nessler reagent (Merck 109028, 1.16 g/cm^3) utilised would determine the concentration of ammonia ranging from 0-10 mg/l. The colours are most distinct at these low concentrations and at higher concentrations (>10 mg/l), the solution maintains a dark orange colour which does not vary with increasing ammonia content.

The effluent was passed through deionised water for a 20-30 minutes time interval. Depending on the flow rate and activity of catalyst, the ammonia absorbed by the water would exceed that of 10 mg/l; hence the solution would be diluted using volumetric flasks to obtain a concentration that could be analysed.

10 mL of the diluted sample would be transferred into a glass sample holder using a volumetric pipette. A colourimetric ammonia test kit (Merck 111117), with a colour card and sliding comparator, would be used to determine the approximate ammonia concentration. This method is not accurate and thus should not be used to determine

the true ammonia concentration. However it was used to verify that the concentration level is within the measurable limits (0-10 mg/l) before spectrophotometric analysis.

The determination of ammonia was determined by carrying out a procedure known as ultraviolet-visible spectroscopy.

Ultraviolet-visible (UV/Vis) spectroscopy

The concentration of the absorbing species in solution was obtained applying the Beer-Lambert law to the spectrometer measurement. A Jenway 6405 UV/Vis. spectrometer was used to carry out ultraviolet-visible spectroscopy (see Appendix A.2.2).

$$A = log_{10}\left(\frac{I_0}{I}\right) = \epsilon \times c \times l$$

(Where A is absorbance based on transmittance, I is the pathlength through the sample, c the concentration of the absorbing species and ε is a constant known as molar absorptivity or extinction coefficient)

A small volume of the ammonium salt solution was transferred to the cuvette which was placed within the spectrometer. It was determined that the intensity of the colour stays constant after the addition of 7 drops of Nessler's reagent to a 10 mL sample . Therefore solutions which contain 10 mL of the diluted sample and 7 drops of Nessler's reagent were taken for spectroscopy analysis (see Appendix A.2.2, Figure A.2). This process was repeated to obtain 2 sample bottles for error analysis.

To calibrate the spectrometer, ammonium nitrate (Kimix, 97%) solutions at different concentrations (0-10 mg/l) were prepared by weighing the appropriate mass and dissolving it in water before adding Nessler's reagent. Different colours would result in different light transmissions at various wavelengths. Therefore the relationship between the transmission and concentration is not necessarily linear at every wavelength. The prepared ammonium nitrate solutions were used to calibrate the spectrometer at different concentrations and wavelengths.

As seen in Table 4.1 and Figure 4.5, the measurement at 450 nm yielded the most linear relationship with respect to transmission and concentration. Once the concentration is known, the total amount of NH_3 trapped in the water solution can be determined and the conversion can be deduced based on the amount of unreacted NH_3.

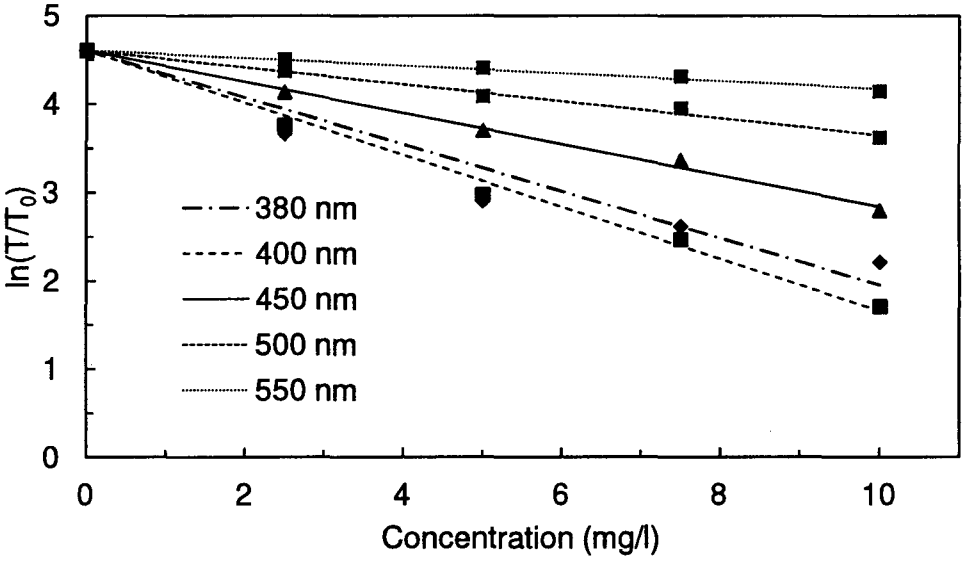

Figure 4.5: Linear relationship between transmission and concentration and various wavelengths

Table 4.1: Relationship between transmission and concentration fitted with a linear equation

Wavelength (nm)	Linear equation	R^2 value
380	y = -0.265x + 4.6	0.921
400	y = -0.295x + 4.6	0.991
450	y = -0.177x + 4.6	0.995
500	y = -0.096x + 4.6	0.988
550	y = -0.043x + 4.6	0.983

All further analysis would be carried out at 450 nm. Two measurements per sample bottle were taken for error analysis.

4.3.3 Ammonia oxidation in the Autochem 2910

Ammonia oxidation was carried out in a different set-up in order to determine the products of the ammonia oxidation reaction using the cobalt based catalysts. In this set-up, a mass spectrometer was connected directly to the reactor effluent stream. Catalyst was loaded into the U-tube quartz reactor within the Micromeritics Autochem 2910. Quartz wool was added above and below the catalyst bed. Approximately 300 mg of SiO_2 (d_p < 75 µm) was added with the catalyst to duplicate the catalyst bed in the experimental rig. A feed gas with a composition of 7.1 vol.-% ammonia, 19.4 vol.-% oxygen and the balance helium was fed at a flow rate of 100 mL(NTP)/min over the catalyst bed. The temperature was ramped up to 850 °C using a linear temperature ramp of 10 °C/min. Samples of the effluent gas were taken by insertion of a stainless steel capillary leading to the mass spectrometer, which was heated and maintained at 120 °C to prevent condensation and blockages to the mass spectrometer.

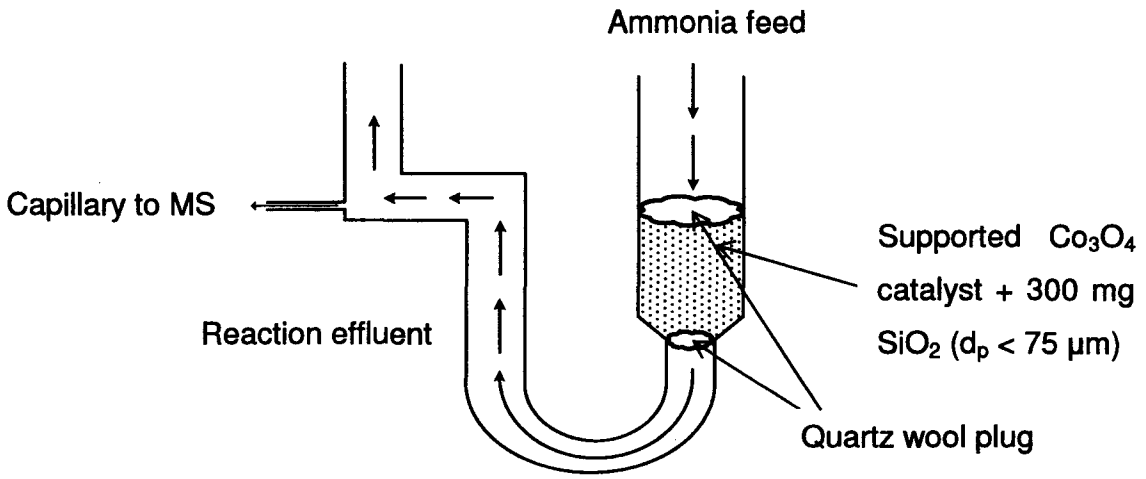

Figure 4.6: Setup of U-tube quartz reactor in Micromeritics Autochem 2910 leading straight to the Pfeiffer Vacuum QMS 200

A Pfeiffer Vacuum Quadrupole Mass Spectrometer 200 (QMS 200) was directly connected to a Micromeritics Autochem 2910. Quadstar 32-bit software was used for control and data acquisition of the QMS 200.

The operational settings on the mass spectrometer were:

- Detector type — Faraday
- Width — 10 a.u.
- Speed — 1 second
- Resolution — 50 (dimensionless)
- RF-Polarity — Normal
- IonRef — 150 V
- Cathode — 60 V
- Admissible max. pressure — 2×10^{-4} mbar

During the initial runs, the mass spectrometer was set to observe every molecular mass ranging from 4 to 100 g/gmol. After the initial runs, the peaks at the relative masses were identified and the mass spectrometer was adjusted to only monitoring the possible molecular masses.

The feed gas and a separate calibration gas containing 1.3% NO, 1.43% N_2O, 1.42% NO_2 and the balance N_2 was used to calibrate the intensities of the mass spectroscopy signals (see Appendix A.2.3).

5 RESULTS

5.1 Catalyst characterisation

5.1.1 Cobalt loading

The cobalt loading of the catalysts was obtained from AAS. The samples were dissolved by acid digestion. Complete dissolution was attained as no solid residue was found after the dissolved samples were filtered with filter paper.

The expected cobalt loading of the in-house catalyst synthesised using the incipient wetness impregnation technique can be calculated from the amount of impregnation solution used per mass of silica and the concentration of the cobalt in the impregnation solution. The Co_3O_4 loading was recalculated from Co-loading.

The expected loading of the catalyst was 9.1 wt.-%. According to AAS, the cobalt loading achieved after a single impregnation was 9.11 wt.-%. Similarly, the correct loading of 17.0 wt.-% and 23.1 wt.-% was achieved using double and triple impregnation respectively. This indicated that the preparation technique could be used to accurately control the cobalt loading on the catalyst.

The commercial catalyst has a Co-loading of 76.69 wt.-% corresponding to pure Co_3O_4 and is thus unsupported containing only Co_3O_4.

Table 5.1: Cobalt metal content of structured catalyst determined from AAS

Catalyst code	Technique	Co-content (wt.-%)	Co_3O_4-loading (wt.-%)
U1	Single impregnation	9.11	12.41
U2	Double impregnation	17.00	23.15
U3	Triple impregnation	23.11	31.48
J1	Commercial catalyst	76.69	100

5.1.2 Phase analysis in the catalysts

XRD analyses were carried out with the purpose of identifying the phases present in the catalyst to determine the average crystallite sizes of the various phases within the catalyst. The XRD analyses were carried out at the diffraction angle (2θ) between 20 – 80 degrees as this is the range where the Co_3O_4 peaks are most prominent.

XRD analysis of the support, SiO_2, was first carried out to achieve an indication of how the pattern would appear without any cobalt present.

Figure 5.1 represents the pure silica support spectrum plotted with the SiO_2 reference spectrum (PDF 00-051-1377). Using the "Topas" refinement software, the silica loading was determined to be 100 wt.-%, indicating that no other phases are present within the support. The sample displayed a wide peak ranging from 15-40 °. This was taken into account when analysing the catalyst samples.

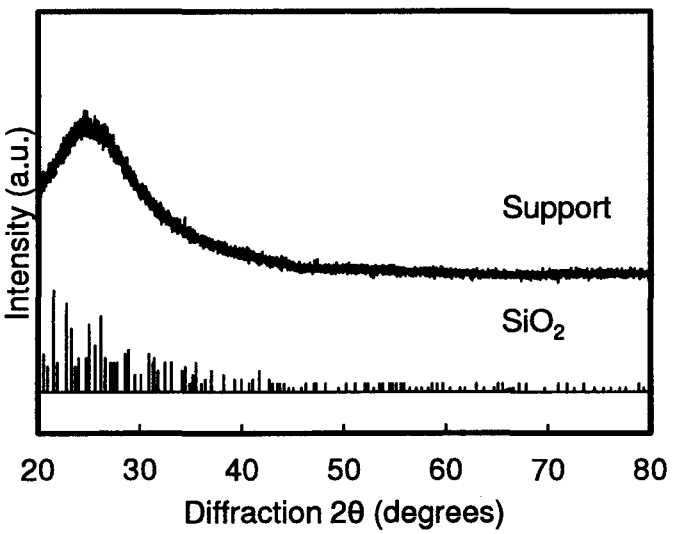

Figure 5.1: XRD diffraction pattern of the SiO_2 support (Degussa†, Aerolyst 3038) with the reference spectrum for SiO_2 (PDF 00-051-1377)

The XRD patterns of the prepared silica supported catalyst are given in Figure 5.2. As expected, the results of the XRD analyses revealed that a similar pattern was seen for single, double and triple impregnated catalyst.

The XRD pattern of the structure catalysts (U1, U2 and U3) illustrates that the characteristic peaks match the Co_3O_4 (PDF-00-043-1003) reference spectrum. All the peaks were accounted for indicating that no other metal/cobalt phase is present within the catalyst. As shown in the diffraction pattern, the higher cobalt loading resulted in diffraction peaks with a greater intensity.

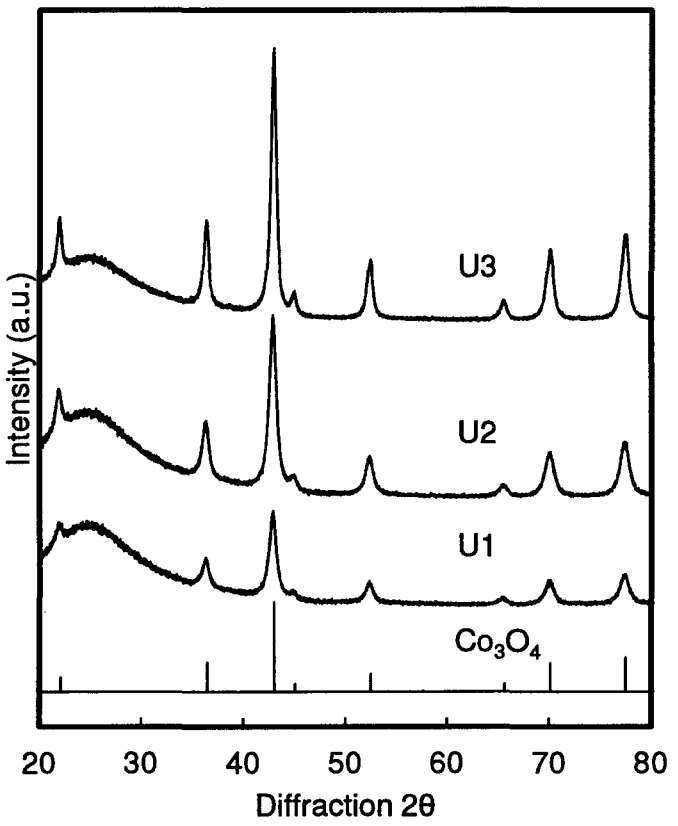

Figure 5.2: XRD diffraction pattern of the synthesised catalyst U1, U2 and U3 superimposed with the reference spectrum for Co_3O_4 (PDF 00-043-1003)

The commercial catalyst was analysed separately and revealed very narrow and sharp peaks. It was determined that the catalyst was unsupported containing a pure Co_3O_4 phase. This result agrees with that obtained using AAS.

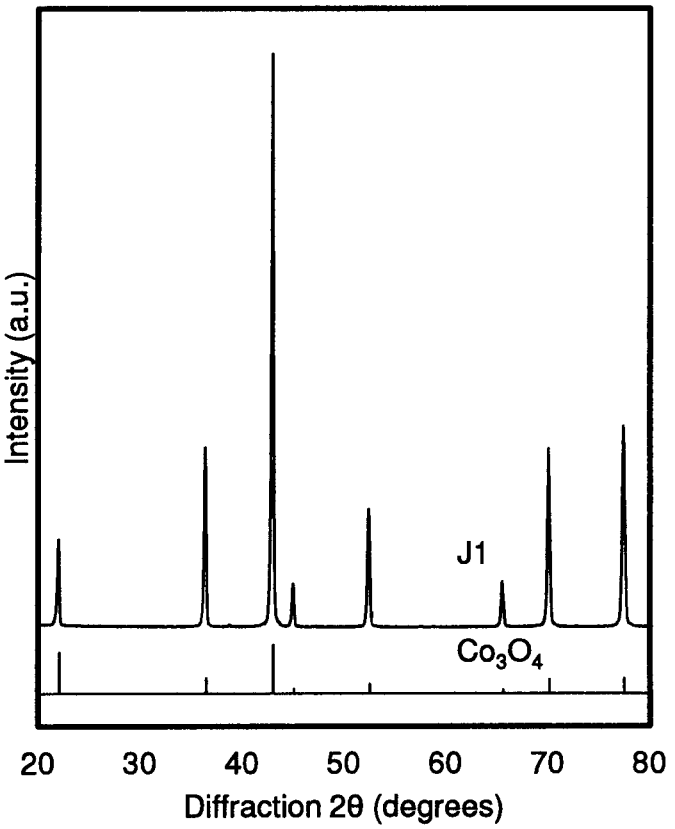

Figure 5.3: XRD diffraction pattern of the commercial catalyst J1 superimposed with the reference spectrum for Co_3O_4 (PDF 00-043-1003)

5.1.3 Cobalt oxide crystallite size determination

The average cobalt crystallite size of the synthesised catalyst was determined using XRD and TEM. SEM was used to analyse the average cobalt crystallite size of the commercial catalyst, as it was observed that the XRD peaks for the commercial catalyst were very narrow with a high intensity. Narrow peaks with a high intensity are subject to error as it becomes difficult to analyse the width of each peak to determine a correct size and the resulting larger sizes could be close the maximum size that can be analysed using the spectrum determined by the XRD instrument. Therefore it was suspected that the large sizes determined for the commercial catalyst could contain errors. The objective was to see if the different techniques agree with each other.

XRD analysis indicates that the crystallite size above 20 nm is obtained using the incipient wetness impregnation technique. The synthesised catalyst showed a slight increase in cobalt crystallite size with the increase in cobalt loading.

The commercial catalyst contained an average cobalt crystallite size of 302.8 nm which is on the verge of the detection limit of the XRD instrument and is to be confirmed using SEM and BET surface area determination.

Table 5.2: Average crystallite size determined using XRD analyses for the respective catalysts

Catalyst code	Technique	Crystallite size (nm)
U1	Single impregnation	21.4
U2	Double impregnation	22.0
U3	Triple impregnation	25.5
J1	Commercial catalyst	302

The synthesised catalyst was further characterised with a transmission electron microscope. The aim was to obtain an average crystallite size and size distribution using the images of the catalyst under the microscope and compare the result to that obtained using XRD analysis.

The TEM images reveal that the Co_3O_4 crystallites are found in clusters with a size range of 60-80 nm. The formation of clusters is common using the incipient wetness impregnation technique (Feller et al., 1999).

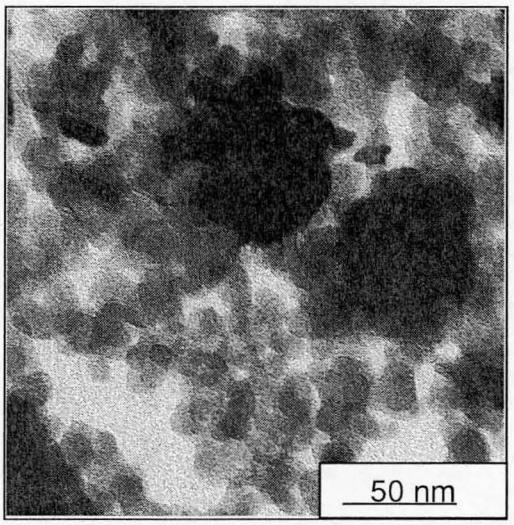

Figure 5.4: An example of TEM image illustrating cobalt clusters within the catalyst

The average crystallite size of the U3 catalyst was determined, using the TEM images, to be 24.4 nm with a standard deviation of 4.5 nm. The high standard deviation could be a result of small clusters being included while measuring the cobalt particles. A cumulative plot which indicates the frequency of the crystallites occurring below a certain size shows that the size distribution is not uniform as a uniform distribution would result in a smooth cumulative plot.

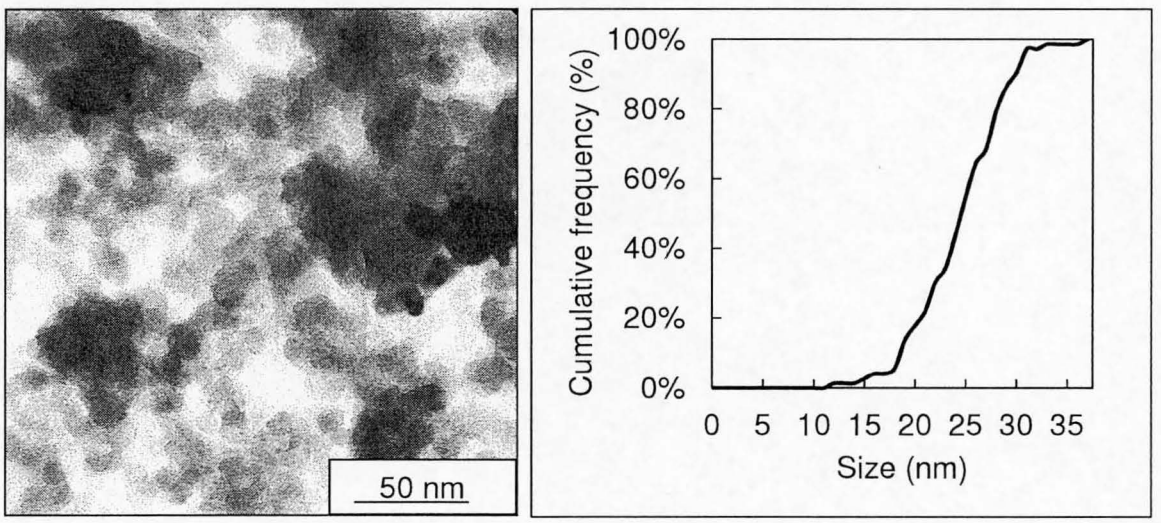

Figure 5.5: TEM image and cumulative frequency of the crystallite sizes of U3 - triple impregnated supported Co_3O_4 catalyst

SEM was used to determine the size of the commercial catalyst as the XRD results indicate that the cobalt crystallites were large. A SEM would further provide a digital image of the catalyst and how the crystallites interact with each other.

The SEM images revealed that the cobalt crystallites are tightly packed into a cluster and the sizes of the individual crystallites are not uniform. The sizes range from 200 to 5000 nm (5 µm). The SEM image displays a region with random sizes of crystallites with the smaller crystallites (~200 nm) attached onto the surface of the larger crystallites (~4 µm). At a different region of the same catalyst (J1), a more uniform crystallite size distribution was found and the crystallites are attached to each other, with an individual size of approximately 2 µm.

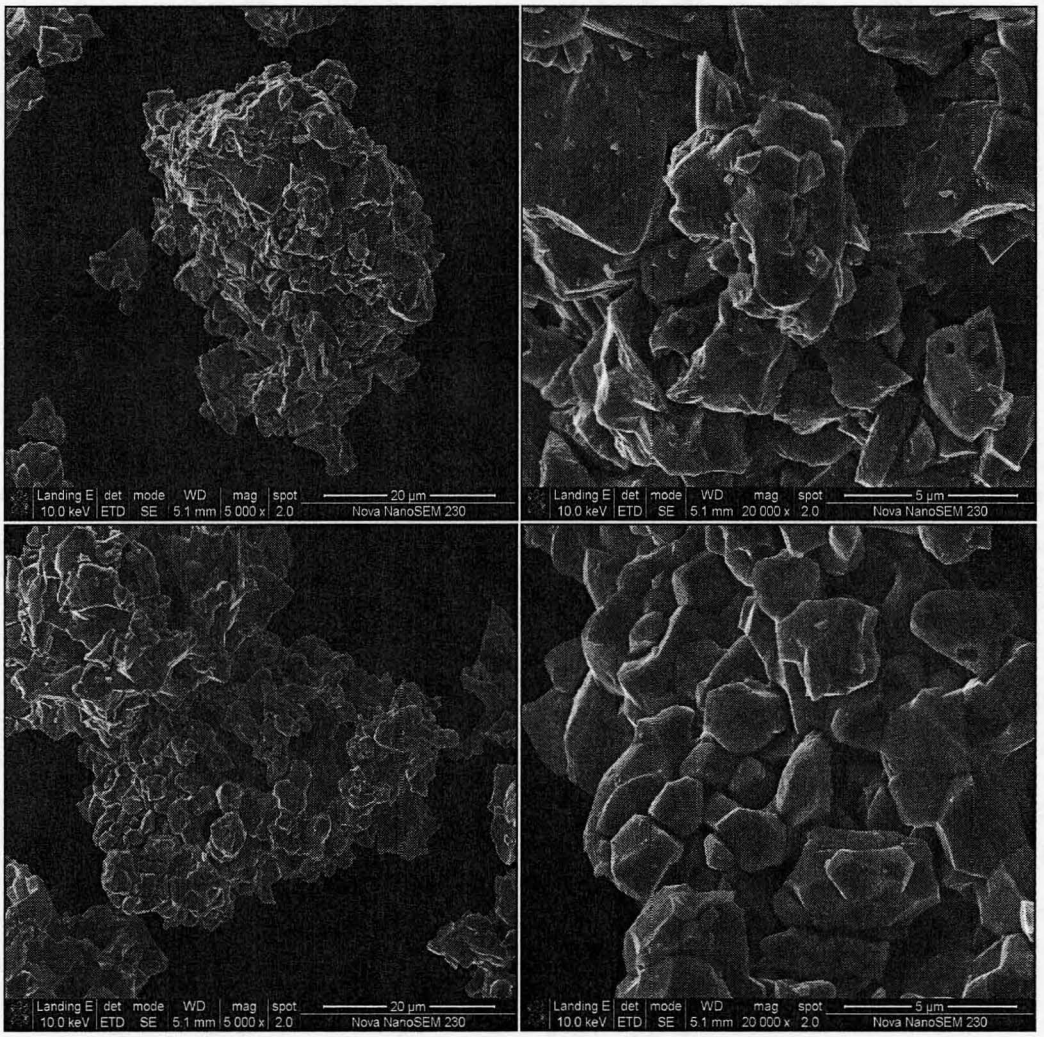

Figure 5.6: SEM image of commercial catalyst J1 at two different regions with its magnified image

Comparing the results using the 3 different techniques, the TEM and XRD results of the U3 catalyst agree with each other (See Table 5.3)

The commercial catalyst contains crystallite sizes over a very wide range which includes large crystallites that cannot be determined accurately using the XRD spectrum due to the small peak width.

The crystallites are attached to each other to form clusters. Therefore, even though the average crystallite size determined using XRD analysis falls within the size range determined using SEM, the average size would be incorrect as it does not take into account the larger sizes. Furthermore, BET surface area analysis on the commercial Co_3O_4 catalyst revealed that the commercial catalyst has a surface area of 0.36 m^2/g, which corresponds to a crystallite size of 2.73 µm (2730 nm) and does not correspond to the size determined using XRD analysis. The commercial catalyst contains a random distribution of crystallite sizes with no obvious observed trend with both crystallite or cluster sizes.

Table 5.3: Comparing TEM, XRD, SEM and BET results on catalyst U3 and J1

Catalyst code	Technique	XRD (nm)	TEM (nm)	SEM (nm)	BET (nm)
U3	Triple impregnation	25.5	24.4 ± 4.5	-	-
J1	Commercial catalyst	302	-	200 – 5000	2730

5.2 Ammonia oxidation activity of the catalyst

The catalysts were tested for the activity in the ammonia oxidation using a feed of 7.1 vol.-% NH_3, 19.4 vol.-% O_2 and the balance He. The conversion of NH_3 was determined spectrometrically using the Nessler reagent (see Appendix A.3.2).

A blank run was carried out using the same reactor packing method but with no catalyst. The SiO_2 and SiC packing showed some activity to convert NH_3 at higher reaction temperatures.

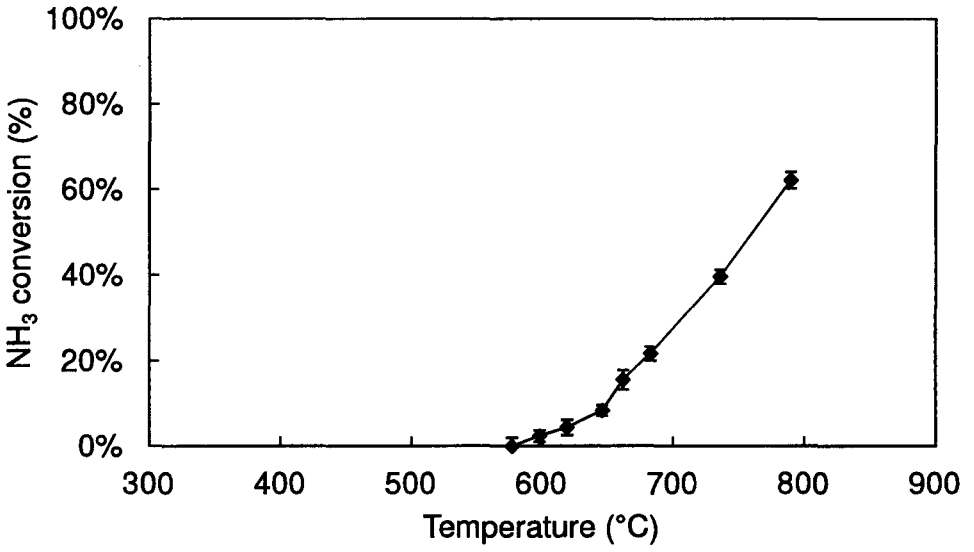

Figure 5.7: Conversion of NH_3 as a function of temperature in the range between 450-800 °C for SiO_2 and SiC packing with no catalyst, with a feed gas flow of 100 mL(NTP)/min

The actual conversion of ammonia due to the cobalt catalyst was determined by subtracting the NH_3 conversion due to the blank run from the measured NH_3 conversion obtained with the catalyst (see Table A.1).

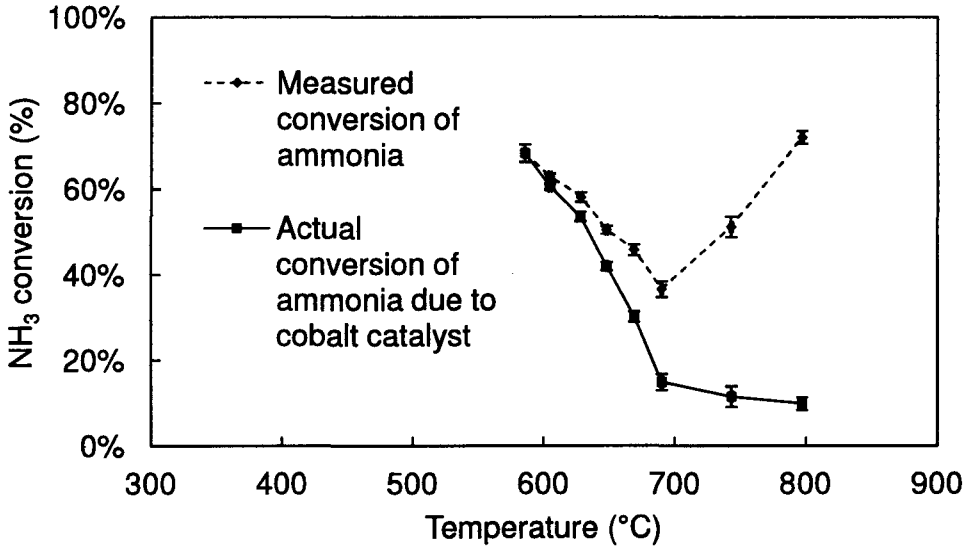

Figure 5.8: Determination of the actual conversion of NH_3 due to the cobalt catalyst as a function of temperature in the range between 450-800 °C for catalyst Co_3O_4/SiO_2 and SiO_2+ SiC packing with no catalyst, with a feed gas flow of 100 mL(NTP)/min

5.2.1 Activity as a function of temperature

In the fixed-bed reactor set-up, the catalyst was packed with the crushed support to fill up the isothermal zone of the reactor. The temperature range between 450-800 °C was investigated. The synthesised (U3) and commercial catalyst (J1) was tested under the same conditions.

To investigate the low conversion range, the catalyst pellets were crushed (size range between 75-1000 µm) to allow for a lower mass of loading. 1 mg of U3 catalyst was loaded into the reactor and a flow rate of 100 mL(NTP)/min of the feed gas was passed through the reactor (space time of 206 g.s/mol NH_3). 1.3 mg of the commercial catalyst J1 was loaded and the same flow rate of 100 mL(NTP)/min of the feed gas was passed through the reactor (space time of 268 g.s/mol NH_3). At a specific temperature, the effluent was passed through a water solution for 20-30 minutes and the solution was further analyzed using Nessler's reagent and UV/Vis spectrometer. The amount of unreacted NH_3 was determined and hence the conversion was deduced.

Figure 5.9 shows the conversion of ammonia as a function of temperature, which indicates that the ammonia conversion pass through a maximum at approximately 600 °C before decreasing with increasing temperature.

The increase in activity of a catalyst is directly related to the increase in the rate constant of the reaction. The rate constant is governed by the Arrhenius equation, where the increase in temperature would result in a larger rate constant. Therefore, the increase in temperature would result in an increase in activity. The decline in activity might indicate that the catalyst undergoes catalyst deactivation at higher temperatures.

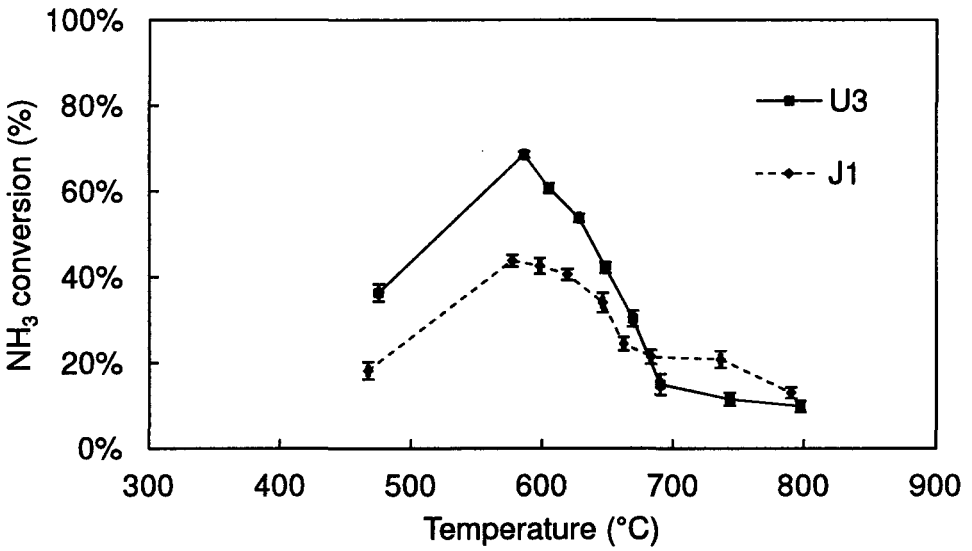

Figure 5.9: Conversion of NH_3 as a function of temperature in the range between 450-800 °C using both synthesised and commercial catalyst (U3 and J1) with a feed gas flow of 100 mL(NTP)/min and a space time of 206 g.s/mol NH_3 and 268 g.s/mol NH_3 respectively for the U3 and J1 catalyst (d_p: 75-1000 µm)

To investigate the high conversion range, the space time of 206 g.s/(mol NH_3) was doubled to 412 g.s/(mol NH_3) by loading twice the mass of catalyst, i.e. 2 mg of U3 catalyst keeping the flow rate of 100 mL(NTP)/min constant. The same trend was observed with the conversion passing a maximum (see Figure 5.10).

When twice the amount of catalyst is loaded, 98% conversion of NH_3 is achieved at ca. 575 °C. If the reaction proceeded via zero order kinetics, having twice the amount of catalyst (doubling the space time) would double the conversion of NH_3, resulting in 72.6% conversion of NH_3 at 475 °C and complete conversion of NH_3 at 580 °C. Alternatively, if the reaction proceeded via 1st order kinetics, having twice the amount of catalyst would result in an NH_3 conversion of 59% and 85% at 475 °C and 580 °C respectively. However having twice the mass did not double the conversion but exceeded the conversion expected for a first order reaction. Therefore indicating that the reaction does not proceed via simple zeroth-order or first-order kinetics as indicated by Sadykov et al. (2000), who expressed the intrinsic rate as a function of both the concentration of ammonia and oxygen with fractions as exponents.

$$r = -r_{NH_3} = k[NH_3]^{0.36}[O_2]^{0.14}$$

Deactivation of the catalyst was still apparent, with the decrease in NH_3 conversion for reaction temperatures higher than 585°C. The gradient at which the conversion decreases is not constant and deactivation is more severe as the temperature increases.

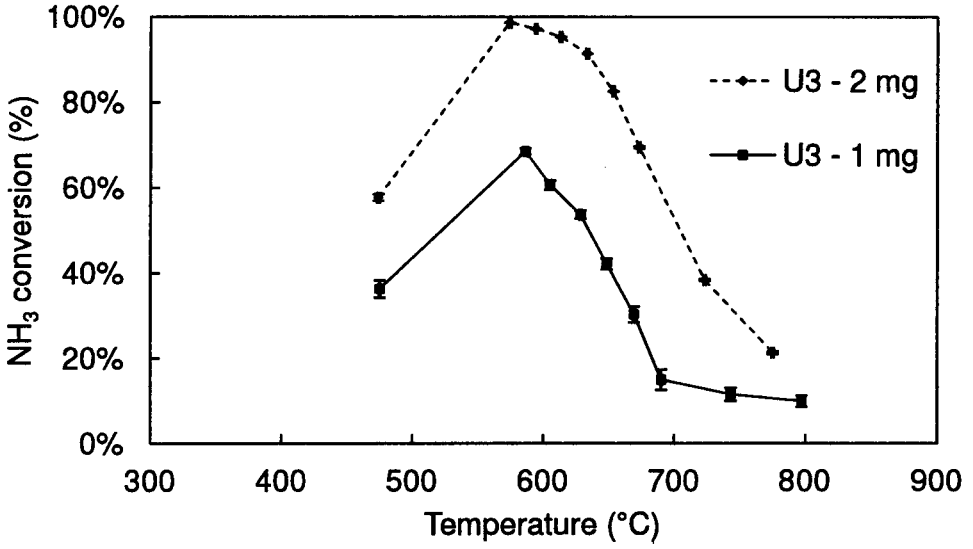

Figure 5.10: Conversion of NH_3 as a function of temperature in the range between 450-800 °C with twice the amount of U3 catalyst (d_p: 75-1000 µm) loaded feed gas flow of 100 mL(NTP)/min and a space time of 206 g.s/mol NH_3 and 412 g.s/mol NH_3 respectively

As industrial solid catalysts are predominantly applied in the form of pellets, the in-house prepared Co_3O_4/SiO_2 pellets were tested under ammonia oxidation conditions. 100 mg of U3 pellets were loaded into the reactor and tested.

The pellets confirm that complete conversion is achieved due to the much larger mass been loaded resulting in an increase in space time by a factor of 100 (20616 g.s/mol NH_3). Complete conversion was achieved in the temperature range of between 570 to 800 °C. At temperatures above 800 °C, the conversion decreases rapidly indicating that the catalyst is undergoing deactivation with increasing temperature. The observed deactivation is thus dependent on the amount of active Co_3O_4 loaded and the space time of the reaction. Complete conversion of ammonia could still be achieved with excess Co_3O_4 on a carrier where some of the active Co_3O_4 phase would be deactivated, most likely to the inactive CoO phase.

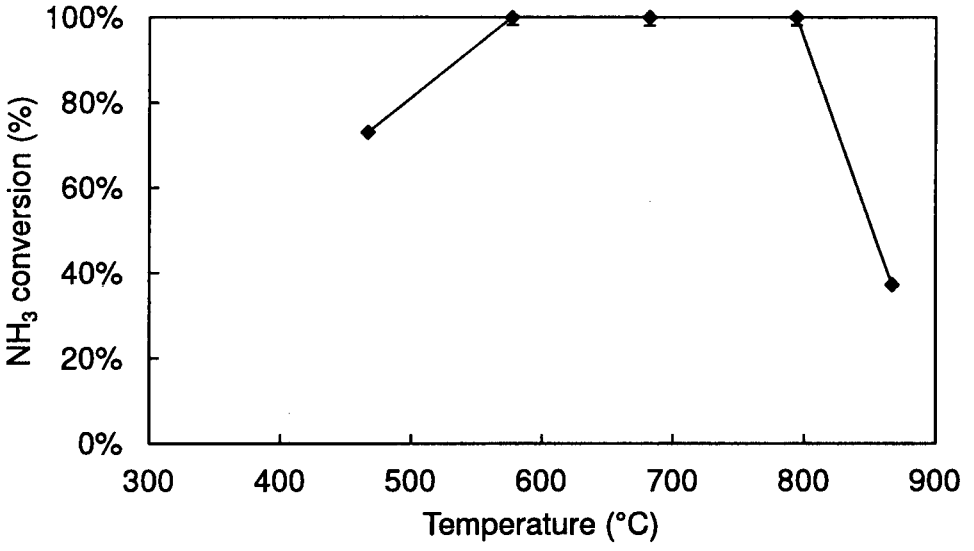

Figure 5.11: Conversion of NH_3 as a function of temperature in the range between 450-800 °C using a supported Co_3O_4 (U3) catalyst in the form of a pellet (d_{pellet}: 2.5 mm, l_{pellet}: 4.5 mm, space time of 20616 g.s/mol NH_3) to represent industrial relevant conditions at complete conversion of NH_3 with a feed gas flow of 100 mL(NTP)/min

The commercial Co_3O_4 catalyst was obtained in the form of pellets. Therefore the entire pellet was tested and compared to the crushed Co_3O_4. A single pellet with a mass of 25.8 mg was loaded (space time of 5320 g.s/mol NH_3) into the reactor.

The pellet showed a higher conversion due to the larger mass loaded and the resulting high space time (5320 g.s/mol NH_3). The activity of the crushed pellet with a lower mass loaded (space time of 268 g.s/mol NH_3) showed a similar trend as a function of temperature but at a lower conversion of NH_3. The space time is close to a factor of 20 times greater than that of the crushed Co_3O_4 catalyst and yet the conversion of ammonia only increases by a factor of less than 2. Complete conversion of ammonia would have been achieved if mass and heat transport limitations and catalyst deactivation were avoided. This indicates that mass and heat transport limitations could be present.

The commercial catalyst pellet starts to deactivate at temperatures greater than 620 °C whereas the crushed catalyst starts to deactivate at temperatures above 570 °C. Similar to the in-house prepared Co_3O_4/SiO_2 catalyst, the increase in mass increases the temperature at which deactivation becomes noticeable.

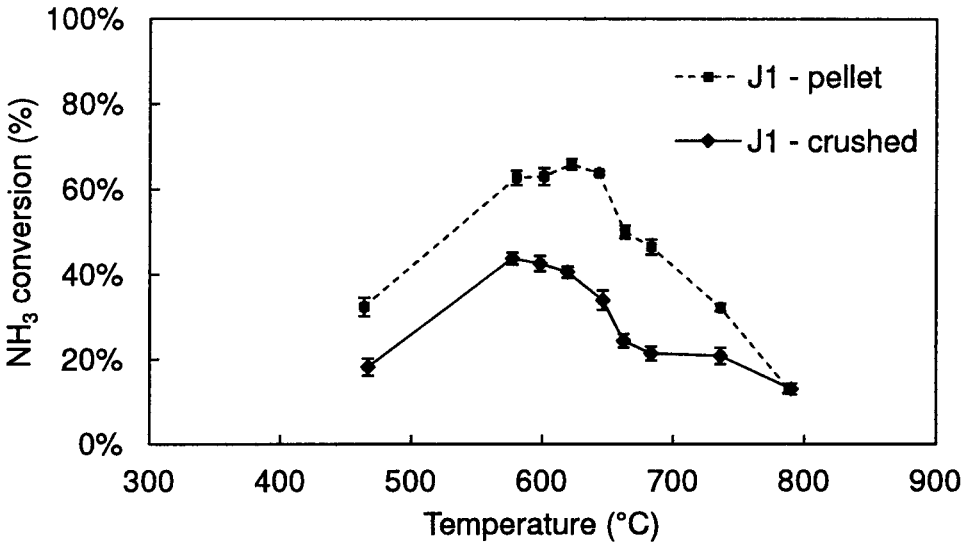

Figure 5.12: Conversion of NH_3 as a function of temperature in the range between 450-800 °C comparing the commercial pellet (space time - 5320 g.s/mol NH_3) to the crushed Co_3O_4 catalyst (space time - 268 g.s/mol NH_3) with a feed gas flow of 100 mL(NTP)/min

5.2.2 Activity as a function of particle size

Catalyst of different particle sizes was obtained by crushing the U3 Co_3O_4/SiO_2 catalyst pellets to obtain a 100% passing through a sieve of its respective size range. As a limited amount of commercial catalyst was obtained, the particle size of the commercial catalyst was not tested. The same space time of 206 g.s/(mol NH_3) for each catalyst was tested under the same temperature. The sizes that were obtained and tested are shown in Table 5.4.

The result indicates that for the Co_3O_4/SiO_2 catalyst, smaller catalyst particles result in a higher conversion of NH_3. In the absence of mass and heat transfer limitations, the observed rate of reaction is independent of the catalyst particle size. Thus, the results show that the catalyst was operating under mass and heat transfer limitation regimes.

Table 5.4: Crushed U3 catalyst with the catalyst code and its respective size range

Catalyst code	Size (µm)
U3-A	710-1000
U3-B	500-710
U3-C	300-500
U3-D	125-300
U3-E	75-125

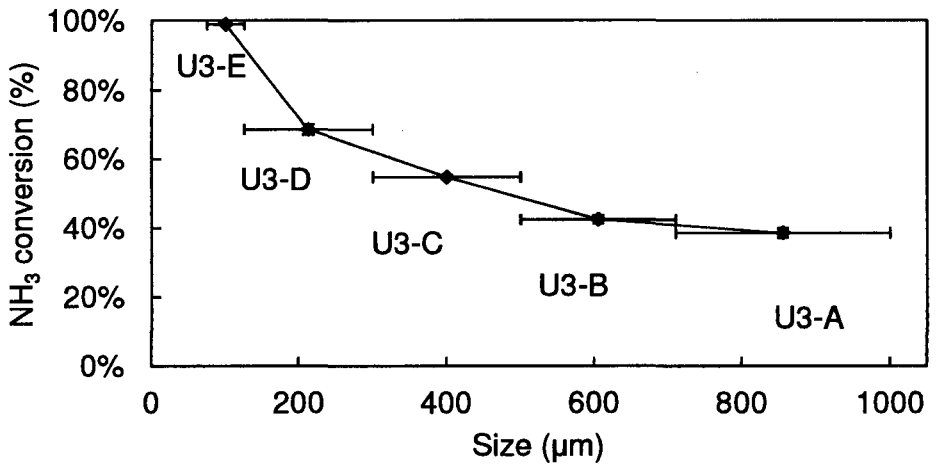

Figure 5.13: Conversion of NH_3 measured at ~580 °C as a function of average particle size between the crushed U3 catalysts with the feed gas flow of 100 mL(NTP)/min and space time of 206 g.s/mol NH_3

5.2.3 Activity as a function of particle size and temperature

Catalysts of different particle sizes were tested at different temperatures (see Figure 5.14). Due to the limited supply of the commercial catalyst, only the U3 catalyst was tested at the different particle sizes.

A decrease in particle size resulted in an increase in ammonia conversion for the lower temperatures prior to catalytic deactivation. A conversion of approximately 100% is achieved using catalyst U3-E (75-125 μm). The conversion increases for all particle sizes when the temperature increases from 450 to approximately 580 °C. Thereafter, severe deactivation occurs as the conversion drops considerably. No obvious trend was observed between particle size and the deactivation of the catalyst.

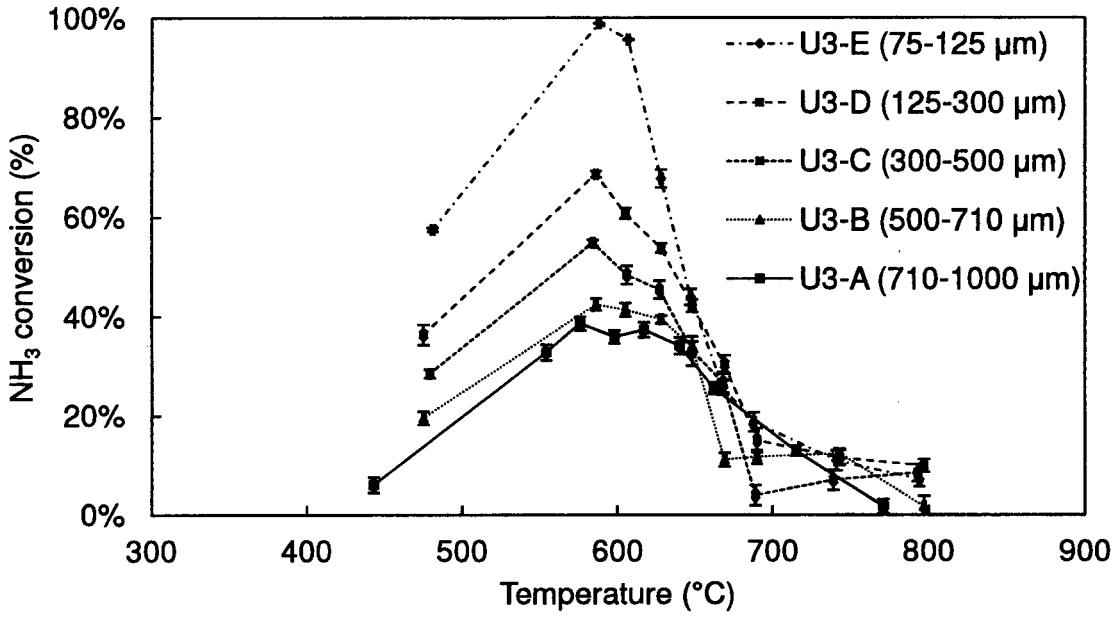

Figure 5.14: Conversion of NH_3 as a function of temperature in the range between 450-800 °C for all particle sizes U3-A to U3-E (see Table 5.4) with a feed gas flow of 100 mL(NTP)/min and space time of 206 g.s/mol NH_3

5.3 Product selectivity of catalysts

Mass spectrometry was used to verify the products synthesised by ammonia oxidation over Co_3O_4. Selectivity as a function of temperature was evaluated and compared at both low and high conversions due to the possible side reactions between the products that could occur at high conversion levels (~100%).

Repeated runs in a different set-up using the same feed gas (100 mL(NTP)/min) and using the same mass of catalyst were carried out to determine the product selectivity of the catalyst. . The selectivity of N_2 could not be determined as the high vacuum inlet had a steady intake of air and thus small changes in N_2 signal could not been observed and thus it was assumed that no N_2 was produced.

5.3.1 Selectivity at low conversions (below 50%) of ammonia

The initial runs confirmed that neither NO_2 nor N_2O_4 were formed using the cobalt based catalyst. Using the same space time (206 g.s/mol NH_3) as the conversion measurements taken in a different set-up, 1 mg of U3-C catalyst was loaded into the U-tube reactor.

The only products that were formed are NO and N_2O. It was seen that the catalyst becomes active above 300 °C and the concentrations of both NO and N_2O increases dramatically. The concentration of NO remains relatively constant from 350 to 500 °C before steadily decreasing and rapidly decreases at temperatures above 650 °C (see Figure 5.15). Similarly the concentration of N_2O remains constant from 360 to 450 °C but starts to decrease at a lower temperature (ca. 450 °C) compared to NO (see Figure 5.16).

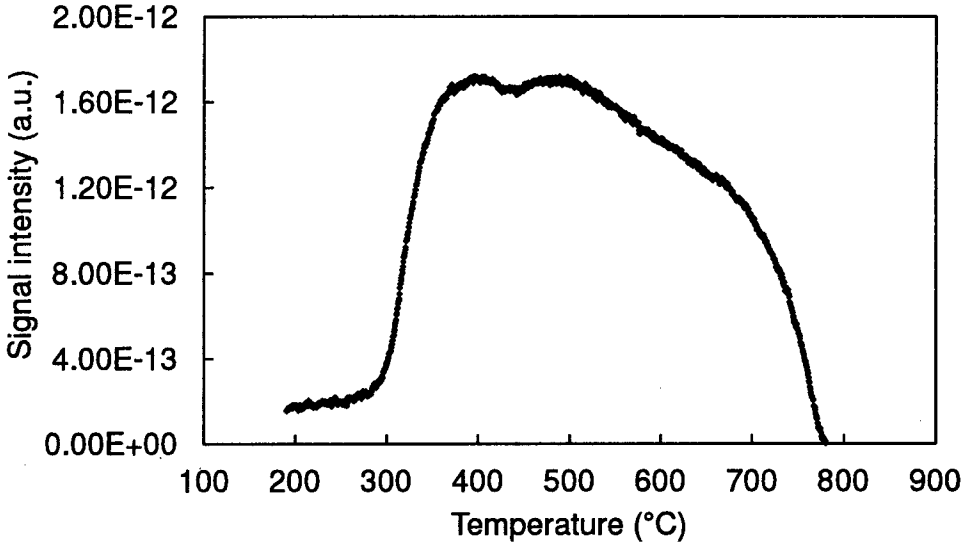

Figure 5.15: Intensity of the NO signal over a temperature range with a space time of 206 g.s/(mol NH_3) and a feed gas flow of 100 mL(NTP)/min using catalyst U3-C (d_p: 300-500 µm) with a temperature ramp of 10 °C/min

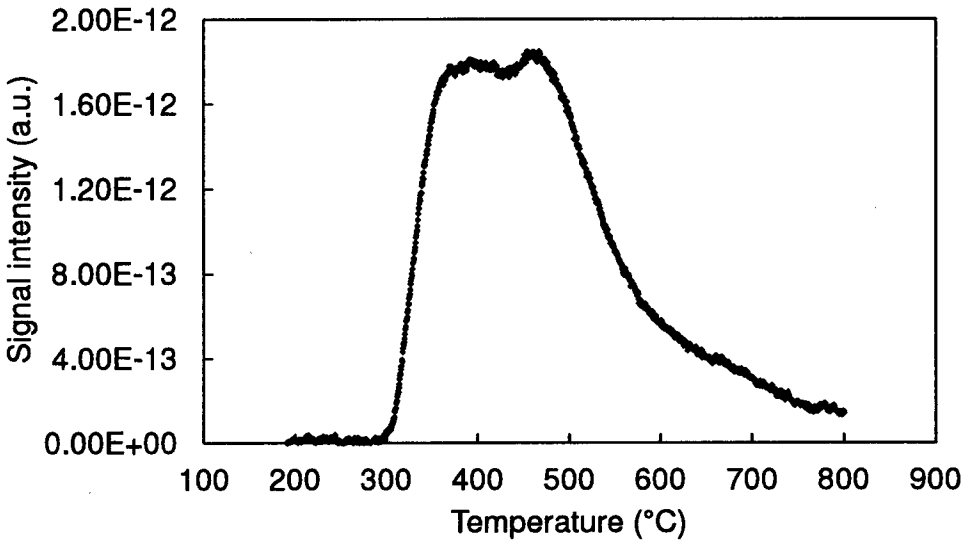

Figure 5.16: Intensity of the N_2O signal over a temperature range with a space time of 206 g.s/(mol NH_3) and a feed gas flow of 100 mL(NTP)/min using catalyst U3-C (d_p: 300-500 µm) with a temperature ramp of 10 °C/min

Using the calibration data obtained by passing a known concentration of gas into the mass spectrometer (see Appendix A.2.3), the NO content and N_2O content were determined.

Figure 5.17 shows the NO content in the fraction of NO plus N_2O. This represents the selectivity of the ammonia converted towards the desired product assuming no formation of N_2. It can be seen that the NO-content increases with increasing temperature before dropping considerably at temperatures above 730 °C, where the catalyst was not active. A minimum temperature of 530 °C was required to obtain at least 90 N-% towards NO content in the fraction of NO plus N_2O, with a maximum of 95 N-% achieved at 720 °C.

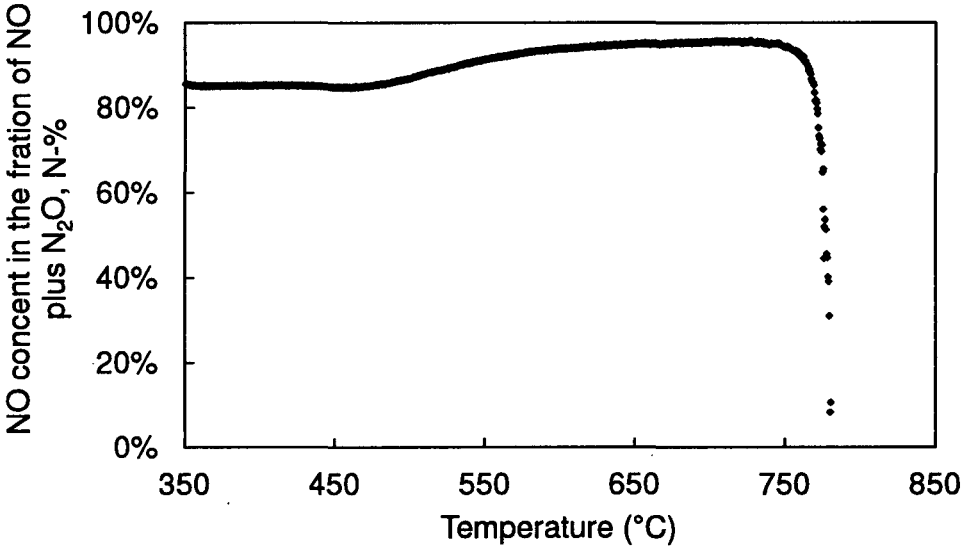

Figure 5.17: NO-content in the fraction of NO plus N_2O in the ammonia conversion with a space time of 206 g.s/(mol NH_3) and a feed gas flow of 100 mL(NTP)/min as a function of the reaction temperature using catalyst U3-C (d_p: 300-500 µm) with a temperature ramp of 10 °C/min

5.3.2 Selectivity at higher conversions by doubling the space time

Higher conversions were obtained by loading higher masses of catalysts. 2 mg of U3-C catalyst was loaded into the U-tube reactor to represent the same scenario as indicated as shown in Figure 5.10, where the space time was doubled to 412 g.s/(mol NH_3).

Even at higher conversions, neither NO_2 nor N_2O_4 are formed using the cobalt based catalyst. The intensity of the signal starts to increase at temperatures just below 300 °C, indicating that the catalyst starts to become active. The signal for both NO and N_2O increases dramatically and reaches a maximum at approximately 350 °C. The concentration of NO decreases slightly but remains fairly constant before declining towards zero at temperatures above 700 °C. The N_2O concentration declines steadily after a maximum is achieved between 350-400 °C. Similar to the NO concentration, the concentration reaches zero at temperatures above 700 °C where the catalyst was not active in producing either NO or N_2O.

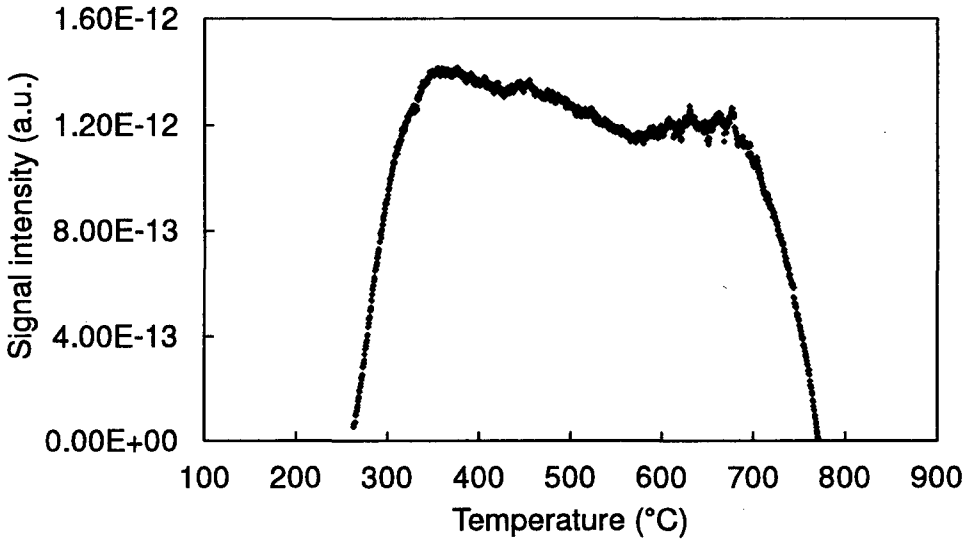

Figure 5.18: Intensity of the NO signal over a temperature range with a space time of 412 g.s/(mol NH_3) and a feed gas flow of 100 mL(NTP)/min using catalyst U3-C (d_p: 300-500 µm) with a temperature ramp of 10 °C/min

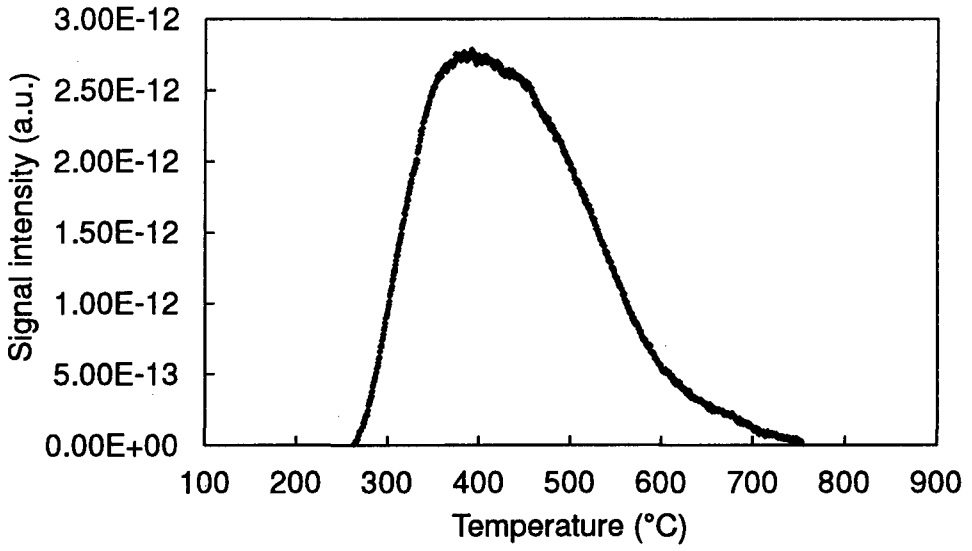

Figure 5.19: Intensity of the N_2O signal over a temperature range with a space time of 206 g.s/(mol NH_3) and a feed gas flow of 100 mL(NTP)/min using catalyst U3-C (d_p: 300-500 µm) with a temperature ramp of 10 °C/min

By representing the NO content in the fraction of NO plus N_2O and assuming no formation of N_2, the relative fraction towards the desired product was observed. The NO content in the fraction of NO plus N_2O increases with increasing temperature before decreasing to zero at temperatures greater than 750 °C. A minimum temperature of 570 °C was required to obtain 90 N-% towards the desired product NO in the fraction of NO plus N_2O. At temperatures above 630 °C, 95 % NO in the fraction of NO plus N_2O was achieved with a maximum selectivity of 99 N-% achieved at temperatures between 740-750 °C before it rapidly decreases to zero at higher temperatures.

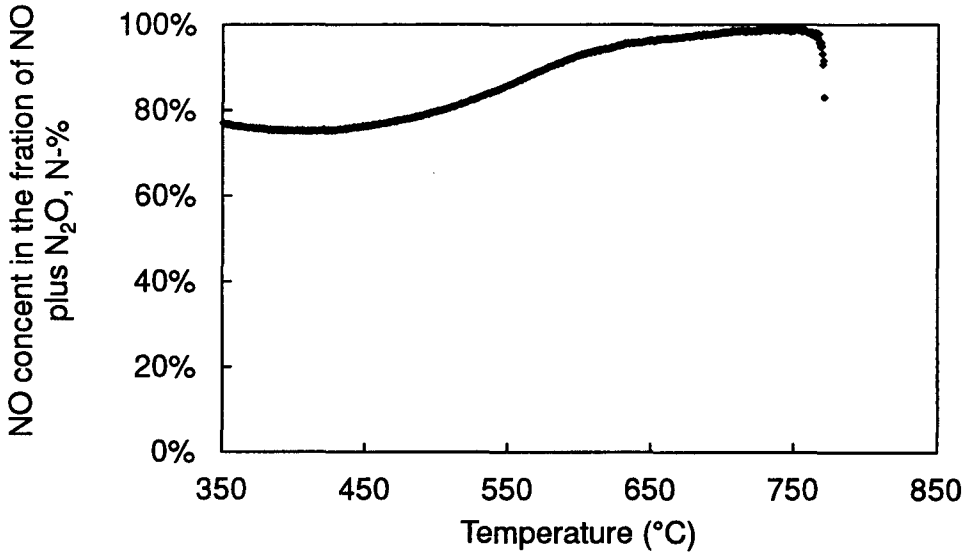

Figure 5.20: NO-content in the fraction of NO plus N_2O in the ammonia conversion with a space time of 412 g.s/(mol NH_3) and a feed gas flow of 100 mL(NTP)/min as a function of the reaction temperature using catalyst U3-C (d_p: 300-500 µm) with a temperature ramp of 10 °C/min

5.3.3 Selectivity at complete conversion using catalyst pellets

Selectivity as a function of temperature was evaluated at complete conversion to represent industrial relevant conditions. A comparison was done between the in-house synthesised Co_3O_4/SiO_2 catalyst pellets and the commercially obtained Co_3O_4 pellets. 50 mg of U3 catalyst was loaded into the U-tube reactor, resulting in space time of 10308 g.s/mol NH_3, keeping the volumetric flow rate of the feed gas of 100 mL(NTP)/min, to ensure that complete conversion was achieved.

Co_3O_4/SiO_2 pellets were active for ammonia oxidation towards NO and N_2O at temperatures greater than 250 °C. The commercial unsupported Co_3O_4 catalyst was only active for ammonia oxidation at temperatures greater than 450 °C. No formation of NO_2 or N_2O_4 was found. For the supported Co_3O_4/SiO_2 pellets, the NO signal increased with increasing temperature before decreasing at temperatures above 700 °C. The N_2O signal for the supported catalyst reached a maximum at approximately 300 °C before steadily decreasing towards zero. For the unsupported commercial Co_3O_4 catalyst, the formation of NO and N_2O was favoured at temperatures between 450-550 °C before decreasing at higher temperatures. As the figures indicate, supported Co_3O_4/SiO_2 favoured the formation of N_2O at lower temperatures with a higher signal compared to the maximum signal achieved on the unsupported Co_3O_4 catalyst. However, the intensity decreased as temperature increased. The formation of NO on the unsupported catalyst is favoured at lower temperatures (430-650 °C) with the NO concentration exceeding the NO concentration obtained from ammonia oxidation over the supported catalyst. At temperatures greater than 650 °C, the NO concentrations were similar with a slight decrease possibly due to catalyst deactivation.

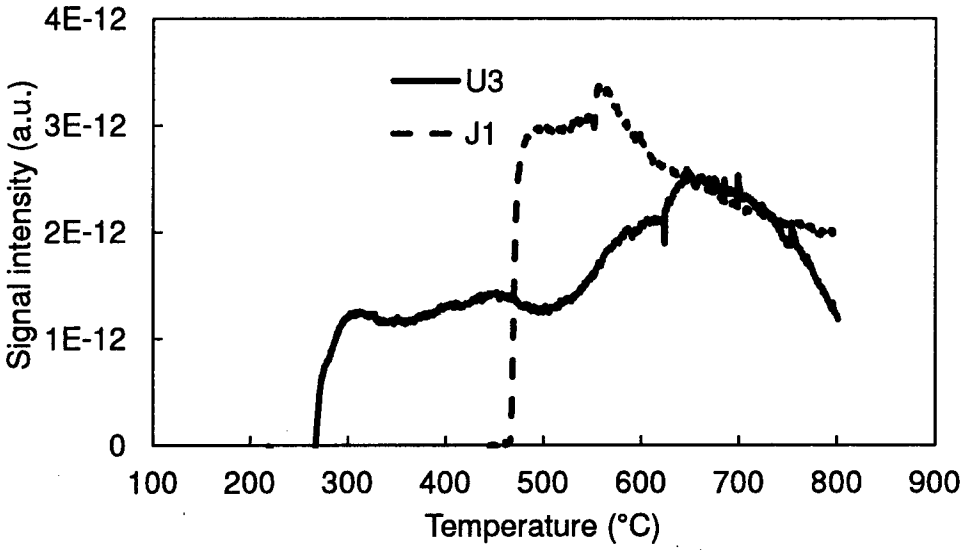

Figure 5.21: Comparison of the intensities of the NO signal over a temperature range with a space time of 10308 g.s/(mol NH_3) and feed gas flow of 100 mL(NTP/min) with a temperature ramp of 10 °C/min for catalyst pellets U3 (d_{pellet}: 2.5 mm, l_{pellet}: 4.5 mm) and J1 (d_{pellet}: 3 mm, l_{pellet}: 3 mm)

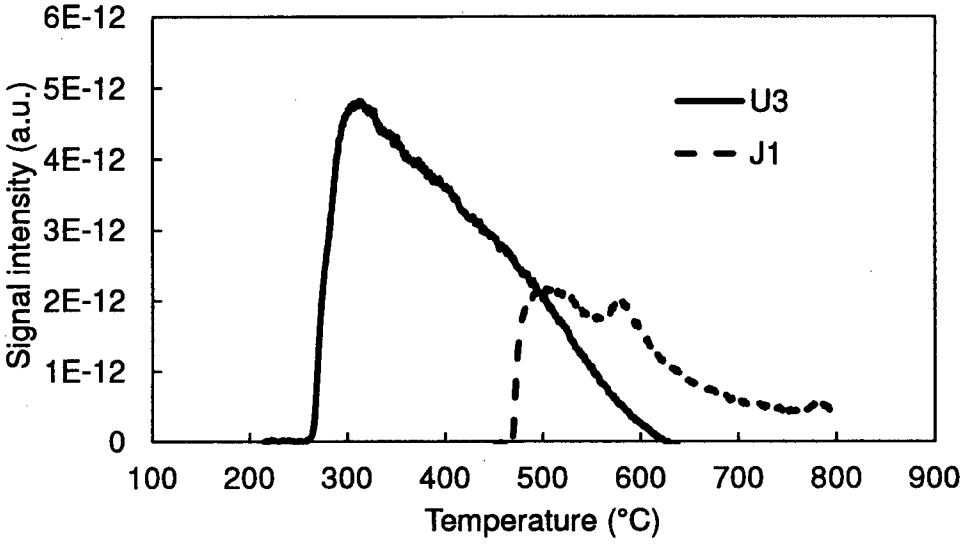

Figure 5.22: Comparison of the intensity of the N_2O signal over a temperature range with a space time of 10308 g.s/(mol NH_3) and feed gas flow of 100 mL(NTP/min) at a temperature ramp of 10 °C/min for catalyst pellets U3 (d_{pellet}: 2.5 mm, l_{pellet}: 4.5 mm) and J1 (d_{pellet}: 3 mm, l_{pellet}: 3 mm)

Comparison between the yields of NO content in the fraction of NO plus N_2O, assuming no formation of N_2 was carried out (see Figure 5.23). A minimum temperature of 550 °C is required to obtain a NO content of 90% in the fraction of NO plus N_2O using the supported Co_3O_4/SiO_2 catalyst. The commercial catalyst is highly selective in producing NO, with the NO content fraction of above 90% achieved from the moment the catalyst is active for ammonia oxidation. At temperatures above 570 °C, the NO content using the synthesised supported catalyst exceeds the NO content using the commercial catalyst. A NO fraction of NO plus N_2O of above 95% is achieved at temperatures above 600 °C and 650 °C for the U3 and J1 catalyst respectively. The maximum NO fraction that the J1 catalyst could achieve in the investigated temperature range was 97.05 % at 800 °C. The maximum NO fraction that was achieved using the supported U3 catalyst was 99.3% at 800 °C. Further increasing the temperature could possibly result in a higher NO content as Figure 5.22 indicates that the concentration on N_2O was approaching zero with increasing temperature.

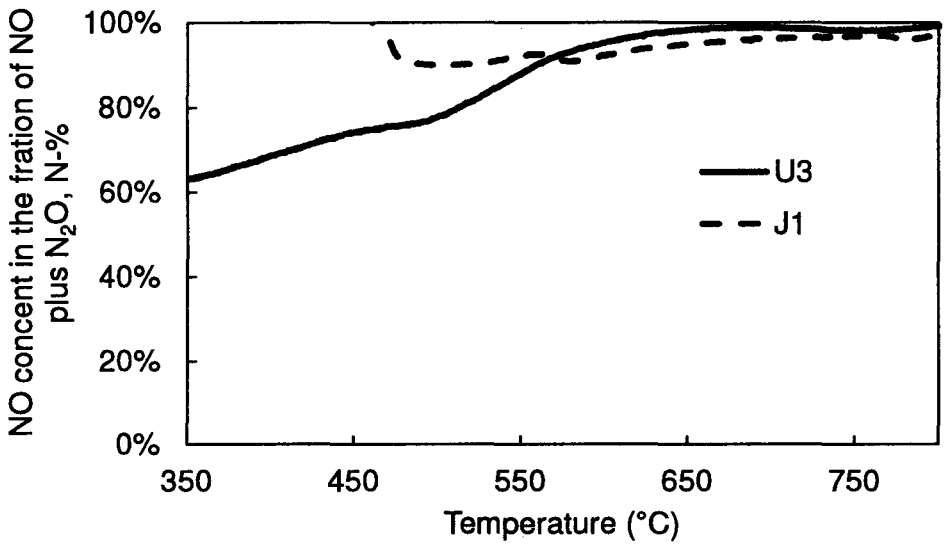

Figure 5.23: NO-content in the fraction of NO plus N_2O for both U3 and J1 pellets in the ammonia conversion with a space time of 10308 g.s/(mol NH_3) and a feed gas flow of 100 mL(NTP)/min as a function of the reaction temperature at a temperature ramp of 10 °C/min for catalyst pellets U3 (d_{pellet}: 2.5 mm, l_{pellet}: 4.5 mm) and J1 (d_{pellet}: 3 mm, l_{pellet}: 3 mm)

5.4 Catalyst deactivation

Catalyst deactivation was investigated to gain an understanding of what deactivation mechanisms are involved for a cobalt oxide catalyst under ammonia oxidation reaction conditions.

As seen in the results, the conversion of NH_3 and consequently the activities of the catalysts decreases at temperatures greater than 600 °C. At higher temperatures, the product selectivity results further confirm that the catalyst was inactive in producing either NO or N_2O as products. The decrease in both the conversion of NH_3 and formation of NO and N_2O as products suggests that severe deactivation occurs at higher reaction temperatures.

XRD analysis was performed on the catalyst after the catalyst was exposed to ammonia oxidation conditions with a feed gas (7.1 vol.-% NH_3) flow of 100 mL(NTP)/min and a maximum temperature of approximately 800 °C. This would indicate whether the cobalt Co_3O_4 phase change occurred and whether any sintering of the catalyst took place by determining the size of the catalyst.

In order to achieve this, sufficient amounts of catalyst have to be loaded into the reactor such that the recovered catalysts was detectable using XRD. Only pellets were loaded as it was not possible to recover the crushed particles.

Deactivation of the U3 and intermediate U2 catalyst was investigated. 100 mg of U3 catalyst (space time of 20616 g.s/mol NH_3) and a slightly higher mass of 110 mg of U2 catalyst (space time of 22678 g/mol NH_3) were loaded into the reactor and exposed to ammonia oxidation conditions at reaction temperatures between 450-800 °C. Due to the high mass of catalyst used, 100% of ammonia conversion was achieved using both the U2 and U3 catalysts, as the conversion of NH_3 decreased to below 50% at higher reaction temperatures and catalyst deactivation was investigated and proved using XRD data,. The catalyst was recovered after ammonia oxidation conditions, crushed up and analysed using XRD.

The U2 catalyst pellets that were recovered were purple in colour while the U3 catalyst maintained its original black colour. The catalyst had undergone some sort of change with the XRD pattern being very different after exposure to ammonia

oxidation conditions at reaction temperatures ranging between 450-800 °C. XRD patterns for both U2 and U3 catalysts displayed signals of the formation of a silicate. For the U2 catalyst, the Co_3O_4 (PDF 00-043-1003) phase seemed to have disappeared with only the signals of the CoO (PDF 00-043-1004) and Co_2SiO_4 (PDF 00-015-0865) corresponding to the XRD spectrum. The Co_3O_4 phase and the silicate phase appear to be present in the U3 catalyst and this was confirmed using the "Topas" software package.

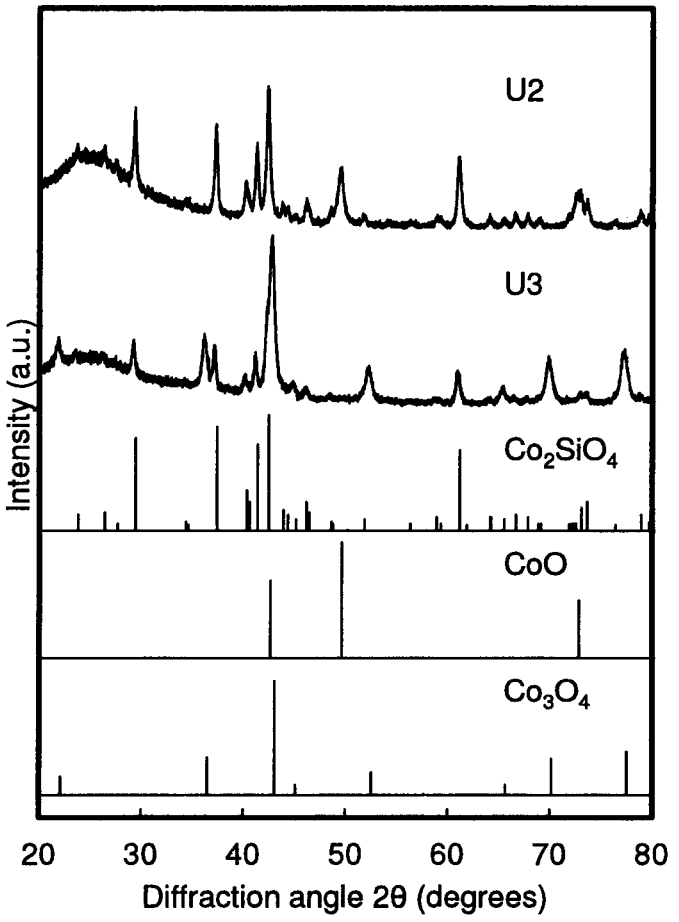

Figure 5.24: XRD diffraction pattern of the U2 and U3 catalyst after exposure to ammonia oxidation conditions respectively, superimposed with the reference spectrum of Co_3O_4 (PDF 00-043-1003), CoO (PDF 00-043-1004) and Co_2SiO_4 (PDF 00-015-0865)

The Topas software analysis of the XRD spectrum confirmed that the Co_3O_4 phase of the U2 catalyst had disappeared. The Co_3O_4 phase and a very low content of CoO (< 1 wt.-%) phase were still present for the U3 catalyst with the higher cobalt loading. Due to the low content of CoO detected, the calculated average crystallite size is rather uncertain. The average crystallite size of the CoO phase (25.2 nm in the case of U2) and the crystallite size of Co_3O_4 phase (26 nm in the case of U3) was very similar to the size of the Co_3O_4 crystallites present in the fresh catalyst. This indicates that sintering is not a major problem with the catalyst. The major problem associated with the catalyst would be the irreversible formation of cobalt silicate under the severe and hydrothermal slightly reducing conditions in the reactor. It was further realised that the amount of cobalt which could be detected using XRD was less than the amount of cobalt originally present as Co_3O_4, indicating the presence of cobalt in some X-ray amorphous form, presumably surface silicate. The formation of cobalt silicate was observed for both the catalysts. The average crystallite size of cobalt silicate, 88.7 nm for the U2 catalyst and 111.2 nm for the U3 catalyst was rather large indicating that the smaller CoO crystallite has reacted with the larger SiO_2 particle.

The commercial catalyst displayed the same XRD pattern as the original with the same distinguished peaks. However after analysis using the "Topas" software package it was determined that a low content of approximately 5.7 wt.-% of the CoO phase was present within the catalyst. As the catalyst was allowed to stand in air for a number of days before it was analysed using XRD, this might have resulted in the re-oxidation of the CoO phase from the active Co_3O_4 phase.

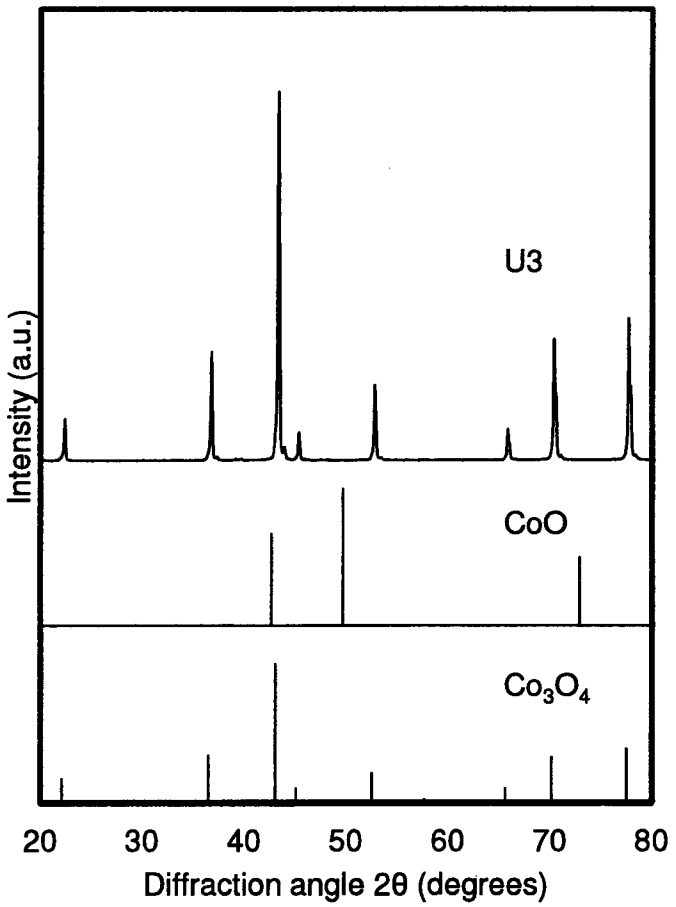

Figure 5.25: XRD diffraction pattern of the commercial J1 catalyst after exposure to ammonia oxidation conditions respectively, superimposed with the reference spectrum of Co_3O_4 (PDF 00-043-1003), CoO (PDF 00-043-1004)

Table 5.5: Average crystallite size determined using XRD analyses for the U2 and U3 catalysts after exposure to ammonia oxidation conditions

Catalyst code	Catalyst phase	Phase present (wt.-%)	Size (nm)
U2	Co_3O_4	0	-
	CoO	3.75	25.2
	Co_2SiO_4	10.5	88.7
U3	Co_3O_4	11.47	26
	CoO	0.24	12.7
	Co_2SiO_4	5.01	111.2
J1	Co_3O_4	94.3	200.5
	CoO	5.7	27.4

6 DISCUSSION

6.1 Catalyst characterisation

Catalyst preparation via the incipient wetness impregnation technique using a cobalt nitrate solution and cylindrical shaped silica pellets (d_{pore}: 12 nm) yielded a catalyst with an average crystallite size of approximately 25 nm with wide size distribution as seen in the TEM images of the Co_3O_4 crystallites supported on SiO_2. The Co_3O_4 was found in the form of clusters, with the larger clusters having a size range of 60-80 nm. Clusters of cobalt are commonly found in supported cobalt catalyst prepared from a cobalt nitrate solution and using the incipient wetness impregnation technique as shown by Feller et al. (1999), where they observed droplets of cobalt nitrate within the catalyst and reported that the droplets of cobalt nitrate and the cobalt clusters were similar in size (Feller et al., 1999).

The cobalt content of the catalyst was obtained from AAS. Cobalt nitrate is hydrophilic and can absorb moisture in air, thus overestimating the amount of cobalt in the impregnation solution, which may lead to lower than expected cobalt loadings. This was avoided as the actual cobalt loading of the synthesised catalyst using the incipient impregnation preparation method corresponded directly with the expected calculated cobalt loading. An accurate loading was achieved using single, double and triple impregnation, indicating that the cobalt content loaded onto the catalyst can be well controlled using this preparation method. The prepared catalyst showed a slight increase in cobalt crystallite size with increase in cobalt content. This phenomenon was reported by Iglesia et al. (1993) where a similar observation was found when preparing a cobalt oxide catalyst for Fischer-Tropsch synthesis (Iglesia et al., 1993).

XRD analyses found a pure Co_3O_4 phase was present for the prepared catalyst (U3) and the intermediates (U1 and U2). The Co_3O_4 crystallite sizes were analysed using both TEM and XRD to obtain a true indication of the actual sizes as each technique encompasses error. The average crystallite size of approximately 25 nm was obtained using XRD analysis which corresponded with the average size using the TEM images.

The commercial catalyst contained a Co-content of 76.69% and hence a Co_3O_4 content of 100%, which was confirmed using XRD. Therefore it was concluded that the commercial catalyst was an unsupported pure Co_3O_4 cobalt catalyst. XRD analysis showed an average crystallite size of 302 nm. SEM images showed that for the commercial catalyst, the crystallites were packed tightly together to form larger clusters. The average crystallite size of 2.73 μm (2730 nm) was determined using BET calculations and does not correlate with the average crystallite size determined using XRD analysis. The cobalt crystallite and cluster sizes were random ranging from 200-5000 nm with no obvious trend observed. This questions the average crystallite size determined from line-broadening in XRD as to whether the larger crystallites/clusters were taken into account accordingly.

The catalyst active surface area of the commercial catalyst was determined using BET analysis to be approximately 0.36 m^2/g of Co_3O_4. The synthesised Co_3O_4/SiO_2 contained much smaller Co_3O_4 crystallites, and taking into account the cobalt loading in the catalyst, resulting in a surface area of 12.2 m^2/g of Co_3O_4 per sample was determined. This would imply that the in-house prepared catalyst would be approximately 34 times more active compared to the commercial catalyst. However, the calculated intrinsic activity constant per m^2 of Co_3O_4 revealed that the commercial catalyst was more active compared to the in-house prepared Co_3O_4/SiO_2 catalyst. Indicating that severe deactivation might have taken place on the synthesised Co_3O_4/SiO_2 catalyst at these temperatures. No further information was provided as to how the commercial catalyst was synthesised or what crystallite size was being targeted. Therefore the true nature of the commercial catalyst is unknown. Nevertheless, a comparison between the in-house prepared Co_3O_4/SiO_2 catalyst and the commercial pure Co_3O_4 catalyst was carried out in terms of activity and selectivity.

6.2 Catalyst activity and product selectivity in the ammonia oxidation

The catalysts were tested for the activity in the ammonia oxidation using a feed of 7.1 vol.-% NH_3, 19.4 vol,-% O_2 and the balance He. The conversion of NH_3 as a function of reaction temperature was determined spectrometrically using the Nessler reagent. Typically, conversion increases with increasing temperature but in this case, the conversion as a function of temperature passes a maximum, indicating severe deactivation of the catalyst at the higher reaction temperatures. The activity of the in-house prepared Co_3O_4/SiO_2 catalyst passes a maximum intrinsic activity at approximately 600 °C, while the commercial catalyst passes a maximum at approximately 620 °C.

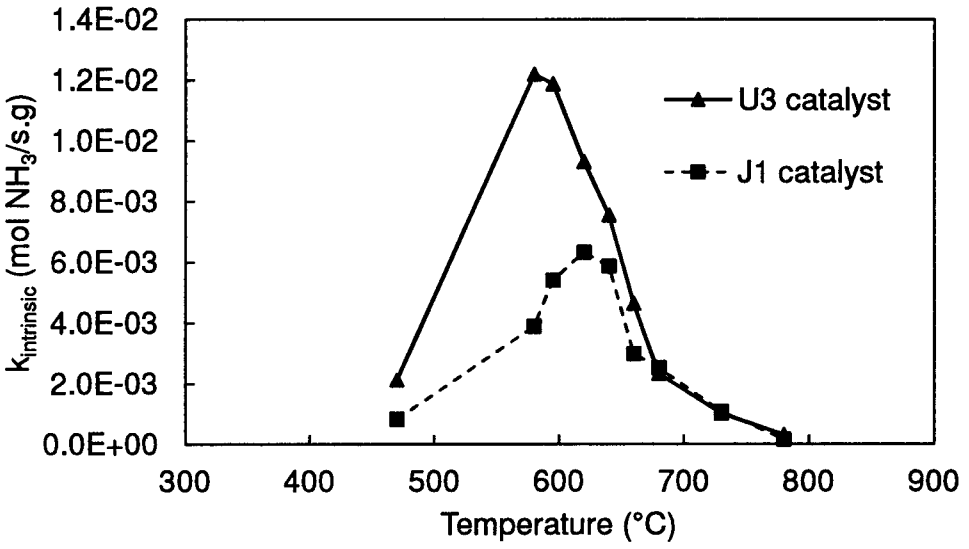

Figure 6.1: Comparison of the intrinsic rate constant of the in-house prepared Co_3O_4/SiO_2 catalyst with the commercial Co_3O_4 pellet catalyst as a function of reaction temperature with a feed gas flow of 100 mL(NTP)/min and a NH_3 content of 7.1 vol.-%, 19.4 vol.-% O_2 and the balance He

An increase in ammonia conversions were achieved by adjusting the space time. By doubling the space time, the conversion of NH_3 did not double which implies that the ammonia oxidation reaction does not proceed via a typical first order or zero order reaction. Complete conversion of ammonia was obtained using Co_3O_4/SiO_2 pellets at temperatures just below 600 °C by increasing the space time with a factor of 100 (20616 g.s/mol NH_3). This confirms that the Co_3O_4 catalyst is active for oxidation

reactions just as in the case with propane and methane oxidation (Liu et al., 2006; Solsana et al., 2008; Liotta et al., 2006).

The synthesised and commercial Co_3O_4 catalyst illustrated that the highest conversion obtained was at the reaction temperatures between 580-600 °C, regardless of the various particles sizes. This indicates that the catalyst is most active within this temperature range. However operating conditions for ammonia oxidation are selected based on both activity and the selectivity of the catalyst to produce the desired NO_x product. Complete conversion of ammonia can be achieved by increasing the space time as seen in Figure 5.11, where NH_3 was completely converted in the temperature range of 570-800 °C. For this reason, the operating temperature should be selected based on the selectivity of the catalyst to product NO_x at complete conversion of NH_3.

The ammonia oxidation reaction yields various nitrogen oxide compounds as products. However, according to the literature, the metal oxide catalysts, specifically over the cobalt oxide catalyst produce N_2, N_2O and the dominant product NO. It was further reported that the decomposition of NO and N_2O gives N_2. Strongly bound surface intermediates are required for molecular nitrogen to form on the oxide catalyst surface and a temperature increase reduces the catalyst coverage by such intermediate species, thus suppressing the formation of N_2 and N_2O (Sadykov et al., 2000; Schmidt-Szałowski et al., 1998).

This observation correlates with the experimental results obtained using the synthesised Co_3O_4/SiO_2 and commercial Co_3O_4 catalyst where the mass spectrometer only detected NO and N_2O as products and the N_2 signal was not quantifiable.

As NO, N_2O and N_2 were the only products formed over the cobalt based catalyst, it follows the speculation by Biausque and Schuurman (2010) that the reaction involves the lattice oxygen and proceeds via a Mars and Van Krevelen mechanism. The characteristic feature of this mechanism is that some products of the reaction leave the solid catalysts' surface with one of more constituents of the catalysts' lattice. NO and N_2O are formed through parallel routes from ammonia via surface nitroxyl (HNO) species and decomposition of NO and N_2O gives N_2 (Biausque and Schuurman, 2010; Doornkamp and Ponec, 2000). The formation of N_2O must be

minimised as the gas is environmentally unfriendly and considered a greenhouse gas.

The content of the desired NO product as a fraction of NO plus N_2O was seen to differ slightly for low and high conversions of ammonia. This was done to evaluate the difference with the increase in space time and to determine whether the NO and N_2O compounds would react further amongst themselves when more of the products are present.

According to Biausque and Schuurman (2010), either increase in space time or temperature would lead to a decrease in NO selectivity and an increase in NH_3 conversion. Comparable observations were obtained when doubling the space time lead to an increase in conversion (see Figure 5.10) and a decrease in the NO content as a fraction of NO plus N_2O. However the relative NO content increased with increasing temperature and the same observation was seen with complete conversion of NH_3. A higher NO content as a fraction of NO plus N_2O for the lower NH_3 conversion was seen at temperatures below 600 ℃ and thereafter the high conversion led to a higher NO fraction, thus not completely agreeing with the findings of Biausque and Schuurman (2010).

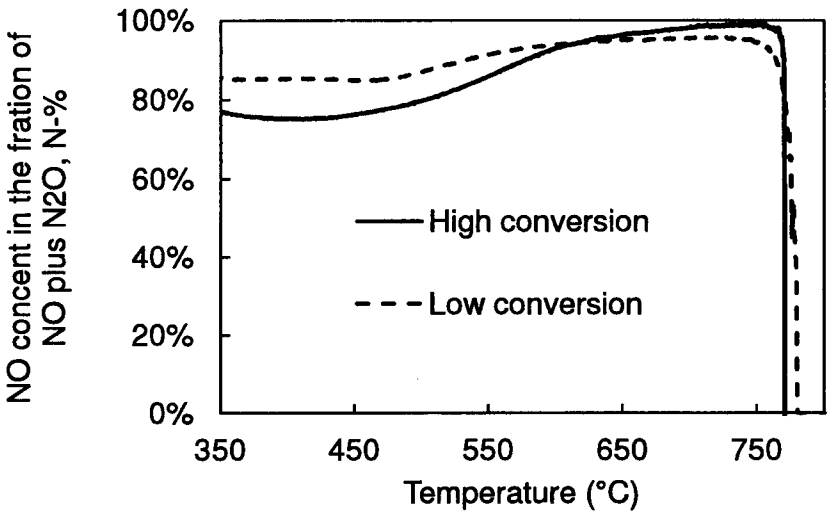

Figure 6.2: Comparing NO-content in the fraction of NO plus N_2O for low and high conversions of NH_3 as a function of reaction temperature

Sadykov et al. (2000) reported that the maximum selectivity to NO of 96% was obtained over a pure Co_3O_4 catalyst at 650 °C under atmospheric pressure. They further reported 94% yield towards NO at 750-800 °C. Both scenarios operating at complete conversion of ammonia. However the selectivity towards N_2O was not provided and thus making it difficult to compare the experimentally obtained data to the literature data. Schmidt-Szałowski et al. (1998), tested the cobalt Co_3O_4 catalyst under ammonia oxidation conditions (720-800 °C and 10 vol.-% NH_3) and provided selectivities towards NO and N_2O under complete conversions of NH_3.

The relative NO fraction as a function of NO plus N_2O was above 97% and close to 99% for the different Co_3O_4 catalyst that underwent different thermal treatments. With similar results, at complete conversion of NH_3, the in-house prepared catalyst achieved a NO content, in the fraction of NO plus N_2O, of 98% at temperature as low as 650 °C. The commercial catalyst was less selective in producing NO with a relative NO fraction of 92.5% at 650 °C and a maximum of 97% at 800 °C.

The selectivity towards NO was increasing as the temperature increased as thermodynamically predicted where the higher temperature would favour the equilibrated formation of NO. This does not correlate with the findings by Sadykov et al. (2000) where the selectivity towards NO passes a maximum and decreases with an increase in temperature from 650 °C to 800 °C. The concentration of NO does go through a maximum as a function of reaction temperature but at the same time the N_2O concentration is relatively high. Hence the temperature at which the maximum amount of NO is formed over the catalyst is not the temperature where NO is the most selective product.

The operating conditions should be optimised to maximise NO selectivity at high conversions of ammonia but limited to below 800 °C to minimise catalyst deactivation seeing that the catalyst severely deactivates at higher temperatures.

6.3 Mass and heat transfer limitations in fixed-bed set-up

Calculations on mass and heat transfer limitations in the fixed-bed set-up was carried out in order to determine the actual activity on the surface of the catalyst and to identify the actual amount of cobalt that is used as a catalyst in the reaction.

6.3.1 External mass and heat transfer limitations

External mass and heat transfer experiments were carried out to determine the effect of the boundary layer around the catalyst particle.

The rate of transport through the boundary layer is dependent on the mass transfer coefficient, which in turn is dependent on the particle size and modelled as follows using the Frössling correlation (Fogler, 1999):

$$r = k_L.a.(C_{A,bulk} - C_{A,s})$$

$$k_L = \frac{D_{A,boundary\ layer}}{d_{particle}}.(2 + 0.6Re^{1/2}Sc^{1/3})$$

$$k_L = \frac{D_{A,boundary\ layer}}{d_{particle}}\left[2 + 0.6\left(\frac{\rho_{fluid}.\mu.d_p}{\mu_{fluid}}\right)^{1/2}.\left(\frac{\mu_{fluid}.d_p}{\rho_{fluid}.D_{A,boundary\ layer}}\right)^{1/3}\right]$$

(Where k_L is the mass transfer coefficient (m/s), a is the external surface area per unit mass (m^2/g), $D_{A,\ boundary\ layer}$ is the diffusion coefficient of reactant through the boundary layer (m^2/s), d_p is the diameter of the particle (m), u the linear velocity (m/s), ρ_{fluid} is the density of the fluid (g/m^3) in the boundary layer and μ_{fluid} is the viscosity of the fluid (g/s.m) in the boundary layer)

Furthermore, by relating the external mass transfer correlation with the internal mass transfer equation, the observed reaction rate could be equated

$$r_{observed} = k_L.a.(C_{A,bulk} - C_{A,s}) = \eta.r_{intrinsic}$$

Upon evaluation of the equations, the maximum concentration gradient is dependent on the observed rate of reaction ($r_{observed}$) and the product of the mass transfer coefficient and external surface area (k_La). k_La and the observed rate of reaction increases with decreasing particle size. Therefore $r_{observed}$ and k_La were evaluated at

both the larger and smaller particle size to determine which regime would enhance external mass transfer limitations.

The catalyst bed contained a low mass of catalyst (ca. 1 mg) and diluted by a much larger mass of SiO_2 (ca. 300 mg, $d_p < 75$ µm). Therefore the calculations carried out relating to the boundary layer investigated were that of the 75 µm SiO_2 support material. The smaller catalyst particles (U3-E, 75-125 µm) resulted in the greater concentration gradient and thus the highest external mass transfer limitations (see Appendix A.3.4). Experiments were carried out using both the smaller and larger catalyst particles to determine the external mass transfer limitations by changing the linear velocity but keeping the space time constant.

1 and 2 mg of U3-E and U3-A catalyst was loaded into the reactor and tested respectively, while keeping the space time constant at 206 g.s/mol NH_3 with a flow of feed gas at 50 mL(NTP)/min and 100 mL(NTP)/min.

The results revealed that changing the linear velocity does not significantly affect the conversion of NH_3 obtained as similar conversion was obtained at various temperatures. The external mass transport limitations were determined for the worst case scenario. Therefore external mass transfer limitations were assumed to be negligible for all particle sizes.

Table 6.1: Investigating external mass transport limitations by varying the linear velocity, i.e. 100 mL(NTP)/min and 200 mL(NTP)/min, and keeping the space time constant at 206 g.s/mol NH_3 using the smallest catalyst particle U3-E (75-125 µm) and U3-A (710-1000 µm)

Liner velocity	Temperature	Conversion of NH_3 (%)	
mL(NTP)/min	°C	d_p (75-125 µm)	d_p (710-1000 µm)
50	480	57.5	6.1
100	580	54.4	5.9
50	480	98.8	32.9
100	580	96.7	29.1

As the external mass transport limitations was assumed to be eliminated, the external heat transfer limitations would also be eliminated due to the link with the boundary layer associated with the catalyst particles (Levenspiel, 1999).

6.3.2 Internal heat transfer limitations in a catalyst particle

The temperature gradient in the catalyst particle can be calculated using the following equation:

$$T - T_S = \frac{D_{eff.}(-\Delta H^{rxn})}{\kappa}.(C_{A,S} - C_A)$$

The maximum temperature difference occurs when the concentration of the reactants in the centre of the catalyst particle approaches zero. Thus the maximum temperature difference can be calculated as follows:

$$T - T_S = \frac{D_{eff.}(\Delta H^{rxn})}{\kappa}.C_{A,S}$$

Molecular diffusion, Knudsen diffusion or configurational diffusion controls the diffusion within the catalyst particle. Therefore it was necessary to investigate which mechanism is more dominant. Configuration diffusion generally applies to catalysts with a pore radius of below 1 nm and thus leaving either molecular diffusion or Knudsen diffusion as the dominant mechanism.

Helium was the diluent and constituted above 70 vol.-% and thus the system was simplified to being a binary gas mixture containing ammonia and helium. The Fuller, Schettler and Giddings relation was used to estimate the molecular gas diffusion and represented by the following equation:

$$D_{NH_3-He} = \frac{10^{-3}.T^{1.75}.\sqrt{\frac{1}{M_{NH_3}} + \frac{1}{M_{He}}}}{p.[(\Sigma v)_{NH_3}^{1/3} + (\Sigma v)_{He}^{1/3}]^2}$$

(Where D_{NH3-He} is the rate of diffusion (cm^2/s), T is the temperature (K), M is the molar mass (g/mol), p is pressure (atm) and v is the molar volume)

Knudsen diffusion is a function of the radius of the pores within the catalyst particle and is given by:

$$D_{NH_3-Knudsen} = \frac{2}{3} . r_{pore} . \sqrt{\frac{8.R.T}{\pi . M_{NH_3}}}$$

(Where $D_{NH3\text{-}Knudsen}$ is the rate of diffusion (m^2/s), r_{pore} is the pore radius (m), T is the temperature (K), M is the molar mass (g/mol) and R the gas constant (J/K.mol))

An average pore diameter (d_{pore}) of 12 nm was determined using mercury porosimetry and the effective diffusivity was calculated as a function of temperature. Molecular diffusion of ammonia in the operating temperature range varied between 3.1 x 10^{-4} m^2/s at 450 °C to a maximum of 5.8 x 10^{-4} m^2/s at 800 °C. Knudsen diffusion of ammonia varied between 3.8 x 10^{-6} m^2/s at 450 °C to a maximum of 4.6 x 10^{-6} m^2/s at 800 °C. Knudsen diffusion is thus the slower rate and hence the dominant mechanism.

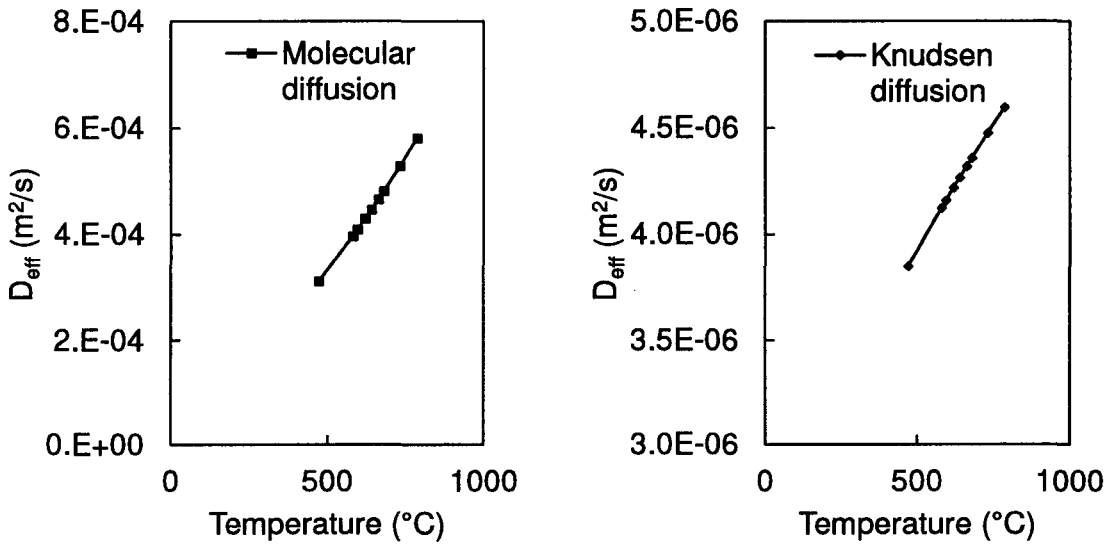

Figure 6.3: Comparison between molecular diffusion of reactant NH_3 and Knudsen diffusion of reactant NH_3 with d_{pore}: 12 nm, to determine the dominant diffusion mechanism

The heat of reaction was calculated on the assumption that only NO is formed as stated in the literature and the product selectivity measurement points out that NO is the dominant product. The heat of reaction decreases (more negative) as the temperature increases (see Appendix A.3.3).

The maximum temperature difference between the catalyst surface and the local temperature in the catalyst particle was calculated under the Knudsen diffusion regime and the calculated heat of reaction at the higher temperatures

The maximum temperature difference was relatively constant, ranging between 2-3 ℃, over the operating temperature range. A temperature change of less than 3 ℃ at high temperatures between 450-800 ℃ is a change of less than 1 percent and thus the catalyst particle was assumed to be isothermal with no heat transfer limitations.

(Note that the thermal conductivity of SiO_2 (1.34 W/(m.K)) was used to represent the temperature difference for the worst case scenario as cobalt oxide has a higher thermal conductivity than SiO_2)

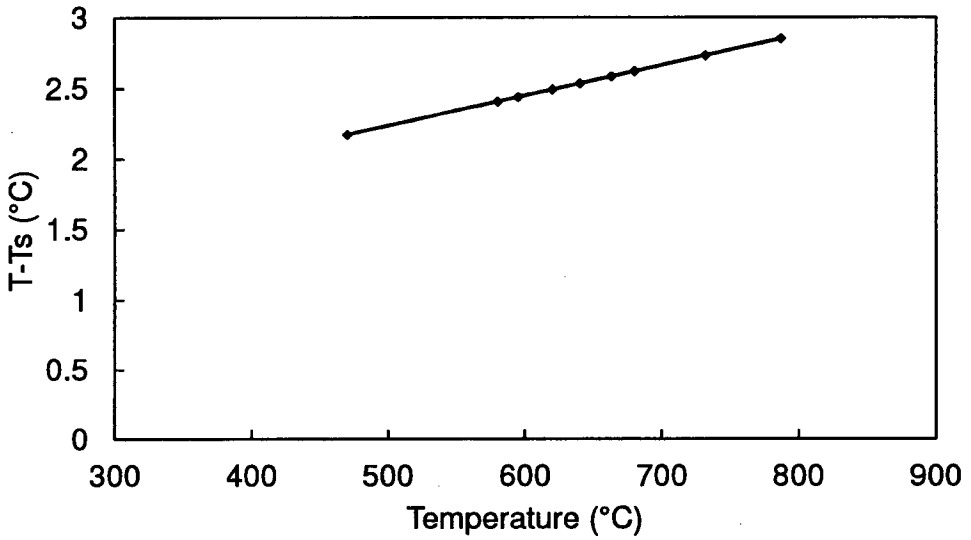

Figure 6.4: Maximum temperature difference between catalyst surface (Ts) and the temperature at the centre of the catalyst particle (T) as a function of reaction temperature

6.3.3 *Internal mass transport in fixed-bed set-up*

The effect of mass transport limitations on the activity of the catalyst can be accounted for by the effectiveness factor (η). The effectiveness factor takes into account the difference between the observed rate of reaction and the intrinsic rate of reaction using the reaction rate proposed by Sadykov et al. (2000):

$$r = -r_{NH_3} = k[NH_3]^{0.36}[O_2]^{0.14}$$

By means of the conversions obtained in the fixed-bed set-up and assuming that NO was the only product formed, the observed rate constant and the resulting observed reaction rate for each of the catalysts was determined (see Appendix A.3.4) .

As the conversion increased with initial increase in temperature from 480 to 580 °C, the activation energy for the individual catalyst could be calculated, assuming that catalyst deactivation has not taken place, using the modified Arrhenius straight line equation with two data points (see Appendix A.3.4):

$$ln(k) = \frac{-E_a}{RT} + ln\,(A)$$

(Where k is the rate constant, E_a is the activation energy and A the frequency/pre-exponential factor)

No noticeable correlation was observed with the activation energy between the different catalysts with the activation energy not showing the expected behaviour where it was expected to decrease with decreasing size, indicating that catalyst deactivation might have been present.

Table 6.2: Reaction activation energy for the individual catalyst at 480-580 °C

Catalyst code	Reaction activation energy (kJ/mol)
U3-A (710-1000 µm)	78.41
U3-B (500-710 µm)	45.52
U3-C (300-510 µm)	41.63
U3-D (125-300 µm)	40.16
U3-E (75-125 µm)	46.92
J1 (pellet) (d_{pellet}: 3 mm, l_{pellet}: 3 mm)	38.01
J1 (crushed) (75-1000 µm)	48.79

The measured NH_3 conversion using Nessler's reagent is an indication of the overall integrated conversion over the entire bed length. Assuming that the total mass of catalyst was uniformly distributed over the bed length within the isothermal zone, the conversion at a particular point in the bed was determined.

By having an initial estimate for the intrinsic rate constant, the intrinsic rate was determined with the concentrations of the reactants calculated at X_0 (first iteration).

The intrinsic rate over the particular section of the bed length/mass of catalyst was used to predict the Thiele modulus (Φ) and consequently the effectiveness factor.

Applying the effectiveness factor to the intrinsic rate, the observed rate and the resulting observed conversion was calculated.

The observed conversion obtained and its concentration was applied as the starting point for the next segment and this iteration was carried out over the total mass of catalyst.

The intrinsic rate constant was solved by equating the final calculated conversion with the overall measured conversion (X_{final} is measured at total catalyst mass = $W_{final} = W_i + dW$).

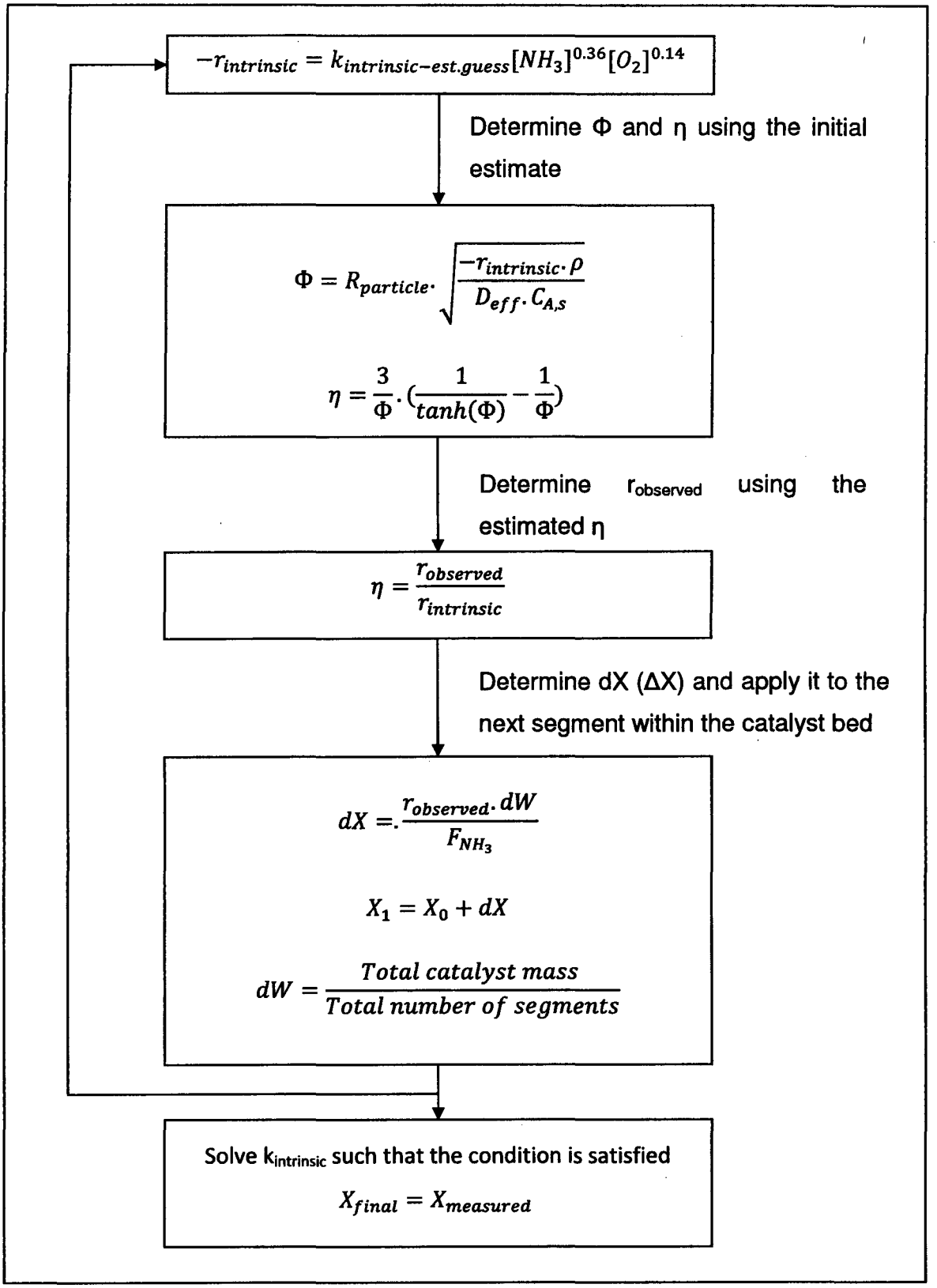

Figure 6.5: Flow diagram showing the layout and equations used to solve for internal mass transport limitations

Mass transport limitations as a function of Co_3O_4/SiO_2 particle size

The Thiele modulus and the resulting effectiveness factor are directly related to the internal mass transfer limitations. Catalyst U3 at its respective particle sizes was tested under ammonia oxidation conditions.

The high errors associated with the Thiele modulus and effectiveness factor will be explained later.

As expected, the effectiveness factor decreases with the increase in Thiele modulus. A maximum effectiveness factor of 0.86 and 0.49 was achieved at reaction temperatures of 470 °C and 580 °C respectively using the catalyst with the smallest particle size (U3-E). The increase in particle size from U3-E to U3-A leads to a decrease in effectiveness factor. At the reaction tempearture of 580 °C, severe mass transfer limitations exist with a Thiele modulus $\Phi > 5$ for all sizes of the catalyst particles with an effectiveness factor of 0.11 for the U3-A catalyst. Mass transfer limitations were less severe at 470 °C with catalyst particles larger than 300 microns resulting in a effectiveness factor of below 0.5.

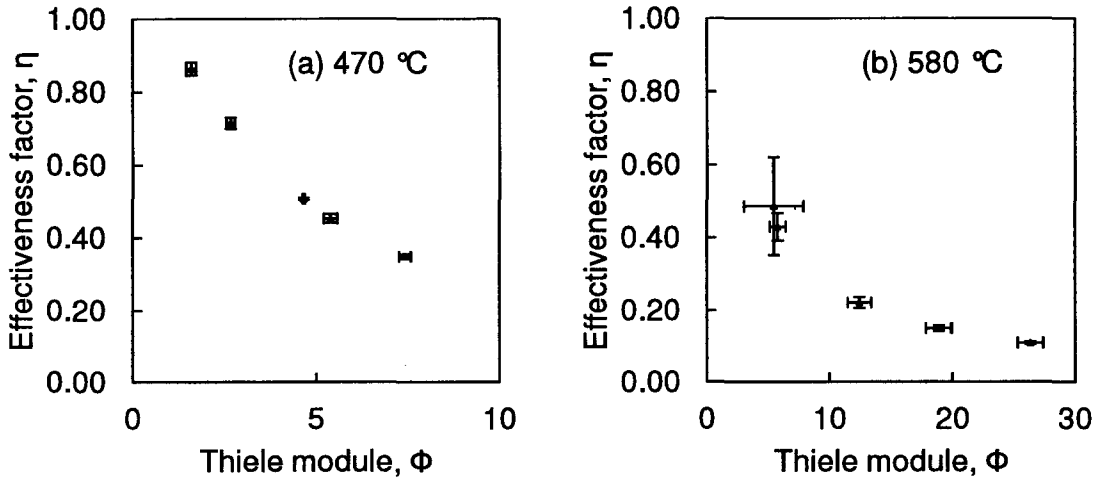

Figure 6.6: Effectiveness factor (η) as a function of Thiele modulus (Φ) for ammonia oxidation at approximate temperatures of (a) 470 °C and (b) 580 °C using the synthesised Co_3O_4/SiO_2 (U3) catalyst

Similar to the outcome obtained at 580 °C, at the reaction temperature of 595 °C, the maximum effectiveness factor of 0.57 corresponded with the U3-E catalyst and a minimum value of 0.1 for the U3-A catalyst. At 620 °C, the U3-E catalyst displayed minor mass transfer limitations with an effectiveness factor of 0.81. Effectiveness factors of below 0.5 were calculated for particles larger than 300 microns.

Similar to the results reported for Figure 6.8, for the reaction temperature of 640 °C, the maximum effectiveness factor of 0.9 was calculated for the U3-E catalyst and a minimum effectiveness factor of 0.1 for the U3-A catalyst. However at a higher temperature of 660 °C less severe mass transfer limitations were observed for the various catalysts with only the U3-A catalyst (size greater than 710 microns) having a Thiele modulus greater than 10 resulting in a effectiveness factor of 0.1. An effectiveness factor of 0.95 was obtained using the U3-E catalyst pointing towards minor mass transport limitations.

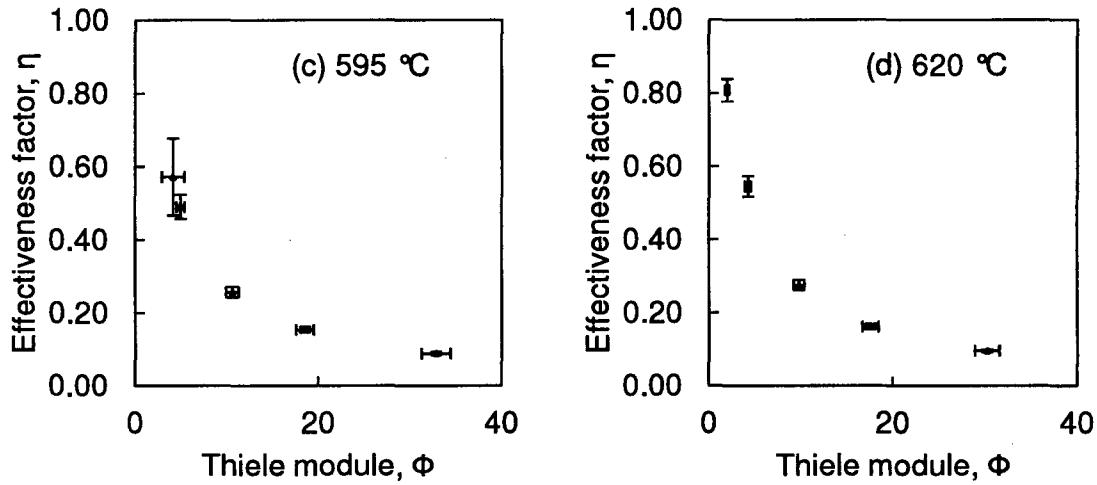

Figure 6.7: Effectiveness factor (η) as a function of Thiele modulus (Φ) for ammonia oxidation at approximate temperatures of (c) 595 °C and (d) 620 °C using the synthesised Co_3O_4/SiO_2 (U3) catalyst

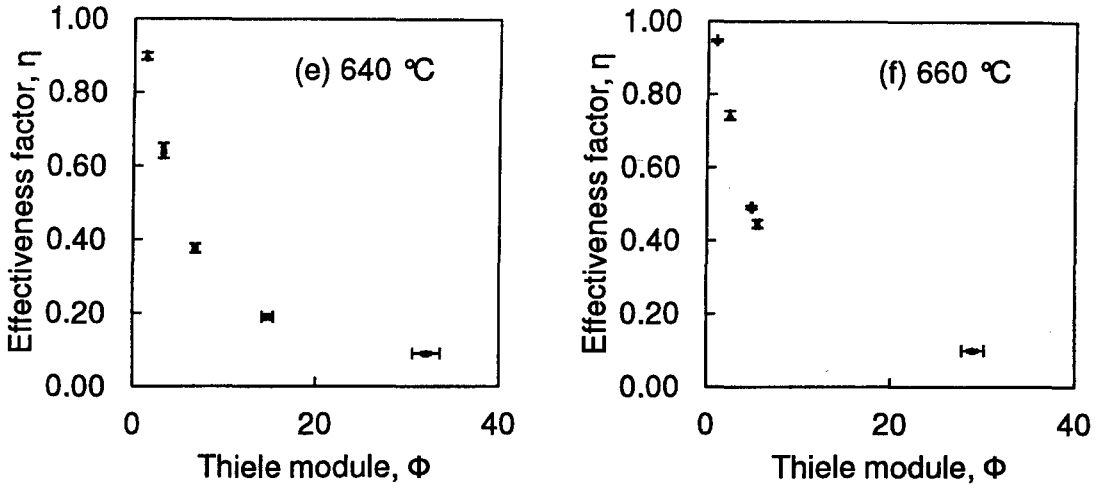

Figure 6.8: Effectiveness factor (η) as a function of Thiele modulus (Φ) for ammonia oxidation at approximate temperatures of (e) 640 °C and (f) 660 °C using the synthesised Co_3O_4/SiO_2 (U3) catalyst

Lower mass transport limitations were observed with an increasing temperature with only the larger particles resulting in an effectiveness factor less than 0.5. Effectiveness factors greater than 0.7 were observed for all the tested Co_3O_4/SiO_2 catalysts when operating at the reaction temperature of 780 °C. However this could be related to the decrease in catalytic activity shown in earlier results with the decrease in ammonia conversion at temperatures above 600 °C (see Figure 5.14).

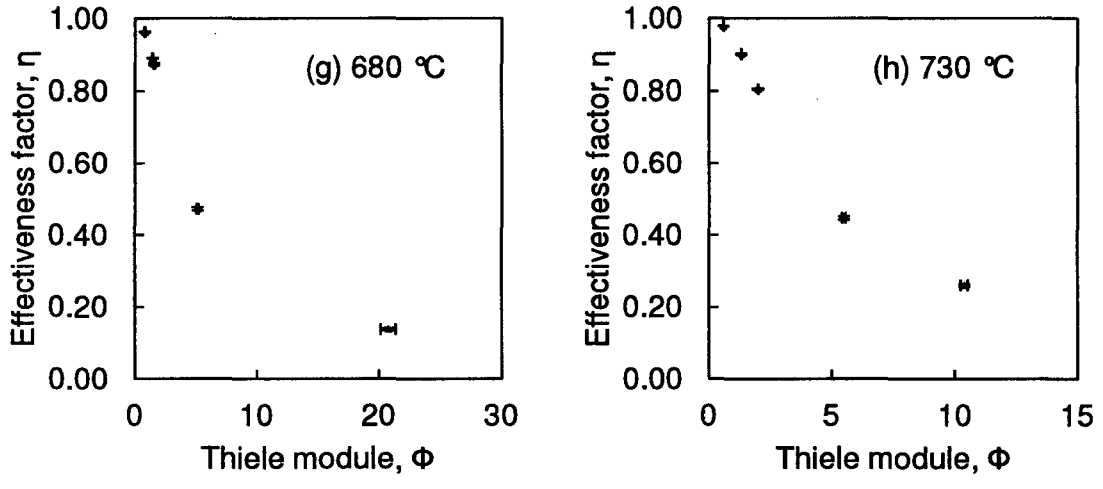

Figure 6.9: Effectiveness factor (η) as a function of Thiele modulus (Φ) for ammonia oxidation at approximate temperatures of (g) 680 °C and (h) 730 °C using the synthesised Co_3O_4/SiO_2 (U3) catalyst

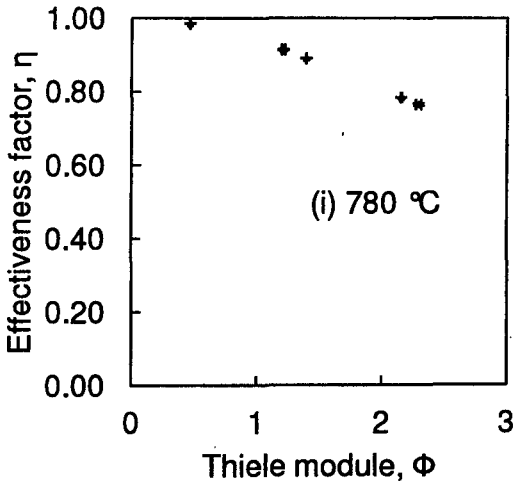

Figure 6.10: Effectiveness factor (η) as a function of Thiele modulus (Φ) for ammonia oxidation at approximate temperatures of (i) 780 ℃ using the synthesised Co_3O_4/SiO_2 (U3) catalyst

Mass transport limitations as a function of temperature

Mass transport limitations as a function of reaction temperature were investigated to find the optimum temperature with the least transport limitations. As the maximum temperature gradient in the catalyst particle was a change of less than one percent of the reaction temperature, the catalyst particle was assumed to be isothermal. Therefore the change in mass transport limitations at the different temperatures would not exist because of the temperature gradient but predominantly due to the change in conversion which leads to a different concentration gradient across the catalyst particle.

Effectiveness factor changes with changes in reaction temperature and is thus dependent of the reaction temperature in the temperature range 450-800 °C. It was evident that the larger catalyst particles illustrated more severe mass transport limitations as compared to the smaller particles. The effectiveness factor was seen to pass through a minimum at conditions where the maximum conversion of ammonia was achieved and thus directly related to the concentration gradient in the catalyst particle. The larger the concentration gradient, the more severe the mass transport limitations would seem. The decrease in conversion and activity of the catalyst would explain the increase in effectiveness factor to approach one at the higher temperatures.

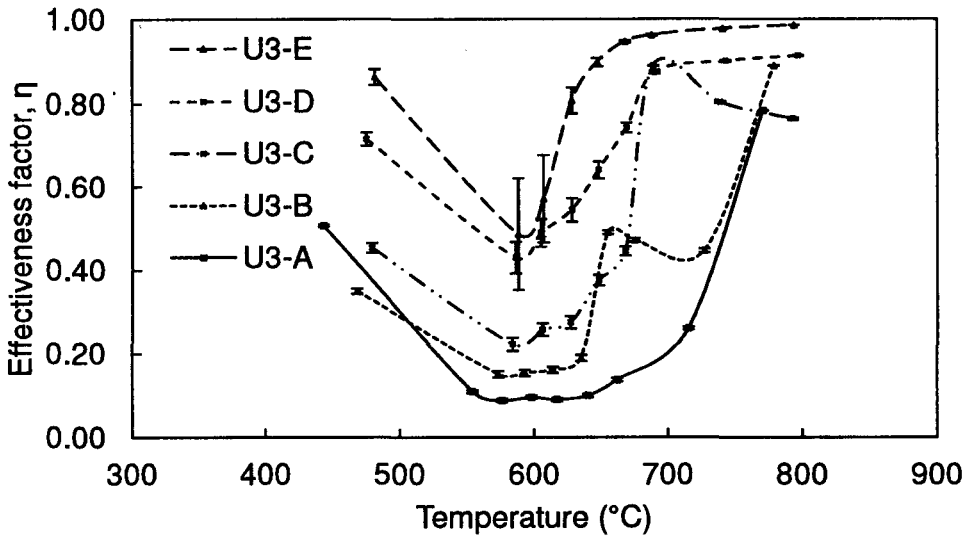

Figure 6.11: Effectiveness factor (η) as a function of reaction temperature for ammonia oxidation at using the synthesised Co_3O_4/SiO_2 (U3) catalyst

The mass transfer limitations of the pure Co_3O_4 commercial catalyst (J1) catalyst were calculated. However, as mentioned before, due to the limited supply of the catalyst, the commercial catalyst was only tested in pellet form and in the crushed form. The pellets were cylindrical in shape with a length and diameter of approximately 3 mm. An average size of 500 microns was assumed for the crushed commercial catalyst based on the average size of the particle sieves used to separate the particles.

The effectiveness factor as a function of reaction temperature was obtained for the commercial catalyst. Effectiveness factors of 0.15 with a minimum effectiveness factor of 0.02 were obtained, indicating severe mass transfer limitation utilising the commercial pellet. The crushed commercial catalyst yielded slightly better results with η ranging between 0.08 and 0.25. Nevertheless, this is still a low value and the commercial catalyst displayed severe mass transport limitations.

Similar to the Co_3O_4/SiO_2 catalyst, the effectiveness factor of the commercial catalyst passes through a minimum having highest mass transport limitations, where a high conversion of ammonia was achieved. In comparison to the synthesised Co_3O_4/SiO_2 catalyst, the commercial catalyst demonstrated smaller changes in effectiveness factor as a function of reaction temperature.

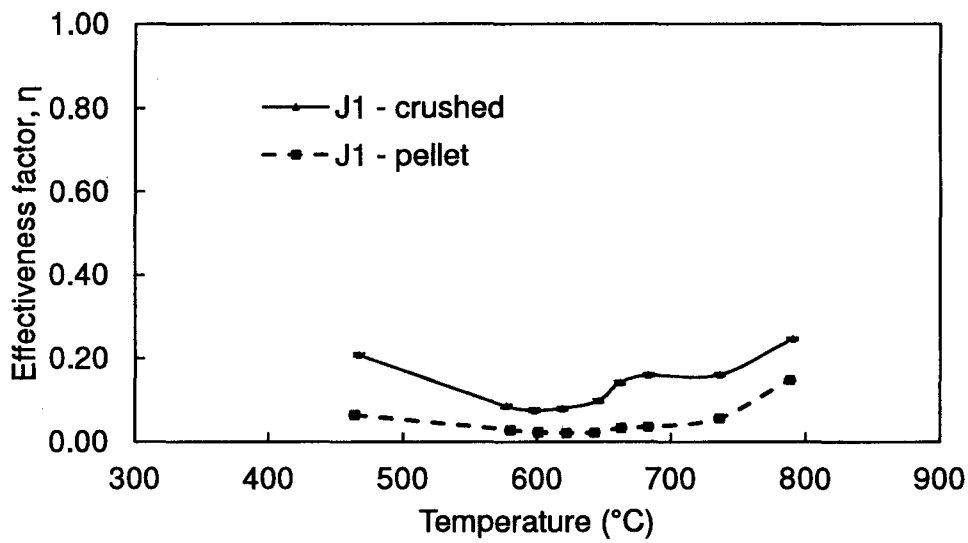

Figure 6.12: Effectiveness factor (η) as a function of reaction temperature for ammonia oxidation at using commercial (J1) catalyst

Therefore it was concluded that the commercial J1 catalyst showed severe mass transport limitations with effectiveness factors of approximately 0.02 for a high conversion of ammonia. This implies that only 2% of the actual cobalt is effectively used as a catalyst in the reaction.

Mass transport parameters over the catalyst bed

To gain a better understanding of the ammonia oxidation fixed-bed set-up, the changes in the mass transport parameters, i.e. conversion, reaction rates, Thiele modulus and effectiveness factors, were investigated down the catalyst bed. This was done by assuming that the catalyst was uniformly distributed down the entire catalyst bed length and by dividing the bed into 100 segments.

$$Total\ mass = \sum_{i=0}^{100} w_i$$

By determining the mass transport parameters after each segment, the changes down the catalyst bed length were observed. The supported in-house prepared catalyst and unsupported commercial catalyst showed similar changes down the catalyst bed. Using the data from the U3-A catalyst at the reaction temperature of 570℃, where the overall observed/integrated conversion of ammonia is below 50%, the changes in mass transport parameters were demonstrated at a specified reaction condition.

The intrinsic rate and the observed rate decreased over the cumulative catalyst mass distributed over the catalyst bed (see Figure 6.13). This was expected as the integrated conversion increased moving down the catalyst bed resulting in a lower concentration of reactants NH_3 and O_2 and thus a lower oxidation rate. The decrease in the rates was seen to be linear with only a small difference in the rates being observed from the top and bottom of the catalyst bed.

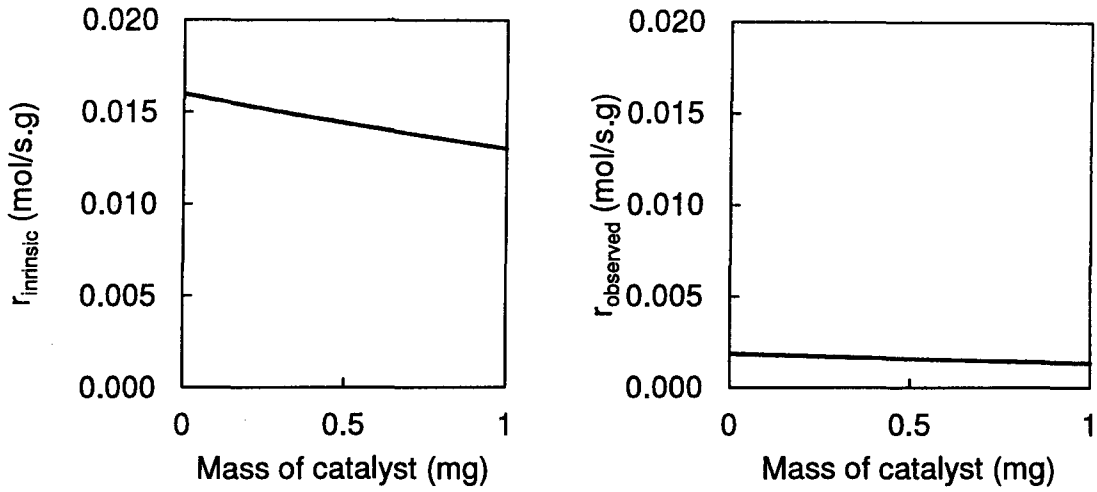

Figure 6.13: For low conversions - change in reaction rates down the catalyst bed, assuming the catalyst is uniformly distributed down the catalyst bed containing 1 mg Co_3O_4/SiO_2

The change in intrinsic rate is exceeded by the change in ammonia concentration, resulting in an increase in the Thiele modulus down the catalyst bed. The increase in Thiele modulus was seen to be a linear increase and thus the effectiveness factor decreases linearly over the catalyst bed. Taking the average value of both Φ and η down the catalyst bed, the relative error for both the parameters was determined to be approximately 4%. Therefore the Thiele modulus and effectiveness factor can be assumed to be constant throughout the catalyst bed.

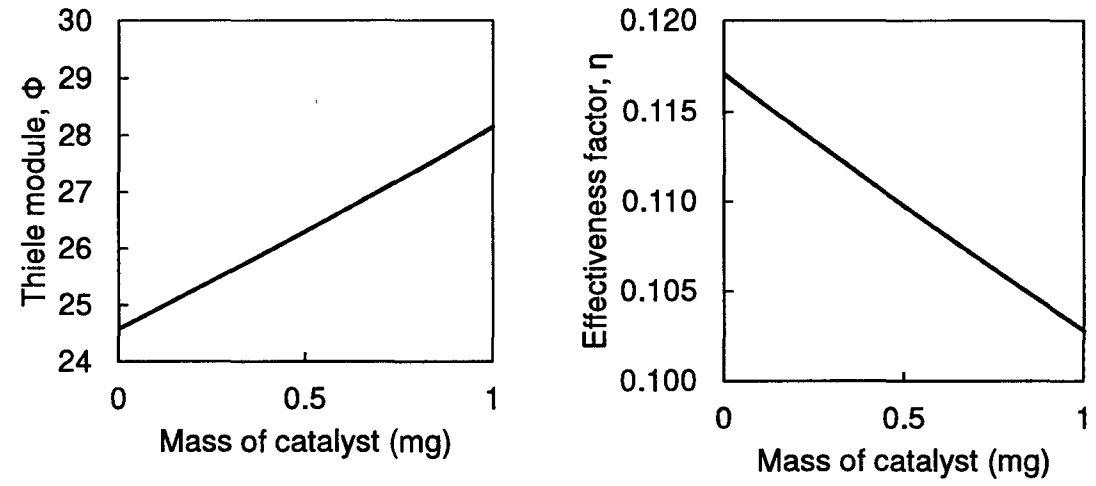

Figure 6.14: For low conversions - change in Thiele modulus (Φ) and effectiveness factor (η) down the catalyst bed containing 1 mg Co_3O_4/SiO_2, assuming the catalyst is uniformly distributed down the catalyst bed containing 1 mg Co_3O_4/SiO_2

The integrated conversion as a function of the catalyst mass was determined to obtain an indication of how the concentrations of the reactants are changing down the catalyst bed. The change in conversion (ΔX) was not constant which indicates that the integrated conversion as a function of catalyst mass was non-linear. However the change in ΔX was not significant and thus a linear fit to the observed conversion yielded similar results.

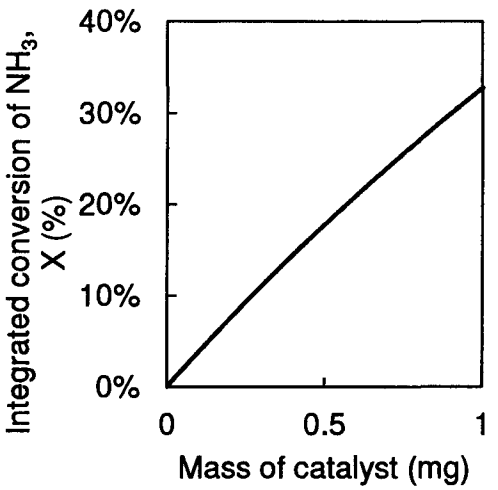

Figure 6.15: For low conversions – the integrated conversion down the catalyst bed, assuming the catalyst is uniformly distributed down the catalyst bed containing 1 mg Co_3O_4/SiO_2

Using the data of the U3-E catalyst, at the same reaction temperature of 570 °C where 98% conversion of NH_3 was achieved, the mass transport parameters displayed a different trend to that observed for the lower conversion.

Similar to the development at the low conversions, the intrinsic rate and the observed rate decreased over the catalyst bed (see Figure 6.13 and Figure 6.16). However the decrease for the high conversion case was not linear and more severe. By taking the average intrinsic rate down the catalyst bed, a much higher relative standard deviation of 45% was calculated in comparison to the 6% at the low conversion of NH_3 indicating severe changes occurring from the top to the bottom of the catalyst bed. Thus explaining the high error associated with all the mass transport parameters at the higher conversions for the previous results (see Figure 6.6 and Figure 6.7).

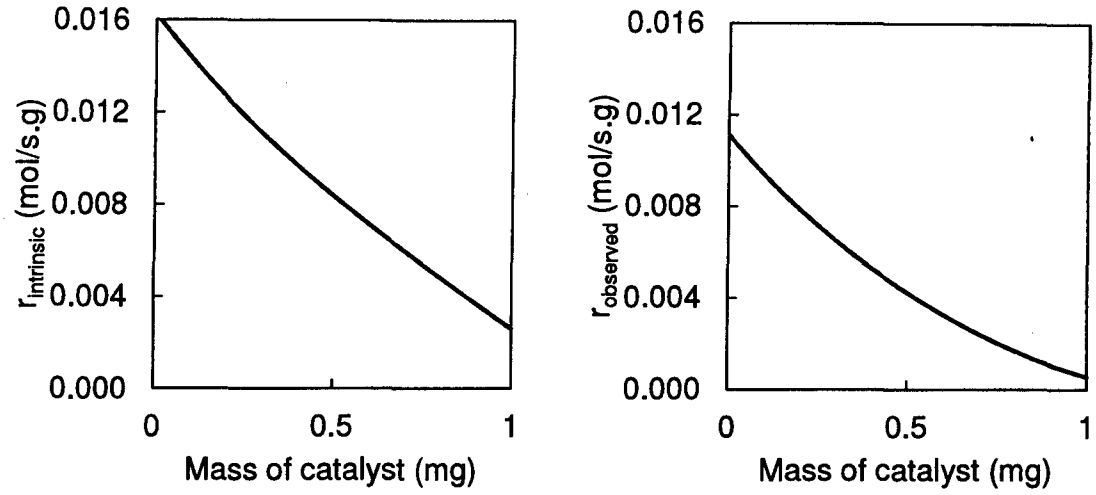

Figure 6.16: For high conversions - change in reaction rates down the catalyst bed, assuming the catalyst is uniformly distributed down the catalyst bed containing 1 mg Co_3O_4/SiO_2

Neither the Thiele modulus nor the effectiveness factor changed linearly as seen for the low conversion case. The Thiele modulus was seen to change by a factor of 5, increasing from just above 2 to a value of 12, down the catalyst bed at the high conversion. The effectiveness factor decreases from 0.7 to approximately 0.23. Therefore by assuming an average value for both the parameters, a large deviation would be associated with the value as seen in the previous results.

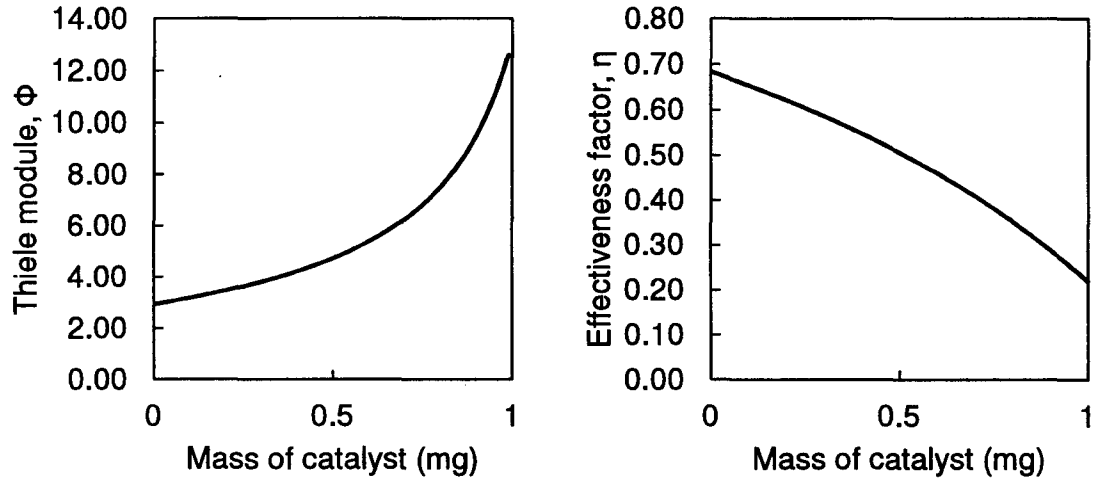

Figure 6.17: For high conversions - change in Thiele modulus (Φ) and effectiveness factor (η) down the catalyst bed, assuming the catalyst is uniformly distributed down the catalyst bed containing 1 mg Co_3O_4/SiO_2

Unlike the case for the low conversion, where the observed conversion can be assumed to increase linearly, the change in conversion was not constant. The change in conversion (ΔX) drops considerably throughout the catalyst bed. As anticipated, the change in conversion is at a maximum where the concentration of reactants is at its maximum, i.e. at the top of the catalyst bed. ΔX is related to the gradient of the integrated conversion, indicating a decrease down the catalyst bed.

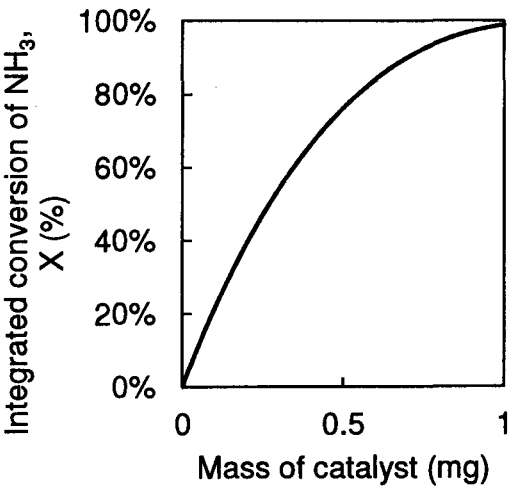

Figure 6.18: For high conversions – the integrated conversion down the catalyst bed, assuming the catalyst is uniformly distributed down the catalyst bed containing 1 mg Co_3O_4/SiO_2

A better understanding of how the parameters change down the catalyst bed length was achieved. The mass transport parameters i.e. $r_{observed}$, $r_{intrinsic}$, Thiele modulus (Φ), effectiveness factor (η) and conversion of NH_3 undergwent significant change at high conversions of NH_3. The changes are less severe at low conversions of NH_3.

6.4 Summary of mass and heat transfer limitations

The ammonia oxidation reaction is an exothermic reaction and has a known heat of reaction associated with it. The amount of heat released by the ammonia oxidation reaction is dependent on the heat of reaction and the rate of reaction, which is a function of the diffusion rate, concentration of compounds involved and the temperature at a certain position within the catalyst particle.

External mass and heat transfer limitations in the fixed-bed set-up were assumed to be negligible with similar conversion of NH_3 obtained while varying the linear velocity and keeping the space time constant.

Diffusion occurs due to the concentration gradient within a catalyst pore via a chemical reaction. The Knudsen diffusion mechanism was determined to be the dominant diffusion mechanism having the slower diffusion rate. This indicates that for the low pressure ammonia oxidation system, the molecules were more likely to collide with the walls of the catalyst pores than with the other molecules and the mean free path lenth between intermolecular collisions are larger than the pore diameter (van Steen, 2010). The Knudsen diffusion rate varied between 3.8×10^{-6} to 4.6×10^{-6} m^2/s for the 450-800 °C temperature range. Assuming that the ammonia oxidation reaction only forms NO, as it is the dominant product, the heat of reaction and the resulting maximum temperature difference (worst case scenario) as a function of reaction temperature was determined.

The maximum temperature difference between the catalyst surface and the local temperature in the catalyst particle does not exceed 3 °C, over the investigated temperature range between 450-800 °C, and thus resulting in a relative temperature difference of below 1%. Therefore the catalyst particle can be assumed to be isothermal with no heat transfer limitations.

Applying the rate law proposed by Sadykov et al. (2000), the activation energy for the commercial catalyst and the in-house prepared catalyst, at its various sizes was determined. Sadykov et al. (2000) reported the activation energy of 37.68 kJ/mol for cobalt catalyst using the proposed rate law. The size and nature of the cobalt catalyst was not given. By comparing the activation energy obtained using the supported and unsupported Co_3O_4 catalyst, the activation energy closest to that

reported by Sadykov et al. (2000) was for an unsupported Co_3O_4 pellet catalyst 38.01 kJ/mol. Thus it could be speculated that the catalyst utilised by Sadykov et al. (2000) was unsupported Co_3O_4 pellets.

The catalyst activity is not measured in a single pore, but rather in the entire catalyst particle. The rate of reaction is governed by the concentration of the compounds and the temperature at the position within the catalyst particle, at which the reaction takes place (van Steen, 2010). It was determined that the temperature is constant, hence the reaction rate and the rate of reaction occurring at the external surface of the catalyst particle may differ due to mass transfer limitations. As mentioned before, the difference in the rate of reaction can be taken into account by defining an effectiveness factor (η).

The effectiveness factor becomes unity for a small Thiele modulus, indicating no transport limitations. The Thiele modulus can be interpreted as the ratio of the rate constant for transport (diffusion) and the rate constant for the reaction and at a given set of reaction conditions, the only parameter that could be varied is the catalyst particle size.

The effectiveness factor for the Co_3O_4/SiO_2 catalyst was severely affected by the different particle sizes at the lower temperatures, before any signs of catalyst deactivation. As expected, the smallest catalyst particle U3-E yielded the effectiveness factor closest to unity. Catalyst particles larger than 300 microns showed severe mass transport limitations with a Thiele modulus value greater than 5 and an effectiveness factor less than 0.5, implying only less than 50% of the actual cobalt is effectively used as a catalyst in the reaction.

The results were obtained by taking an average value down the catalyst bed, and further calculations showed that the mass transport parameter change significantly from the top to the bottom of the catalyst bed, especially in instances where a high conversion of NH_3 was achieved. Both the supported Co_3O_4/SiO_2 catalyst and the commercial pure Co_3O_4 catalyst showed the same trend. A comparison of the change in mass transport parameters between the low conversion of NH_3 below 50% and 98% conversion of NH_3 for the more industrial relevant condition is given as follows:

Table 6.3: Change in mass transport parameters with regards to low and high conversions of NH_3 obtained down the catalyst bed

Change in mass transport parameters	Low conversion	High conversion
$r_{intrinsic}$ and $r_{observed}$	Minimal decrease – constant	Relative deviation from average of 45% for $r_{intrinsic}$ and 65% deviation for $r_{observed}$
Thiele modulus. Φ and effectiveness factor, η	Relative deviation from average of < 6% - constant	Changed by a factor of 5 for Φ and by a factor of 3 for η
Trend of integrated conversion, X	Minimal change in ΔX – linear increase in X	non linear increase in X

The higher conversion resulted in a much greater change in the mass transport parameters from the top to the bottom of the catalyst bed. By taking an average value down the bed a high standard deviation is reflected by use of the error bars for the respective plots. The change from the top to the bottom of the catalyst bed is directly related to the higher conversion achieved. As it was assumed that the particle is isothermal, the significant change is a result of the large concentration gradient down the catalyst bed. The intrinsic and observed rate is directly related to the concentration of the reactants via the proposed oxidation rate by Sadykov et al. (2000). Therefore a high conversion would result in an elevated concentration gradient and significantly change the rates and the subsequent mass transport parameters.

The increase in temperature seemed to result in less severe mass transport limitations with the decrease in Thiele modulus and the resulting effectiveness factor approaching unity. However, the observation was false. As mentioned before, diffusion through the catalyst particle is a result of a concentration gradient which exists due to the catalyst chemical reaction. At higher temperatures, the conversion of NH_3 rapidly decreases, indicating severe catalytic deactivation has occurred. The deactivated catalyst does not promote or enhance the ammonia oxidation reaction any longer and thus no diffusion transport through the particle and hence the intrinsic rate of reaction would be equivalent to the observed reaction rate. Therefore mass transport limitations must be evaluated without any catalytic deactivation.

Mass transport limitations were severely affected by the change in temperature. The increase in temperature did not affect the temperature gradient within the catalyst particle and it could still be assumed to be isothermal. However the increase in temperature did affect the activity of the catalyst as indicated by the conversion of NH_3 passing through a maximum over the temperature range of 450-800 ℃. The maximum mass transport limitations corresponded with the highest conversion of NH_3 obtained at approximately 600 ℃. This means that the higher conversion resulted in a greater concentration gradient and hence more severe mass transport limitations. It was further verified that for the supported Co_3O_4/SiO_2 catalyst, the larger catalyst particles illustrated more severe mass transport limitations (see Figure 6.11). The commercial catalyst showed more severe mass transport limitations compared to the U3 catalyst (see Figure 6.12) but demonstrated smaller changes in effectiveness factor as a function of reaction temperature. For both catalysts, catalyst deactivation was the cause of the less severe transport limitations at the higher temperatures.

6.5 Catalyst deactivation under ammonia oxidation conditions

The in-house prepared catalyst and commercial catalyst experience major deactivation at higher temperatures as indicated by the decrease in NH_3 conversion.

At a particular set of reaction conditions, the pre-exponential factor could be used as an indication of the activity of the catalyst as it is directly related to the amount of catalytically active sites. Using the rate expression given by Sadykov et al. (2000) , the activation energy (see Table 6.2) and rate constants were determined used to calculate the pre-exponential factors at the relative reaction temperatures by applying the Arrhenius equation (see Appendix A.3.4, Table A.4). A decrease in the frequency factor and hence the activity was observed for both the U3 and J1 catalyst.

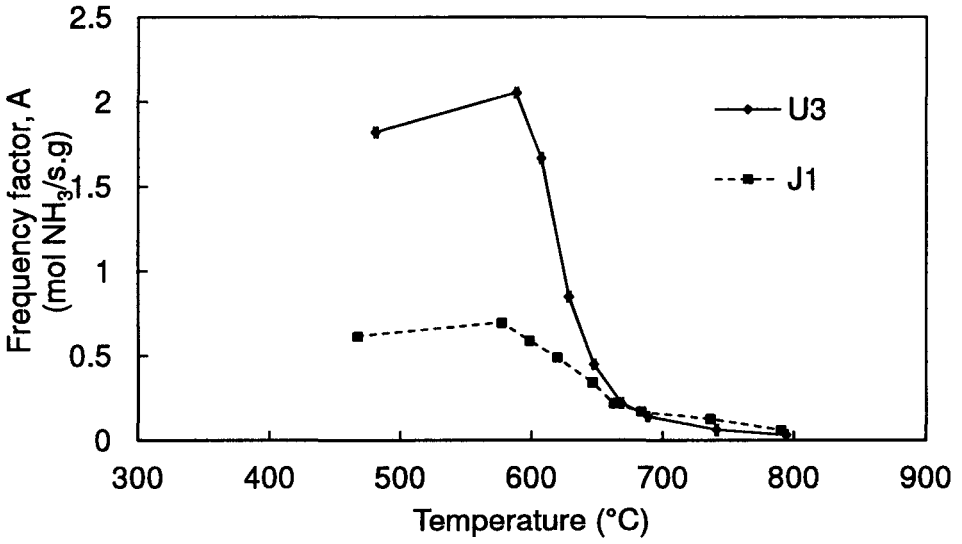

Figure 6.19: An example of the decrease in frequency factor for both the crushed U3 (d_p: 75-125 µm) and J1 (d_p: 75-1000 µm) catalysts during ammonia oxidation as a function of reaction temperature

A higher catalyst mass (ca. 1 mg) was loaded into the reactor so that the catalyst pellets could be recovered and analysed using XRD. The higher mass used resulted in an ammonia conversion of 100% and a higher temperature before decrease in activity was observed: both catalysts U2 and U3 at different cobalt loadings were investigated.

The recovered U2 catalyst was purple in colour but the recovered U3 catalyst maintained the original black colour of the fresh catalyst. The XRD pattern (see Figure 5.24) obtained with the U2 and U3 catalyst after the ammonia oxidation treatment indicated that the catalyst has undergone some change and the pure Co_3O_4 phase has transformed to other cobalt phases. The U2 catalyst showed that the Co_3O_4 phase disappeared with CoO and Co_2SiO_4 being formed. With catalyst U3 some Co_3O_4 was still present and less cobalt silicate was formed. CoO was also observed in this deactivated U3 catalyst but at a very low level. The amount of cobalt which could be detected using XRD was less than the amount of cobalt originally present as Co_3O_4, indicating the presence of cobalt in some X-ray amorphous form, presumably surface silicate. This indicated the deactivation was related to the amount of cobalt content within the catalyst.

The formation of the silicate required the reduction of Co_3O_4 to CoO and should therefore be viewed as a consecutive reaction (Stoia et al., 2010). The CoO phase would be an intermediate in the reaction and could perhaps explain the smaller size and higher deviation shown by the U3 catalyst due to its ongoing transformation. Seeing that the ammonia oxidation reaction proceeds via the Mars and Van Krevelen mechanism, the involvement of lattice oxygen implies a reduction of the oxide under reaction conditions, which may lead to the transformation of the Co_3O_4 phase to the catalytically inactive CoO phase and hence the formation of the silicates.

The phase transition from Co_3O_4 to CoO was reported by both Schmidt-Szałowski et al. (1998) using 10 vol.-% NH_3 content in air and Liotta et al. (2006) using 0.3 vol.-% methane with O_2 and He, where they reported that the transition occurs at temperatures above 700 °C operating with a Co_3O_4 catalyst. The catalyst deactivation seemed to occur at a lower temperature of 600 °C using the synthesised catalyst under ammonia oxidation conditions in the fixed-bed set-up. Hutchings et al. (2006) reported that the transition is dependent on the thermodynamic driving force and thus changing the partial pressures (ammonia content and oxygen content) would affect the temperature range at which the transition occurs. This was further confirmed by Sadykov et al. (2000), who operated using a pure Co_3O_4 catalyst at 1-1.5 vol.-% of ammonia and reported that higher ammonia content would promote the transformation to the inactive CoO phase.

Therefore the point at which the phase transformation occurs is highly dependent on the temperature, ammonia content and the cobalt content within the catalyst.

Using excess oxygen in the reaction could decrease the formation of CoO as it is a reversible transformation (van Steen et al., 2005). However the involvement of the support silica allows the transformation to proceed further to a silicate, which is irreversible. Therefore this could be one of the reasons why the commercial catalyst uses an unsupported pure Co_3O_4 body.

The unsupported catalyst displayed a low content of CoO after exposure to ammonia oxidation conditions. As the Co_3O_4 phase could be recovered by using excess oxygen, low CoO content could be a result of the catalyst being left in a atmospheric environment where oxygen is present, allowing the catalyst to reduce. Therefore the unsupported catalyst undergoes a reversible deactivation mechanism where the active phase of the catalyst could be recovered. This could be the reason why the commercial catalyst is unsupported.

The average crystallite size of the CoO phase (25.2 nm in the case of U2) and the crystallite size of Co_3O_4 phase (26 nm in the case of U3) was very similar to the size of the Co_3O_4 crystallites present in the fresh catalyst. This indicates that sintering and agglomeration is not a major problem with the catalyst as mentioned by Trimm (1995). The structure and activity with time online would be constant if the silicate is not formed. The size of the cobalt silicate phase was much larger, 88.7 nm for the U2 catalyst and 111.2 nm for the U3 catalyst indicating major clustering of the cobalt crystallites with the larger silica support material.

7 CONCLUSIONS

Supported cobalt on silica catalyst was successfully synthesised using the incipient wetness impregnation technique. The size of the cobalt crystallites is dependent on the type and source of the support. Using the incipient wetness impregnation method, the cobalt loading onto the catalyst can be accurately controlled. However, with the preparation method and using a cobalt nitrate solution, cobalt clusters are likely to be formed and thus resulting in a wider size distribution. A pure cobalt Co_3O_4 phase was obtained for the synthesised Co_3O_4/SiO_2 supported catalyst. The commercial catalyst sample for the oxidation of ammonia was an unsupported, pure Co_3O_4 catalyst.

Ammonia oxidation can be successfully carried out using either a supported cobalt Co_3O_4/SiO_2 catalyst or an unsupported pure Co_3O_4 catalyst. The activity of the catalysts passes a maximum with both the supported and unsupported catalyst yielding the highest conversion of NH_3 at approximately 600 °C. The smaller catalyst particle resulted in a higher conversion. Severe catalytic deactivation takes place at higher temperatures. Thermodynamic calculations showed that a higher temperature would favour the formation of NO_x. Only NO, N_2O and N_2 products are formed over the cobalt oxide catalyst. The products NO and N_2O are thought to be formed through the intermediate HNO specie and N_2 is formed through the decomposition of NO and N_2O. The selectivity of NO and N_2O increases with decreasing space time, meanwhile the ammonia conversion is increased by increasing space time and complete conversion of ammonia could be achieved with both supported and unsupported cobalt catalyst. The relative selectivity of NO, as a fraction of NO plus N_2O, increases with increasing temperature before catalyst deactivation takes place. The relative selectivity of NO is higher at lower conversions of ammonia and at lower reaction temperature. The in-house prepared Co_3O_4/SiO_2 catalyst displayed a higher relative NO selectivity compared to the commercial Co_3O_4 catalyst under industrial relevant conditions at complete conversion of ammonia.

Under the regime where Knudsen diffusion is the dominant diffusion mechanism, the maximum temperature difference between the catalyst surface and the local temperature in the catalyst particle can be assumed to be constant, over the

investigated temperature range between 450-800 °C. Therefore the catalyst particle can be assumed to be isothermal with no heat transfer limitations.

Using the rate equation proposed by Sadykov et al. (2000), the commercial catalyst pellets showed severe mass transport limitations with an effectiveness factor 0.02 under conditions where the catalyst is most active. The supported Co_3O_4/SiO_2 catalyst showed severe mass transfer with particles greater than 300 microns. The operating reaction temperature which resulted in the highest conversion of NH_3 would also result in greater mass transport limitations. The catalyst pellets showed smaller change in effectiveness factor as a function of reaction temperature. The mass transport parameters, i.e. intrinsic reaction rate, observed reaction rate, Thiele modulus and effectiveness factor, exhibit small changes over the catalyst bed at low conversions and display significant changes at higher NH_3 conversions which represents more industrial relevant conditions.

Understanding that the ammonia oxidation reaction proceeds via the Mars and Van Krevelen mechanism, the involvement of lattice oxygen implies the reduction of Co_3O_4 to the catalytically inactive CoO phase; a similar phenomenon was observed in literature. The deactivation is reversible by using excess oxygen, however the inclusion of the silica support resulted in the formation of cobalt silicate which is irreversible. The deactivation is highly dependent on temperature, ammonia content in the feed gas and cobalt loading in the catalyst. Sintering of the catalyst was observed to be a minor factor.

Supported Co_3O_4/SiO_2 catalyst with small Co_3O_4 crystallites is an effective catalyst for ammonia oxidation to NO. However, severe mass transport limitations existed with larger catalyst particles and severe irreversible catalytic deactivation in the formation of cobalt silicate occured at higher temperatures.

Support material which can react with CoO under hydrothermal conditions, i.e. silica and alumina should be avoided in the preparation of cobalt catalysts for ammonia oxidation. The operating conditions and the catalyst choice should be optimised to maximise NO selectivity at high ammonia conversion with minimal catalyst deactivation.

8 RECOMMENDATIONS FOR FUTURE WORK

Based on the conclusions drawn from this study, the following recommendations are made:

- Develop a new rate expression determined experimentally and compare the rate expression with that presented by Sadykov et al. (2000).
- Carry out a mass balance on the water produced to determine the ammonia uptake and investigate the product selectivity using on SiC as a catalyst.
- The appropriate choice of support material is crucial and the conventional support materials such as silica cannot be used. Therefore further work would involve an alternative support material. An alternative support material could be zinc aluminate, a material which is highly stable and used as a catalyst support for the STAR-process.
- Larger particles and especially pellets showed severe mass transport limitations implying that a low amount of the actual cobalt is effectively being used as the catalyst in the reaction. An alternative would be to distribute the supported Co_3O_4 as a thin layer on a monolith. The use of a monolith would also aid in reducing the pressure drop in the ammonia oxidation reactor.
- It would help to have a dedicated mass spectrometer directly connected to the effluent stream of the reactor in the same set-up for a more accurate selectivity determination.

9 REFERENCES

Bell, B.H.J. 1960, "Platinum catalyst in ammonia oxidation", *Platinum Metals Review,* vol. 4, pp. 122-126.

Bezemer, G.L., Bitter, J.H., Kuipers, H.P.C.E., Oosterbeek, H., Holewijn, J.E., Xu, X., Kapteijn, F., van Dillen, J.A. & de Jong, K.P. 2006, "Cobalt particle size effects in the Fischer-Tropsch reaction studied with carbon nano-fibre supported catalysts", *Journal of the American Chemical Society,* vol. 128, pp. 3956-3964.

Biausque, G. & Schuurman, Y. 2010, "The reaction mechanism of the high temperature ammonia oxidation to nitric oxide over $LaCoO_3$", *Journal of Catalysis,* vol. 276, pp. 306-313.

Chen, J.G., Wang, X.Z., Xiang, H.W. & Sun, Y.H. 2001, "Stability of $Co/ZrO_2/SiO_2$ catalyst for FT synthesis" in *Natural Gas Conversion 6*, eds. E. Iglesia, J.J. Spivey & T.H. Fleisch, 1st edn, Elsevier, Amsterdam, The Netherlands, pp. 525-529.

Chernyshev, V.I. & Zjuzin, S.V. 2001, "Improved start-up for the ammonia oxidation reaction", *Platinum Metals Review,* vol. 45, no. 34, pp. 40.

Clarke, S.I. & Mazzafro, W.J. 2005, "Nitric acid" in *Kirk-Othmer Encyclopedia of Chemical Technology*, 17th edn, John Wiley & Sons, , pp. 1-27.

Doornkamp, C. & Ponec, V. 2000, "The universal character of the Mars and Van Krevelen mechanism", *Journal of Molecular Catalysis,* vol. 162, pp. 19-32.

EPA 2009, 29 June-last update, *Six Common Air Pollutants* [Homepage of United States Enviromental Protection Agency], [Online]. Available: http://www.epa.gov/air/nitrogenoxides/index.html [2010, April 19] .

Feller, A., Claeys, M. & van Steen, E. 1999, "Cobalt cluster effects in zirconium promoted Co/SiO_2 Fischer-Tropsch catalysts", *Journal of Catalysis,* vol. 185, pp. 120-130.

Fogler, H.S. 1999, *Elements of Chemical Reaction Engineering,* 3rd edn, Prentice Hall, New Jersey.

Hunt, L.B. 1958, "The ammonia oxidation process for nitric acid manufacture", *Platinum Metals Review,* vol. 4, pp. 129-134.

Hutchings, K.N., Wilson, M., Larsen, P.A. & Cutler, R.A. 2006, "Kinetic and thermodynamic considerations for oxygen absorption/desorption using cobalt oxide", *Solid State Ionics,* vol. 177, pp. 45-51.

Iglesia, E., Reyes, S.C., Madon, R.J. & Soled, S.L. 1993, "Selectivity control and catalyst design in Fischer-Tropsch synthesis: Sites, pellets and reactors", *Advances in Catalysis,* vol. 39, pp. 221-302.

Il'chenko, N.I. & Golodets, G.I. 1975, "Catalytic oxidation of ammonia", *Journal of Catalysis,* vol. 39, pp. 73-86.

Kim, C.H., Qi, G. & Li, W. 2010, "Strontium-doped perovskites rival platinum catalysts for treating NO_x in simulated diesel engine", *Science,* vol. 327, pp. 1624-1627.

Levenspiel, O. 1999, "Reactions catalysed by solids" in *Chemical Reaction Engineering,* 3rd edn, John Wiley & Sons, United States of America, pp. 369-427.

Liotta, L.F., Di Carlo, G., Pantaleo, G., Venezia, A.M. & Deganello, G. 2006, "Co_3O_4/CeO_2 composite oxides for methane emissions abatement: Relationship between Co_3O_4-CeO_2 interaction and catalytic activity", *Applied Catalysis B: Environmental,* vol. 66, pp. 217-227.

Liu, Q., Wang, C.L., Chen, M., Cao, Y., He, H.Y. & Fan, K.N. 2009, "Dry citrate-precusor synthesized nanocrystalline cobalt oxide as highly active catalyst for total oxidation of propane", *Journal of Catalysis,* vol. 263, pp. 104-113.

Nell, J. & O'Neill, H.S.C. 1996, "Gibbs free energy of formation and heat capacity of PdO: A new calibration of the Pd---PdO buffer to high temperatures and pressures", *Geochimica et Cosmochimica Acta,* vol. 60, no. 14, pp. 2487-2493.

Ning, Y. & Yang, Z. 1999, "Platinum loss from alloy catalyst gauzes in nitric acid plants", *Platinum Metals Review,* vol. 43, pp. 62-69.

O'Neill, H.S.C. 1987, "Free energies of formation of NiO, CoO, Ni_2SiO_4 and Co_2SiO_4", *American Mineralogist,* vol. 72, pp. 280-291.

Perry, R.H. & Green, D.W. 1997, *Perry's Chemical Engineers' Handbook,* 7th edn, McGraw-Hill, New York.

Petryk, J. & Kołakowska, E. 2000, "Cobalt oxide catalysts for ammonia oxidation activated with cerium and lanthanum", *Applied Catalysis B: Environmental,* vol. 24, pp. 121-128.

Pradyot, P. 2003, *Handbook of Inorganic Chemistry,* McGraw-Hill, New York.

Sadykov, V.A., Isupova, L.A., Zolotarskii, I.A., Bobrova, L.N., Noskov, A.S., Parmon, V.N., Brushtein, B.A., Telyatnikova, T.V., Chernyshev, V.I. & Lunin, V.V. 2000, "Oxide catalysts for ammonia oxidation in nitric acid production: properties and perspectives", *Applied Catalysis A: General,* vol. 204, pp. 59-87.

Schmidt-Szałowski, K., Krawczyk, K. & Petryk, J. 1998, "The properties of cobalt oxide catalyst for ammonia oxidation", *Applied Catalysis A: General,* vol. 175, pp. 147-157.

Skoog, A.D., Holler, F.J. & Crouch, S.R. 2007, "Ultraviolet spectroscopy and UV lasers" in *Principles of Instrumental Analysis*, 6th edn, Thomson Brooks/Cole, , pp. 169-173 and 349-351.

Smith, J.M., Van Ness, H.C. & Abbott, M.M. 1999, "Chemical equilibrium" in *Chemical Engineering Thermodynamics* McGraw-Hill, Singapore.

Solsona, B., Davies, T.E., Garcia, T., Vázquez, I., Dejoz, A. & Taylor, S.H. 2008, "Total oxidation of propane using nanocrystalline cobalt oxide and supported cobalt oxide catalysts", *Applied Catalysis B: Environmental,* vol. 84, pp. 176-184.

Stoia, M., Stefanescu, M., Dippong, T., Stefanescu, O. & Barvinschi, P. 2010, "Low temperature synthesis of Co_2SiO_4/SiO_2 nanocomposite using a modified sol-gel method", *Journal of Sol-gel Science and Technology,* vol. 54, pp. 49-56.

Trimm, D.L. 1995, "Materials selection and design of high temperature catalytic combustion units", *Catalysis Today,* vol. 26, pp. 231-238.

Trimm, D.L. 1980, *Design of Industrial Catalysts,* Elsevier, Amsterdam.

van de Loosdrecht, J., Balzhinimaev, B., Dalmon, J.-A., Niemantsverdriet, J.W., Tsybulya, S.V., Sadykov, V.A., van Berge, P.J. & Visagie, J.L. 2007, "Cobalt Fisher-Tropsch synthesis: Deactivation by oxidation ?", *Catalysis Today,* vol. 123, pp. 293-302.

van Steen, E. 2010, *Heterogeneous catalysis - Basic principles, catalyst synthesis and characterisation, and industrial applications*, Notes edn, University of Cape Town.

van Steen, E., Claeys, M., Dry, M., van de Loosdrecht, J., Viljoen, E.L. & Visagie, J.L. 2005, "Stability of nanocrystals: Thermodynamic analysis of oxidation and re-reduction of cobalt in water/hydrogen mixtures", *Journal of Physical Chemistry B,* vol. 109, pp. 3575-3577.

Vogel, A.I. 1961, "Determination of ammonia" in *Quantitative Inorganic Analysis*, third edn, Longmans, London, pp. 783-785.

Zhuang, Y. 2009, *The performance of structured cobalt catalysts in Fischer-Tropsch synthesis*, PhD Thesis, University of Cape Town.

A APPENDICES

A.1 Thermodynamic product distribution – Scilab code

```
clear;clc;format(20);
function f=eqb(x)
R=8.314; //joules per mole
T=2073; // temp in Kelvin

NH3f=0.071;
O2f=0.194;
Nf=1-O2f-NH3f;
total=10; //total moles basis
NH3=NH3f*total;
O2=O2f*total;
N=Nf*total;
NO=NH3;
H2O=1.5*NH3;

// all delG in kJ/mol
delGO2=0*1000; delGNO=86.6*1000; delGH2O=-228.6*1000; delGNO2=51.3*1000;
delGN2O=104.2*1000; delGN2=0*1000; delGN2O4=97.9*1000;

// x=(yO2(1), yNo(2), yH2O(3), yNO2(4), yN2O(5), yN2(6), yN2O4(7), lamN/RT(8),
lamO/RT(9), lamH/RT(10) )

yo2=x(1); yno=x(2); yh2o=x(3); yno2=x(4); yn2o=x(5); yn2=x(6); yn2o4=x(7);
lamN=x(8); lamO=x(9); lamH=x(10); tot=x(11);
//total=x(1)+x(2)+x(3)+x(4)+x(5)+x(6)+x(7)+x(8); //total moles

f(1)=log(yo2*tot)+2*lamO; //O2
f(2)=delGNO/R/T+log(yno*tot)+lamN+lamO; //NO
f(3)=delGH2O/R/T+log(yh2o*tot)+2*lamH+lamO; //H2O
f(4)=delGNO2/R/T+log(yno2*tot)+lamN+2*lamO; //NO2
f(5)=delGN2O/R/T+log(yn2o*tot)+2*lamN+lamO; //N2O
f(6)=log(yn2*tot)+2*lamN; //N2
f(7)=delGN2O4/R/T+log(yn2o4*tot)+2*lamN+4*lamO; //N2O4
f(8)=NO+2*N-yno*tot-yno2*tot-2*yn2o*tot-2*yn2*tot-2*yn2o4*tot; //N balance
f(9)=(2*O2)-2*yo2*tot-yno*tot-yh2o*tot-2*yno2*tot-yn2o*tot-4*yn2o4*tot; //O balance
f(10)=2*H2O-2*yh2o*tot; //H balance
f(11)=tot-yo2*tot-yno*tot-yh2o*tot-yno2*tot-yn2o*tot-yn2*tot-yn2o4*tot; //total balance
endfunction

//initial guesses for temp at 2073 K
x0 = [0.130 0.000399 0.105 0.0071 0.000285 0.75 0.000735 -
1.01778272527361668 -0.138 8.7 10.12]

//options=optimset("display","iter");
[x, fval]=fsolve(x0,eqb,0.0001)
```

A.2 Instrument calibration

A.2.1 Calibration of mass flow controller

The mass flow controller calibration data sheet sourced from the manufacturers shows that the mass flow controller could achieve a maximum flow rate of 500 mL(NTP)/min for a gas mixture containing 7% NH_3, 19% O_2 and the balance He. The calibration gas mixture that the manufacturers used is different from the feed gas mixture. Therefore the MFC had to be recalibrated using the feed gas, a bubble meter and a stop watch. At each set percentage, multiple readings were taken and by taking the average value and the deviations associated with the average value, the flow and error bars were determined.

The mass flow controller fits a linear profile with respect to flow rate and the set-point percentage. As a result, the maximum flow rate that the MFC can achieve is 564 mL(NTP)/min at a set-point of 100%.

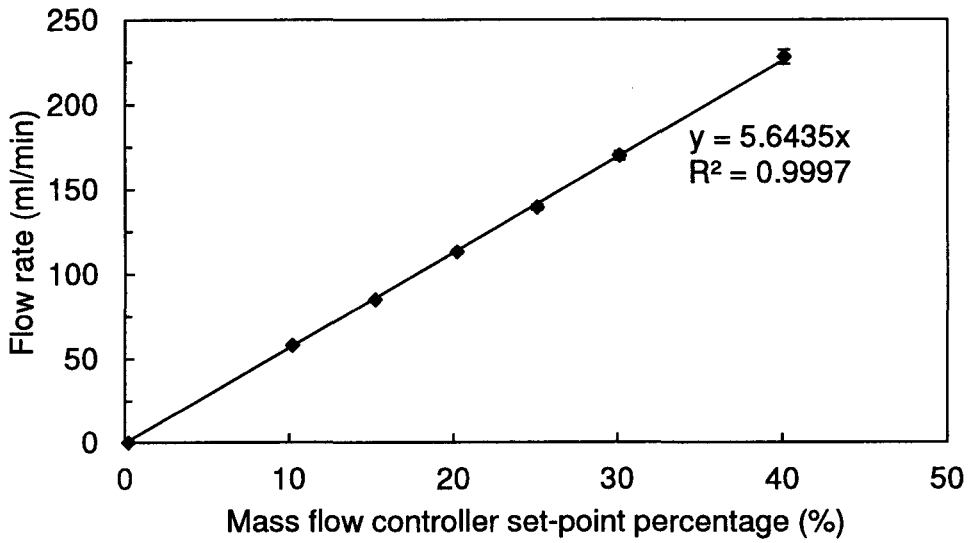

Figure A.1: Calibration of MFC using feed gas mixture

A.2.2 Ultraviolet-visible spectroscopy

In ultraviolet-visible spectroscopy (UV/Vis), the ratio of the intensity of light passing through the sample (I) with the intensity of light before it passes the sample (I_0) is used to determine the concentration of the sample.

This ratio is also otherwise known as transmittance and by applying the Beer-Lambert law, the concentration of the absorbed species can be determined (Skoog et al., 2007).

$$A = log_{10}\left(\frac{I_0}{I}\right) = \epsilon \times c \times l$$

$$A = -log_{10}(\frac{T\%}{100})$$

Nessler's reagent is not a clear solution and thus the amount of reagent added to the ammonium salt solution would affect the intensity of the colour and hence the transmission. An approximately concentration of approximately 10 mg/l NH_3^+ sample was prepared by diluting a 30 wt.-% NH_4OH solution. A test was conducted to determine the amount of Nessler's reagent that should be added to 10 mL of a 10 mg/l NH_3^+ sample that would provide a relatively constant transmission.

It was established that after adding 6-7 drops of Nessler's reagent to a 10 mL sample, the colour intensity stays constant (see Figure A.2). Therefore every sample analysed contained 10 mL of the ammonium salt solution and 7 drops of Nessler's reagent.

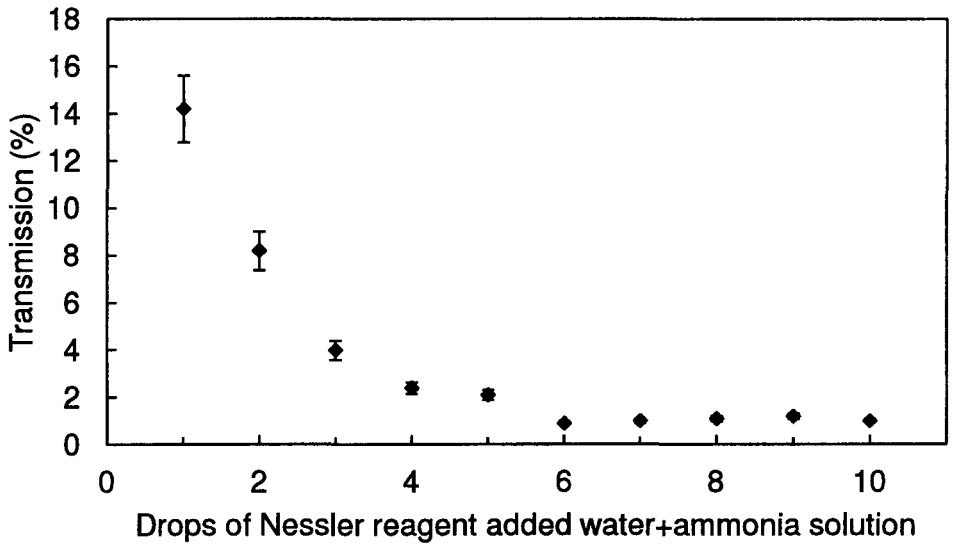

Figure A.2: Determining the amount of Nessler's reagent necessary to obtain a constant transmission reading using 10 mL of a 10 mg/l NH_3^+ sample

A.2.3 Calibration of mass spectrometer

The gas with known concentrations containing 1.3% NO, 1.43% N_2O, 1.42% NO_2 and the balance N_2 was used to calibrate the intensities of the mass spectroscopy signals. The signals were normalised with the baseline and the standard deviation being calculated and the following calibration curve was obtained:

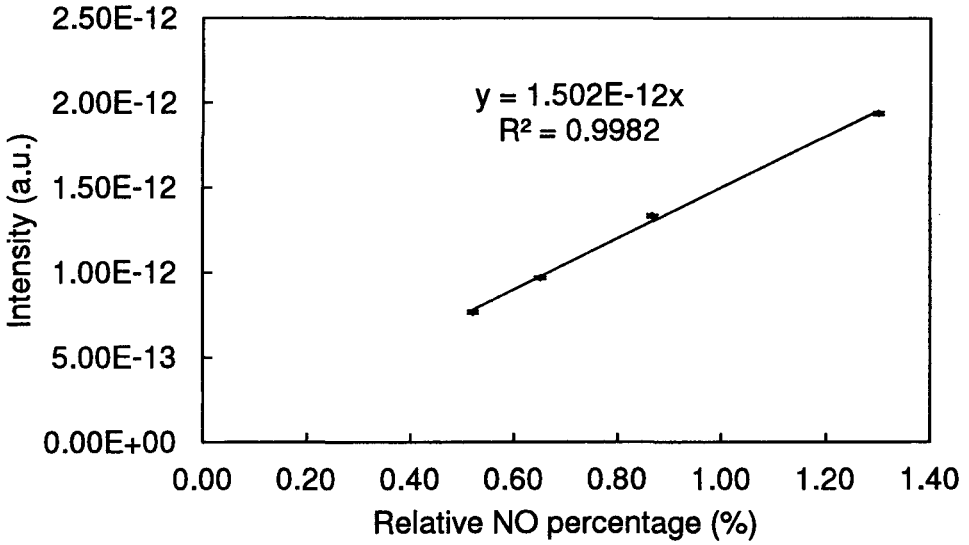

Figure A.3: Calibration curve of the normalised intensity signals with the known concentrations of NO

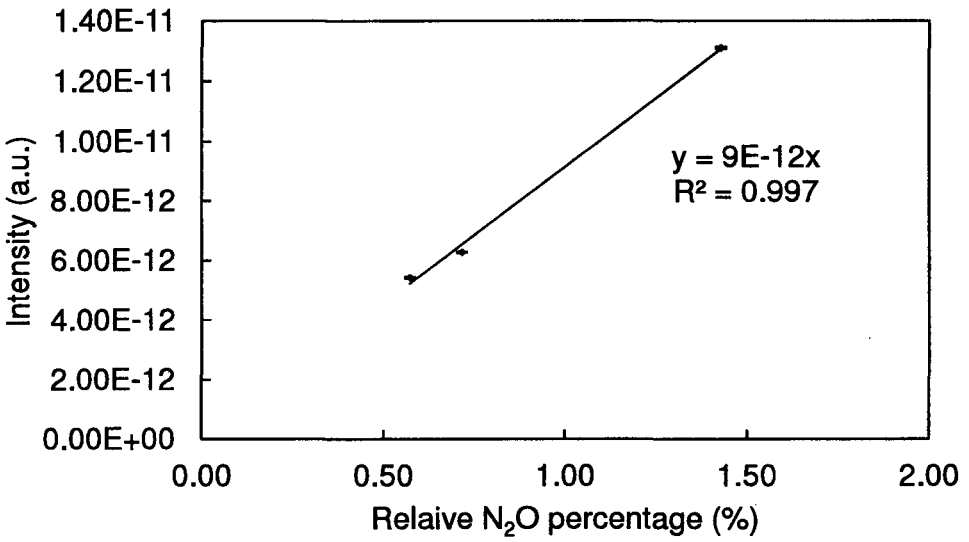

Figure A.4: Calibration curve of the normalised intensity signals with the known concentrations of N_2O

A.3 Catalyst characteristics and ammonia oxidation test

A.3.1 TEM image analysis

Image J was used to convert the picture to a greyscale image. The image was then manipulated in terms of its contrast and brightness to isolate the cobalt metal particles. The software allows the user to set a scale and take measurements accordingly.

It was observed that the image which has been adjusted improves the outline of the cobalt crystallites which allows the user to gain a better analysis of the TEM image and achieve a more accurate measurement of the particles.

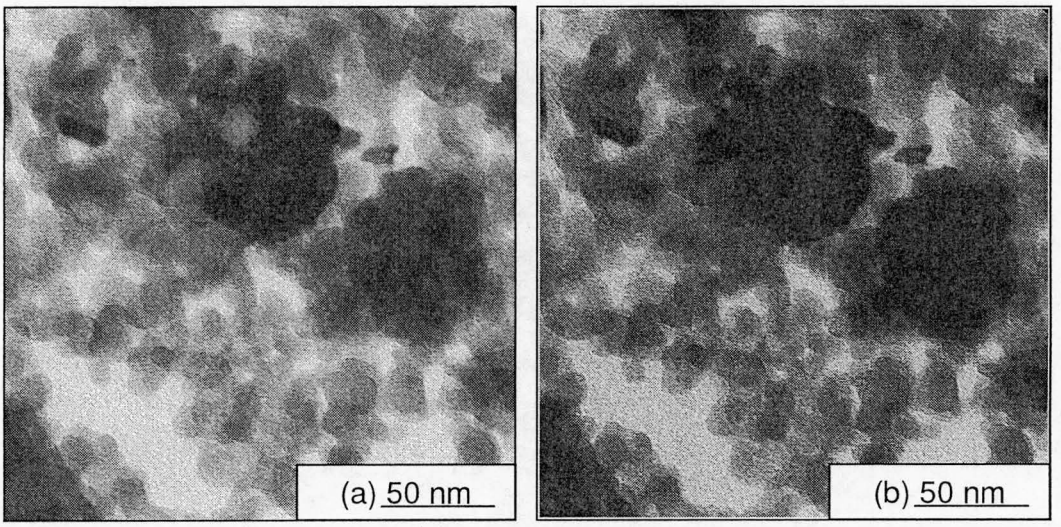

Figure A.5: TEM image of U3 catalyst before and after contrast and brightness adjustments (a) Raw TEM image of catalyst U3 (b) adjusted TEM image

A.3.2 Ammonia conversion calculations

Below is a sample calculation of how the conversion of NH_3 was determined:

The effluent was passed through a water solution for 20 min.; thereafter the water solution transferred and filled up to a 500 mL volumetric flask. 10 mL of this ammonia + water solution was taken and diluted to a total volume of 500 mL.

Operating temperature of 550 ℃ using U3-A catalyst:

Spectrophotometric readings using Nessler's reagent: 4 readings: 34.9; 33.9; 33.4; 33.7

Average reading: 33.60 with a standard deviation of 0.245

$$\frac{T}{T_0}(\%) = \frac{Average\ reading}{Blank\ reading} \times 100 = \frac{33.60}{53.733} \times 100 = 62.53$$

$$y = \ln\left(\frac{T}{T_0}\right) = 4.136$$

$$Using\ the\ straight\ line\ equation\ y = mx + c\ @450nm = y = -0.177x + 4.6$$

$$ammonia\ concentration\ \left(\frac{mg}{l}\right) = x = \frac{y - c}{m} = \frac{4.136 - 4.6}{-0.177} = 2.66$$

$$As\ the\ solution\ came\ from\ a\ 500ml\ bottle, the\ ammonia\ mass = \frac{2.66}{2} = 1.33\ mg$$

$$1.33\ mg\ resulted\ from\ 10\ ml\ of\ the\ ammonia + water\ solution,$$

$$Total\ ammonia\ recovered\ in\ effluent = 1.33 \times 50 = 66.50\ mg = 3.911\ mol\ NH_3$$

$$Total\ moles\ in\ using\ ideal\ gas\ equation = 100\frac{ml}{\min} = 4.09\frac{mmol}{min}$$

$$Total\ ammonia\ in = 7.10\% \times 4.09\frac{mmol}{min} \times 20\ min = 5.81\ mmol$$

$$Ammonia\ conversion\ (\%) = \frac{NH_3in - NH_3out}{NH_3in} \times 100 = \frac{5.81 - 3.911}{5.81} \times 100 = 32.68\%$$

The measured conversion of ammonia was then subtracted from the conversion obtained during the blank run to determine the conversion of ammonia due to the catalyst.

Similarly, the conversions using different catalyst and different conditions were calculated.

Table A.1: Calculated conversion of NH_3 for each the catalysts at the various reaction temperatures

Approx. Temp. (℃)	Measured conversion of NH3						
	U3-A	U3-B	U3-C	U3-D	U3-E	J1 - pellet	J1 - crushed
470	6.08%	19.54%	28.51%	36.36%	57.49%	32.47%	18.25%
580	32.78%	42.46%	54.83%	68.61%	98.94%	62.75%	43.81%
595	38.62%	41.34%	48.37%	60.75%	95.64%	63.09%	42.62%
620	35.91%	39.43%	45.42%	53.78%	67.71%	65.92%	40.61%
640	37.35%	33.93%	33.03%	42.20%	43.94%	63.89%	34.03%
660	34.12%	11.16%	26.73%	30.34%	25.67%	50.05%	24.42%
680	25.53%	11.70%	3.97%	15.04%	18.74%	46.55%	21.44%
730	12.94%	12.38%	7.07%	11.57%	10.98%	32.26%	20.84%
780	1.75%	1.67%	8.48%	9.92%	7.22%	13.04%	13.07%

The errors associated with the measurements were also calculated and taken into account:

$$Ammonia\ conversion = X = 1 - \frac{NH_3out}{NH_3in}$$

$$\partial X = \left(\frac{\partial X}{\partial NH_3out}\right)_{NH_{3,in}} \times \partial NH_3out + \left(\frac{\partial X}{\partial NH_3in}\right)_{NH_{3,out}} \times \partial NH_3in$$

Taking the derivative of the initial equation,

$$\partial X = -\frac{1}{NH_3in}.\partial NH_3out + \left(\frac{NH_3in}{NH_3in^2}\right).\partial NH_3in$$

$$\partial X = -\frac{-NH_3out}{NH_3in}\left(\frac{\partial NH_3out}{NH_3out}\right) + \left(\frac{NH_3in}{NH_3in}\right)\left(\frac{\partial NH_3in}{NH_3in}\right)$$

By substituting initial equation

$$\frac{\partial X}{X} = -\left(\frac{1-X}{X}\right)\left(\frac{\partial NH_3out}{NH_3out}\right) + \left(\frac{1-X}{X}\right)\left(\frac{\partial NH_3in}{NH_3in}\right)$$

$$\left(\frac{\partial X}{X}\right)_{max} = \left(\frac{1-X}{X}\right)\left|\left(\frac{\partial NH_3out}{NH_3out}\right) + \left(\frac{\partial NH_3in}{NH_3in}\right)\right|$$

A.3.3 Heat of reaction

The heat of reaction changes with temperature and assuming only NO is formed, the heat of reaction for the ammonia oxidation reaction as a function of temperature was calculated at represented as follows:

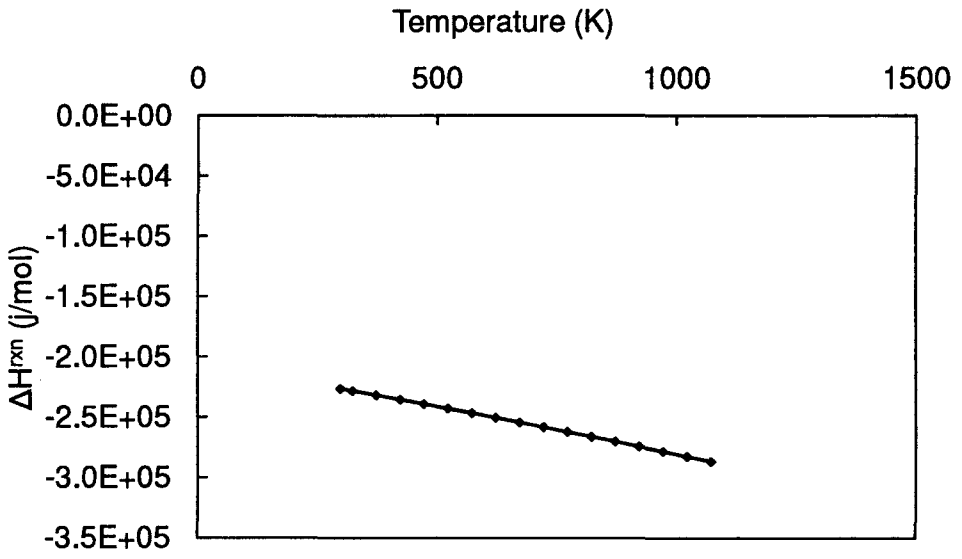

Figure A.6: ΔH^{rxn} as a function of temperature for the ammonia oxidation reaction to determine heat and mass transport limitations

A.3.4 External and internal mass and heat transfer

Calculating the observed rate constant:

Using the rate law proposed by Sadykov et al. (2000):

$$\frac{dX}{dW} = -r_{NH_3} = k[NH_3]^{0.36}[O_2]^{0.14}$$

Applying the definition of a gas-phase reaction, the definition of concentration of ammonia and oxygen along with the stoichiometric reaction and assuming an isothermal particle with no pressure difference and ε represents the change in moles within the system relative to the reactant NH_3:

$NH_3 + 1.25O_2 \rightarrow NO + 1.5H_2O$ $\Delta H^{rxn}_{25℃} = -226$ kJ/mol

$$C_{NH_3} = \frac{F_{NH_3}}{v} = \frac{F_{NH_3,in}(1-X)}{v} = C_{NH_3,in}\frac{(1-X)}{(1-\varepsilon X)}$$

$$C_{O_2} = \frac{F_{O_2}}{v} = C_{O_2,in}\frac{(\frac{19.4}{7.1} - 1.25X)}{(1-\varepsilon X)}$$

$$Where\ \varepsilon = 1.5 + 1 - 1.25 - 1 = 0.25$$

$$\frac{dX}{dW} = k\left[C_{NH_3,in}\frac{(1-X)}{(1-\varepsilon X)}\right]^{0.36}\left[C_{O_2,in}\frac{\left(\frac{19.4}{7.1} - 1.25X\right)}{(1-\varepsilon X)}\right]^{0.14}$$

$$kW = \int_0^X \frac{1}{\left[C_{NH_3,in}\frac{(1-X)}{(1-\varepsilon X)}\right]^{0.36}\left[C_{O_2,in}\frac{(\frac{19.4}{7.1} - 1.25X)}{(1-\varepsilon X)}\right]^{0.14}}$$

Taking the integral from zero to the measured conversion and dividing by space time, the observed rate constant was determined

Table A.2: Observed rate constants for each the catalysts at the various reaction temperatures

Approx. Temp. (℃)	Observed rate constant, k (mol NH_3/s.g)						
	U3-A	U3-B	U3-C	U3-D	U3-E	J1 - pellet	J1 - crushed
470	2.39E-04	7.97E-04	1.20E-03	1.57E-03	2.69E-03	5.35E-05	5.70E-04
580	1.49E-03	1.99E-03	2.70E-03	3.61E-03	6.82E-03	1.24E-04	1.59E-03
595	1.81E-03	1.96E-03	2.35E-03	3.11E-03	6.26E-03	1.27E-04	1.56E-03
620	1.69E-03	1.88E-03	2.21E-03	2.70E-03	3.63E-03	1.36E-04	1.49E-03
640	1.78E-03	1.60E-03	1.56E-03	2.05E-03	2.15E-03	1.32E-04	1.24E-03
660	1.63E-03	4.95E-04	1.25E-03	1.43E-03	1.19E-03	9.83E-05	8.70E-04
680	1.20E-03	5.26E-04	1.74E-04	6.84E-04	8.62E-04	9.12E-05	7.65E-04
730	6.00E-04	5.72E-04	3.21E-04	5.33E-04	5.05E-04	6.16E-05	7.60E-04
780	8.06E-05	7.60E-05	3.97E-04	4.69E-04	3.37E-04	2.41E-05	4.77E-04

External mass transfer calculation:

Using the data prior to catalyst deactivation at 480 °C for catalyst U3-A (710-1000 µm - large particle) and U3-E (75-125 µm – small particles) the external mass transport limitations were solved simultaneously with the internal mass transport limitation to determine whether the smaller or larger particles would result in the higher external mass transfer limitation. An iterative process was carried out where an initial surface concentration was estimated and the equation solved such that $r_{observed}$ initial is equal to the final calculated $r_{observed}$.

$$r_{observed} = k_L . a . (\Delta C_A)$$

$$k_L = \frac{D_{A,boundary\ layer}}{d_{particle}} . (2 + 0.6 Re^{1/2} Sc^{1/3})$$

$$k_L = \frac{D_{A,boundary\ layer}}{d_{particle}} \left[2 + 0.6 \left(\frac{\rho_{fluid} \cdot \mu . d_p}{\mu_{fluid}} \right)^{1/2} . \left(\frac{\mu_{fluid} \cdot d_p}{\rho_{fluid} \cdot D_{A,boundary\ layer}} \right)^{1/3} \right]$$

$$-r_{intrinsic} = k_{intrinsic} [NH_3]^{0.36} [O_2]^{0.14}$$

$$\Phi = R_{particle} \cdot \sqrt{\frac{-r_{intrinsic} \cdot \rho}{D_{eff} . C_{A,S}}} \quad ; \quad \eta = \frac{3}{\Phi} . \left(\frac{1}{tanh(\Phi)} - \frac{1}{\Phi} \right)$$

$$r_{observed} = \eta . r_{intrinsic}$$

$$\Delta C_A = \frac{r_{observed}}{k_L . a}$$

Note that the size of 75 µm was used for d_p as the catalyst particle was highly diluted by the smaller SiO_2 particles. Thus the boundary layer along the bed would be that or the silica particle.

The following results were obtained:

Table A.3: Change in $r_{observed}$ and k_La to determine which particle size would result in higher mass transfer limitations

	NH_3 conversion (%)	$r_{observed}$ (mol/s.g)	k_La (m^3/s.g)	ΔC_A, $r_{observed}/k_La$ (mol/m^3)
U3A	6.1	2.95E-04	1.62E-03	0.18
U3-E	57.5	2.73E-04	6.91E-03	0.40

Therefore this indicates that the smaller particles would result in the maximum external mass transport limitations.

Sample calculation of activation energy and pre-exponential factor:

Using the data obtained from U3-D catalyst, the rate constant (k) determined at 470 ℃ (1.57 x 10^{-3} mol/s.g) and 580 ℃ (3.61 x 10^{-3} mol/s.g) was used to determine the activation energy of the catalyst.

Applying the rate constants to the Arrhenius straight line equation, the activation energy and pre-exponential factor (y-intercept) and activation energy (line gradient) was determined.

$$ln(k) = \frac{-E_a}{RT} + ln\,(A)$$

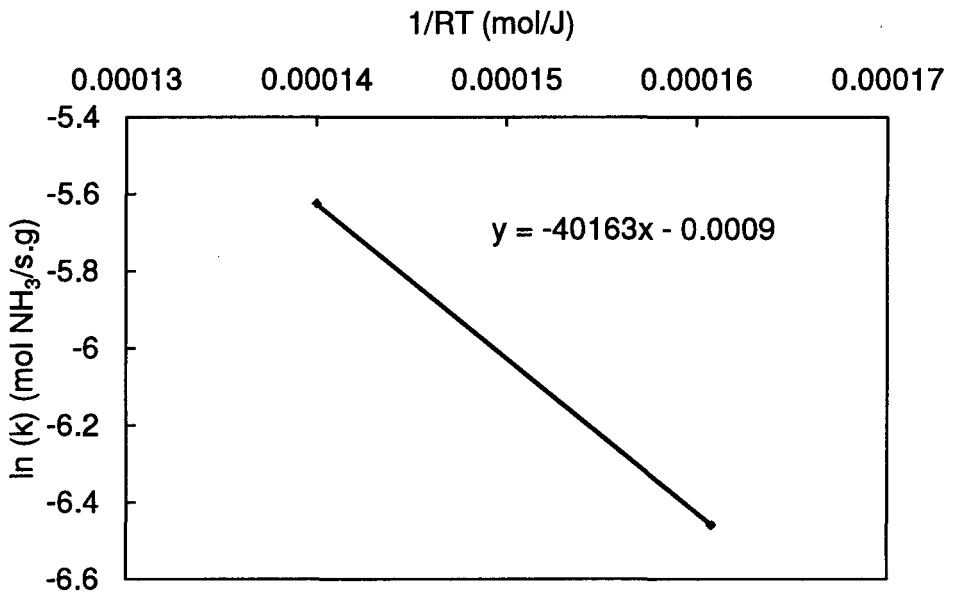

Figure A.7: Sample linear plot of the modified Arrhenius equation to determine the activation energy of the reaction

The pre-exponential factor was determined by assuming constant activation energy and using the respective rate constants:

$$ln(A) = ln(k) - \frac{-E_a}{RT}$$

Table A.4: Pre-exponential factor (A) for each the catalysts at the various reaction temperatures

Approx. Temp. (℃)	Pre-exponential factor (A) (mol NH_3/s.g)						
	U3-A	U3-B	U3-C	U3-D	U3-E	J1 - pellet	J1 - crushed
470	126	1.290	0.932	0.999	4.786	0.026	1.585
580	134	1.290	0.932	0.999	4.786	0.026	1.585
595	122	1.091	0.700	0.159	3.815	0.024	1.315
620	85.5	0.901	0.577	0.128	1.905	0.022	1.074
640	71.8	0.666	0.357	0.095	0.992	0.019	0.734
660	50.2	0.181	0.255	0.064	0.479	0.013	0.463
680	29.0	0.170	0.032	0.030	0.306	0.011	0.354
730	8.44	0.137	0.045	0.018	0.132	0.006	0.255
780	0.68	0.014	0.043	0.013	0.067	0.002	0.119